Real-time Simultaneous Myoelectric Control of Multiple Degrees of Freedom

by

Ali Ameri

B.Sc., Electrical Engineering, Sharif University of Technology, 2004
M.Sc., Electrical Engineering, Shahid Beheshti University, 2007

A Dissertation Submitted in Partial Fulfillment of the Requirements for the Degree of

Doctor of Philosophy

In the Graduate Academic Unit of Department of Electrical and Computer Engineering

Supervisor(s): Kevin Englehart, Ph.D., Electrical and Computer Engineering
Philip Parker, Ph.D., Electrical and Computer Engineering
Erik Scheme, Ph.D., Electrical and Computer Engineering

Examining Board:
Eduardo Castillo Guerra, Ph.D., Electrical and Computer Engineering
Jon Sensinger, Ph.D., Electrical and Computer Engineering
Michael Fleming, Ph.D., Computer Science

External Examiner:
Dario Farina, Ph.D., Electrical Engineering, Georg-August University

This dissertation is accepted by the Dean of Graduate Studies

THE UNIVERSITY OF NEW BRUNSWICK

May, 2014

©Ali Ameri, 2014

Abstract

Natural limb control during activities of daily living involves simultaneous motions of multiple degrees of freedom (DOFs) (such as feeding or grooming, which require simultaneous activation of hand, arm, and wrist in multiple directions). A strategy for simultaneous myoelectric control is to train the system with EMG as the input and the corresponding joint force or position (angle) as the target. For prosthesis control, since it is not possible to measure force/position from an absent limb, a strategy called *mirrored bilateral training* was proposed (with unilateral amputees) in previous work, in which force/position was recorded from the opposite limb during mirrored contractions.

In this work, the effect of alternative feature sets, estimators, feature projection, and coordinate systems on estimation performance was studied with force and position based paradigms. Furthermore, a real-time control test was performed to assess the system usability. It was shown that when the EMG (and effort) levels were similar, no significant difference (p>0.1) was found between the force and position based methods in both offline and real-time control tests.

A novel training paradigm for simultaneous control is described, in which users were prompted to synchronize their contractions with a moving target cursor on a computer screen. The cursor displacements were used as targets to train the estimators. The system usability was assessed with a real-time control test, and the performance was found to be equivalent (p>0.1) to that of the mirrored bilateral training. The proposed visual target based training is more practical than mirrored training because it does not require force and position sensing equipment, and can be potentially used by both unilateral and bilateral amputees.

Finally, a novel application of a support vector machine (SVM) was evaluated in simultaneous myoelectric real-time control of DOFs. It was shown with able-bodied and amputee subjects that the proposed SVM based method outperformed the widely used multilayer perceptron artificial neural network (ANN) in a Fitts' law style real-time control test. Moreover, the processing time required for training and estimation with the SVM was significantly lower than that of the ANN. This approach is shown to provide a robust and computationally efficient system for simultaneous and proportional myoelectric control.

Table of Contents

List of Tables

List of Figures

Chapter 1- Introduction

1.1 Motivation

Persons with transradial amputation form approximately 60% of those with major upper limb loss [1], and include individuals with congenital or acquired deficiencies. Available prostheses can be broadly categorized into passive and active devices. Passive prostheses are purely for cosmetic and body symmetry purposes, while active prostheses assist amputees to perform functional tasks. There are two major groups of active prostheses including body powered and electrically powered devices. The body powered prostheses use harness and cable systems and require body movements (such as shoulder or arm motions) to open or close a hand/prehensor.

The electrically powered prostheses are more complex than the body-powered devices but can potentially provide multiple functions. A battery is used to power electric motors that drive the device. *Myoelectric* prostheses are electrically powered prostheses in which the user motion intent is estimated based on the electrical activity of muscles, obtained by sensors placed on the skin surface. The muscles' electrical signals are referred to as the *electromyogram* (EMG) or *myoelectric signal* (MES). In case of trans-radial amputees, the EMG is measured from the remaining musculature of the residual limb distal to the elbow.

Existing commercial prostheses use rather simple myoelectric control techniques that generally map EMG amplitude to device velocity. Control is usually limited to a single

degree of freedom[1] (DOF) at a time, although a co-contraction or hardware switch can alternate control between multiple DOFs [2]. To overcome this issue, a significant amount of research has been focused on classification based pattern recognition systems which do not require mode switching to change between DOFs. Pattern classification systems have recently become commercially available [3] and are expected to grow in the coming years. The challenges for clinical use of this approach include socket fitting issues [4], and variations in EMG patterns over time [5]. However, the main disadvantage of classification based approaches is that they do not typically accommodate combined motions (for instance performing wrist flexion and pronation at the same time), and thus the selection of DOFs is sequential (multiple motions are performed in series). The requirement for sequential control leads to significant motor planning challenges and prohibits fluid life-like motions. Recent preliminary work [6],[7] has investigated the use of pattern recognition for combined but dependent motions. However, it is desired to control multiple DOFs simultaneously and independently (controlling the intensity of each DOF independent of others'). It is proposed that the simultaneous and proportional control of multiple DOFs can improve the intuitiveness of prosthesis control.

[1] A degree of freedom or DOF refers to rotation about a joint or a movement axis of a prosthesis. The DOFs most often encountered are open/close of a hand and pronation/supination of a wrist. More sophisticated wrists are becoming available than have additional DOF of flexion/extension and adduction/adduction, and more dexterous hands with multiple grasp profiles.

1.2 Objectives

The general objective of this work was to investigate strategies that allow simultaneous and proportional myoelectric control of multiple DOFs and to conduct real-time control tests to assess the usability of these methods. These approaches may be used in multifunction prostheses for transradial amputees. A strategy for independent simultaneous control of multiple DOFs, is using measured joint force or position (angle) as the target to train a supervised estimator with EMG as the input. However, force or movement measurement in amputees is not feasible from the absent limb. To address this issue in the case of unilateral amputees, *mirrored bilateral training* has been employed in previous work, e.g. [8], in which force/position is measured from the opposite (intact) limb during mirrored contractions. With this strategy, the intact limb may be constrained (the force is measured), or unconstrained (the position is measured). It is useful to compare these paradigms to determine their relative performance during real-time control tests. During real-time control, the user interacts with the system as he/she receives visual feedback of the control output, whereas the user interaction effect does not exist in offline results.

1.3 Document Outline

Chapter 2 reviews the physiological background, motor control theories, and myoelectric control schemes. In Chapter 3, force and position estimation using mirrored training are investigated and various analytical analyses using different estimators, feature sets, dimensionality reduction techniques, and alterative coordinate systems are examined. In

Chapter 4, force and position based control methods are assessed in a real-time usability test. Chapter 5 describes a novel training strategy using visual targets. In Chapter 6, a new control scheme based on the support vector machines (SVM) is proposed. A comparison between the usability of the SVMs and a baseline estimator, a multilayer perceptron artificial neural network (ANNs), is conducted using a Fitts' law test. Chapter 7 concludes the document and provides a summary of the results, a list of contributions, and a discussion of the future research.

Chapter 2- Literature Review

2.1 Muscle Contractions

The central nervous system (CNS) has a very important role in the generation of force and movement. The CNS uses the information coming from different receptors in the skeletal muscles, joints, eyes, ears, etc. to accomplish an action. The impulses travelling through the α-motoneurons encode the CNS motor commands and activate the muscles [9]. When a muscle is activated by its α-motoneuron, tension across actin and myosin filaments is generated, which in turn produces force [9]. This results in muscle shortening (concentric contraction), lengthening (eccentric contraction) or no length change (isometric contraction). The nervous system, skeletal muscle, and external load all affect the movement direction, magnitude, and velocity [9]. Muscle resists against stretching due to its elastic characteristics [9]. The opposing force of muscle is called the passive force. The muscle active force is produced by activation through its motor axon. The total muscle force is the sum of active and passive forces [9].

2.2 Proprioception

The sense of joint position is referred to as proprioception while kinesthesia is the sense of joint motion [10]. However, often these terms are mixed, and the term proprioception is used to refer to the sense of body motion, position and force received from peripheral receptors.

The skin may participate in proprioception, but most information comes from two types of receptors, Golgi tendon organs (GTOs) and muscle spindles [10]. GTOs are positioned at the connection between muscle and its tendons, and are innervated by the ending of type Ib afferent sensory nerve fibers. In general, GTOs are considered as force feedback receptors [10]. Muscle spindles are known as receptors of position, velocity and acceleration [10]. Two types of sensory endings innervate the spindles; type Ia (primary) and II (secondary) afferents. The type Ia afferents have large diameter and conduct action potentials faster and usually transmit velocity and acceleration information, while type II afferents are smaller with slower conduction speed and typically convey position [10]. A third type of peripheral receptors is referred to as joint receptors that reside in joint capsules and convey joint movement [10].

2.3 Force Generation

The muscle force is determined by the number of active motor units, their size (diameter), and their firing rates [11]. With the arrival of a single action potential through an α-motoneuron, a MUAP is produced. After a delay (3 to 5 ms or more depending on the muscle type), the motor unit generates a force twitch which is monophasic with a duration of 50-150 ms that is longer than that of the MUAP [12]. Because of the twitch duration, twitches overlap and add even at low firing rates. The force increases with increasing firing rate until it levels off at typically around 30-40 pulses per second, which is less than the maximum motor unit firing rate [13]. A firing rate that is greater than that of the saturation point is only reflected in the EMG signal and not in the force. Typically

EMG-force models do not consider this behavior, and therefore it can degrade the quality of EMG based force estimation [12].

2.4 Myoelectric Control

EMG is an electrical signal that reflects the neuromuscular activation during muscle contraction. EMG is often measured by bipolar surface electrodes and its magnitude prior to amplification typically ranges between 50 μv to 30 mv [14], depending on the muscle. The ionic flow across the cell membrane of the muscle fibers (generating an action potential as depicted in Figure 2.1) propagates (at a speed of around 5 m/s [15]) through the surrounding tissues and arrives at the electrode surface placed on the skin (or underneath the skin in case of intramuscular electrodes) [16].

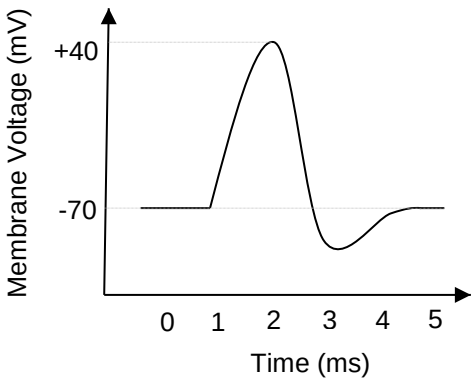

Figure 2.1. An example of an action potential generated in the cell membrane of muscle fiber.

A motor unit comprises of an α-motoneuron (a neuron that transmit motor signals from the spinal cord to muscles) and the skeletal muscle fibers innervated by the motoneuron's axonal branches. The number of muscle fibers innervated by a motor unit is referred to as the innervation ratio, which typically ranges from 2 to 2000 depending on the muscle

[15]. The innervation ratios of muscles responsible for delicate movements are typically lower, whereas muscles required for gross motions usually have higher innervation ratios. Groups of motor units work together to generate contractions of a single muscle. The number of motor units in a muscle varies typically from 10 to 200 [15].

When a motor unit is activated, a motor unit action potential (MUAP) is generated (Figure 2.2), and consequently a force twitch is produced [16]. The activation by the central nervous system (CNS) continues until the muscle no longer needs to produce force. This repeated activation produces MUAP trains. The spatial and temporal superposition of MUAP trains from active motor units forms the EMG signal. Each MUAP is associated with the generation of a force twitch. The total force is the superposition of the force twitches produced by all motor units. When the CNS excitation increases to produce a larger force in the muscle, a larger number of motor units are activated and the firing rates in all motor units are increased.

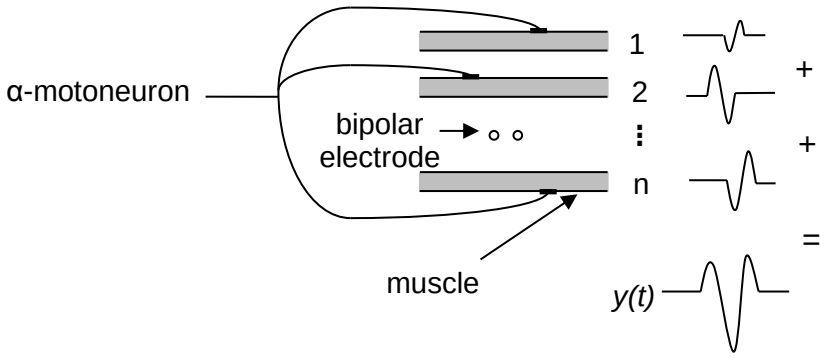

Figure 2.2. When a motor unit is activated through its α-motoneuron, a MUAP is generated. The measured MUAP i.e. *y(t)* (using a bipolar surface electrode) is the superposition of the action potentials of individual muscle fibers.

The EMG amplitude increases with increasing generated force (Figure 2.3). Thus, intentional increased effort and contraction intensity leads to higher amplitude EMG signals [17]. This property is used to estimate user intent from EMG to control powered prostheses in a process called *myoelectric control*. Typically two EMG sensors control one motion or DOF, whereas several EMG sensors are needed to control multiple DOFs.

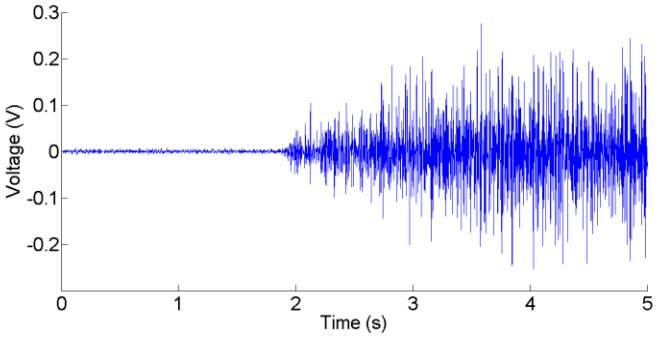

Figure 2.3. The EMG signal measured using a bipolar electrode placed on the skin surface (the signal has been amplified by the acquisition system). The EMG amplitude (envelope) increases with increasing generated force (contraction intensity).

An important feature of the human body is proprioceptive feedback which facilitates limb movement [10]. However, in prostheses there is only some proprioceptive feedback via interaction of socket/device with joint/skin, and auditory feedback from motors. Sensory feedback can be employed to improve the usability of the device [18]. This work, however, focuses on the user intent estimation, and providing sensory feedback is considered outside the scope of this work.

2.5 EMG-Force Relationship

Extensive research has been conducted to determine the relationship between surface EMG and force. Both linear [11],[19]-[22], and nonlinear relationships [23]-[29] have been reported. It should be noted that the net moment of all muscles spanning a joint is measured in these studies. Only in some muscles can individual muscle force be measured using invasive methods [30]. A single bipolar electrode has been used for EMG acquisition.

This relationship between twitch force and MUAP amplitude affects the EMG-force relationship [31]. Motor unit recruitment is generally in order of the smallest to largest (and thus slow to fast twitch motor units) as contraction increases. This is referred to as the *size principle*. According to the *size principle*, the force increase with increasing number of motor units is estimated to be more than proportional [32]. However, an increase in the motor unit size does not necessarily result in a more than proportional increase in the EMG amplitude, because the MUAP amplitude detected by an electrode also depends on the distance between the motor unit and the electrode [33].

Furthermore, the increase in force and EMG with increasing firing rate is less than proportional [32].These effects, however, may be different between the force and EMG. Therefore, since the effects of motor unit recruitment and firing rate on muscle force can be different from those on the EMG, the relationship between force and EMG is not necessarily linear [12]. It depends on the motor unit recruitment range and therefore on the configuration of muscle fiber type. In experiments with muscles of uniform fiber

composition, more linear relationships were observed, and in muscles composed of more mixed fiber types, nonlinear relationships have been reported [34].

2.6 EMG-Force Relationship during Dynamic Contractions

The muscle force at a given EMG amplitude depends on muscle length and velocity (rate of length change) [35]. Muscle active force has an inverse parabolic relationship with muscle length, with the maximum occurring at the muscle resting length (L_0). The passive force increases in an exponential fashion above L_0. The sum of the active and passive forces shows an approximately monotonic increase with increasing muscle length above L_0 [12]. During muscle shortening, force reduces in a hyperbolic fashion with increasing velocity. During muscle stretching, force increases with increasing velocity, levelling off at high speeds [12]. The force-length and force-velocity relationships suggest that force estimation requires not only EMG data, but kinematic information as well [36],[37]. Several studies have investigated force estimation from EMG and kinematics in different joints such as trunk [38], shoulder [39], elbow [40], wrist [41], and knee [42].

2.7 Human Arm Motor Control Models

Human arm motor control has been an active research area for many years. A motor control task can be defined as producing the series of muscle activations that best result

in the completion of a task, given the proprioceptive information from the body sensors [43]. This section reviews some important motor control theories.

2.7.1 Descriptive Models

The purpose of descriptive models is to predict human motion trajectories without having to consider the biological principles that cause the motion features [43]. Empirical relationships observed in human arm movements have resulted in a number of theories including the Fitts' law [44], the bell shaped velocity curve in straight movements [45], and the 2/3 power law [46]. Fitts' law concerns fast, goal directed movements and relates the movement duration time to the distance and size of the target as in the Equation (2.1).

$$MT = a + b\ log_2(1 + \frac{D}{W}) \tag{2.1}$$

where *MT* is the time taken to complete the movement, *a* and *b* are regression coefficients, *D* is the distance between the starting point and target, and *W* is the target width. The index of movement difficulty (*ID*) is defined as:

$$ID = log_2(1 + \frac{D}{W}) \tag{2.2}$$

The 2/3 power law states that in curved movements, the velocity (*v*) of the hand is derived from the inverse of the curve radius (*r*) as in the Equation (2.3).

$$v(t) = \gamma r(t)^{-\frac{1}{3}} \tag{2.3}$$

where γ has been empirically determined as 0.33. The drawback of the power law is that it cannot be applied to paths including straight segments or inflection points. Also, it is

inaccurate during slow movements and it does not predict the velocity reduction at the end of the path.

An important feature of human arm motion is the bell shaped velocity profile in straight movements. Flash and Hogan [47] employed this feature to introduce a new model called minimum *jerk* model (*jerk* is the derivative of acceleration). This model states that the movement smoothness determines the trajectory and is obtained by minimizing the *jerk, (J),* as defined in Equation (2.4) for planar movements:

$$J = \sqrt{(\frac{d^3x}{dt^3})^2 + (\frac{d^3y}{dt^3})^2} \tag{2.4}$$

2.7.2 Dynamic Models

Dynamic models concentrate on the dynamics of the arm and use the joint torques and external forces to describe motor control [48]. The most important dynamic model is the *minimum torque change* model [49]. This model states that the human motor system uses a motion trajectory that minimizes the total torque change (Equation (2.5)).

$$C = 1/2 \int_0^{t_f} \sum_i (\frac{dz_i}{dt})^2 dt \tag{2.5}$$

where C is the total torque change and z_i is the torque of the ith joint, and t_f is the time to reach the final point.

2.7.3 Stochastic Models

Harris and Wolpert [50] presented a different concept of motor control and suggested that motor planning is not based on minimization of *jerk* or torque change, but on the minimization of the end-point variation. It was shown that the existence of biological noise in the firing of motor neurons, explains the differences that occur in repeated movements. The noise increases linearly with the command signals amplitude (the standard deviation of the motor neuronal firing increases, with the mean level, with a coefficient of variation between 10% to 25% [51],[52]). Therefore, the end-point variance minimization involves not only kinematics but also dynamics adjustments. It was demonstrated that the end-point error minimization results in the well-known motion features such as *jerk* minimization and Fitts' law.

Previous models assumed that planning was performed before execution, and consequently in a feedforward manner. However, Todorov and Jordan [53] presented an optimal feedback control based model in which planning and execution are carried out simultaneously. In a theory termed “minimum intervention principle”, they proposed that the control system only corrects for the deviations in the task-relevant directions of the control space. This theory concerns the redundancy of motor control as different trajectories can be used for movement between desired points. They showed that the optimal feedback control model predicted a decrease in variance near the desired points (via-point and end-point) at the expense of increase in variance of other regions in the path.

2.8 Control Variables encoded in the CNS Signals

It has been shown that cell discharge in the primary motor cortex is related to both dynamic (force related) [54]-[57] and kinematic features [58]-[60] of the motion. Furthermore, different parameters may be encoded in the same cell under different conditions [54],[57].

Motor cortical cells receive a complex combination of sensory inputs, and therefore their discharge cannot be related to a single mechanical variable [54],[61]. As described earlier, muscle spindle group II afferents are typically known as muscle length receptors, group Ia afferents as length plus velocity receptors, and Golgi tendon organs as force receptors [62]. However, muscle length and force nonlinearly interact with each other, which is reflected in muscle afferent discharge [61]. Also, in many cases, muscle spindles and Golgi tendon organs converge into the same neurons which causes mixed representations [61]. Therefore, it is likely that the discharge patterns of populations of neurons encode global information rather than single, artificially isolated mechanical variables [61].

2.9 Myoelectric Systems

Myoelectric control systems use EMG signals (typically recorded using surface electrodes placed on the skin) to estimate motor intent, and have been used for many years to control powered upper limb prostheses. The general procedure of myoelectric control [2] is shown in Figure 2.4.

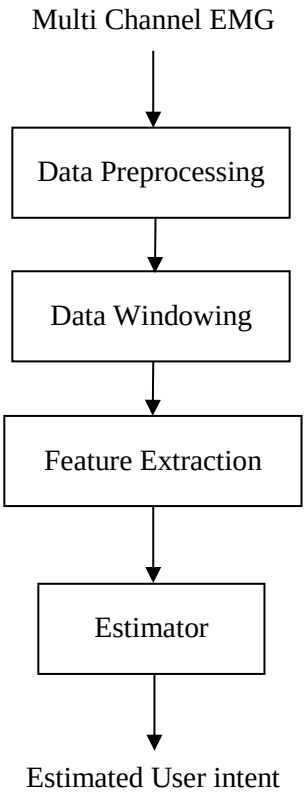

Figure 2.4. Block diagram of myoelectric estimation of motor intent.

2.9.1 Data Preprocessing

Various noise sources may contaminate the surface EMG signal. The goal of data preprocessing is to filter the maximum amount of noise while preserving as much of the signal frequency spectrum as possible. Using bipolar electrodes, the EMG frequency spectrum typically ranges from above 0 to 400 Hz [63]. This range depends on factors such as the inter-electrode spacing in the bipolar sensors, muscle type, the shape of the action potentials and the amount of fatty tissues between the muscle and skin [63]. During preprocessing, the EMG may be lowpass filtered. De Luca et al. [63] suggested a

cutoff frequency in the range 400 to 450 Hz for lowpass filtering the EMG. Modern EMG sensors employ built-in anti-aliasing filters.

There are several low frequency noise sources that can affect the signal. Two extrinsic noise sources, *power line interference* and *cable motion artifact*, are rendered largely insignificant in modern sensor systems [63]. Two low frequency intrinsic noise sources namely *thermal noise* and *electrochemical noise* are produced in the amplification system and at the skin-electrode interface, respectively [64]. The *thermal noise* and *electrochemical noise* together form the *baseline noise [*63].

Movement artifact is another low frequency noise source which is also generated at the electrode-skin interface and generates a time-varying voltage across the two electrodes of the bipolar sensor. Movement artifact may be produced due to either muscle movement under the skin, or by a travelling force pulse [63]. The low frequency noise components (baseline noise and movement artifact) can be reduced using a highpass filter. The suggested cutoff frequency in the literature ranges from 5 to 20 Hz [63], [65]-[67].

2.9.2 Data Windowing

The instantaneous value of EMG is not useful for intent estimation [68], and consequently EMG features are extracted from an analysis window. There is a trade-off in choosing the window length. Longer window lengths result in higher delay which may degrade the system responsiveness [69], while lower window lengths lead to lower estimation accuracies [70],[8]. Most myoelectric systems use window lengths between 100-250 ms.

Based on the system processing speed, disjoint or overlapped windows may be used for analysis. In the disjoint method, new windows are formed using new samples, and the estimation rate is $1/W$, where W is the window length. In the overlapped method, overlapped windows are used and the estimation rate exceeds $1/W$.

The choice of disjoint or overlapped windows depends on the system processing speed for feature extraction and estimation for the window of the data. Overlapped windows are highly preferable because a desired estimation rate is faster than typical window lengths (100-250 ms), and they result in smoother and more continuous control which enhance the usability.

2.9.3 Feature Extraction

Following data windowing, signal features are computed for each window. Many myoelectric systems use an estimate of EMG envelope using mean absolute value [2], mean square value [71] or root mean square [72] features. Most pattern recognition based schemes ([72]-[76]) include additional features to improve the performance. Various time domain variables have been employed. A well-known feature set called the TD features proposed by Hudgins et al. [73] consists of four time domain features including mean absolute value, waveform length, zero-crossings, and slope signs changes. The waveform length, zero-crossings, and slope signs changes provide information about the frequency content of the signal. The calculation of the TD statistics for an analysis window of N samples including $x_1, x_2,..., x_N$ is described below.

The mean absolute value (*MAV*) is computed as in Equation (2.6).

$$MAV = \frac{1}{N}\sum_{i=1}^{N} |x_i| \tag{2.6}$$

The waveform length (*WL*) is the cumulative sum of the absolute values of the differences between consecutive samples and defined as in the Equation (2.7).

$$WL = \sum_{i=2}^{N} |x_i - x_{i-1}| \tag{2.7}$$

The zero-crossings feature is the number of times the signal crosses zero. To decrease the number of noise induced zero-crossings, a threshold (ε) is included in the computation of the zero-crossings. For each two consecutive values of the signal i.e. x_{i-1} and x_i, the zero-crossings count is incremented if

$$\{x_i > 0 \; and \; x_{i-1} < 0\} \; or \; \{x_i < 0 \; and \; x_{i-1} > 0\}$$

and (2.8)

$$|x_i - x_{i-1}| > \varepsilon$$

The value of ε depends on the noise of the acquisition system and must be determined based on the noise level of data.

The slope signs changes feature is the number of times the slope of the signal changes sign. In other words, it is the zero-crossings of the derivative of the signal. Again, to account for noise interference, a threshold (ε) is used for calculation of the slope signs changes. For each three consecutive samples of the signal i.e. x_{i-1} , x_i and x_{i+1}, the slope sign change count is incremented if

$$\{x_i > x_{i-1} \; and \;\; x_i > x_{i+1}\} \; or \; \{x_i < x_{i-1} \;\; and \;\; x_i < x_{i+1}\}$$

and

$$\{|x_i - x_{i-1}| > \varepsilon\} \ or \ \{|x_{i+1} - x_i| > \varepsilon\} \tag{2.9}$$

Other features such as the autoregressive coefficients, short time Fourier transform coefficients, wavelet transform coefficients, wavelet packet transform coefficients, and different combinations of these features have been widely used in the literature. A comparison between all feature sets is difficult due to their large variety (examples of feature comparison studies include [77]-[79]).

2.9.4 Estimation Paradigms

There have been several strategies to estimate user intent using EMG. Current commercial prostheses use a heuristic method which typically involves estimating the EMG amplitude [80] or rate of change [81] from one or two muscles to determine the direction and speed of a device. This cannot be extended to the control of more than one DOF without some means of "mode switching" (usually a contraction burst or hardware toggle), resulting in an awkward means of multi-DOF manipulation [82].

To address this issue, classification based pattern recognition techniques has been investigated for more than 30 years (e.g. [72]-[76]). This approach is based on the assumption that EMG features from a given electrode location are repeatable for a given state of muscle group activation, and are different from one state of activation to another [83]. This method potentially allows control of more DOFs than conventional approaches because they a one-to-one mapping between the DOF and control site is not required [72].

However, the classification schemes in the literature mostly do not inherently provide proportional control, although many studies has proposed methods for its inclusion (e.g. [84],[85],[72],[108],[118]-[120]). Furthermore, the pattern classification based approaches do not typically allow combined motions, and thus the selection of DOFs is sequential. Recently, preliminary work [6],[7] has investigated the use of classification for control of combined (simultaneous) DOFs. Despite these modifications, however, a classification based approach combining both aspects of simultaneous and proportional control of multiple DOFs has yet to be developed. Using current pattern classification based control methods, a user is required to perform movements sequentially in order to complete a given task, which imposes significant motor planning challenges, and prevents fluid functional motions.

For independent simultaneous control of multiple DOFs, recent work has focused on regression techniques to map EMG to a continuous representation of user intent (such as force or position) so that the simultaneous activation of multiple DOF can be estimated. This requires measuring force or position to be used as the training target for a supervised estimator. In the case of robotic teleoperation (e.g. [86]), the user's limb is assumed to be intact, so the EMG and the force/position target can be acquired from the controlling limb. In the case of upper limb prostheses, the amputee is unable to produce movement or force with the absent limb. A strategy (applicable to unilateral amputees) to accommodate this is to have the amputees generate *mirrored bilateral contractions* with the intact (contralateral) limb producing the movement/force target. The consistency in EMG between the upper limbs is motivated by the observation that a significant correlation exists between the left and right upper limb motions during mirrored bilateral maximal

and submaximal contractions [87]. As well, a high correlation between the movement related cortical potentials (MRCP) recorded from the left and right motor areas during mirrored bilateral maximal and submaximal contractions has been reported [87]. This high correlation indicates the interneuronal connectivity between both motor areas linked by common inputs [87]. Furthermore, the "common drive" to the motor units proposed by De Luca et al. [88] suggests that when the right and left upper limbs are activated simultaneously to generate force, the nervous system views them as one unit and controls them in a similar fashion.

For force/position estimation from EMG in case of intact limb, the limb may be *constrained* (unable to move, isometric, the force is measured), or *unconstrained* (movement allowed, the position is measured).

In constrained (force targeted) experiments, Jiang et al. [71] proposed a method using non-negative matrix factorization to estimate, from EMG, the wrist force in the three DOF of flexion-extension, abduction-adduction, and pronation-supination. This method was semi-unsupervised as it did not require force data for training but only needed the information on which DOF was active in a training trial (training trials involved single DOF contractions). This approach was applicable to bilateral amputees. The performance however, was poor in pronation-supination (zero correlation between the measured and estimated force in this DOF was found). This might be because the pronators and supinators are deep muscles and their activities may be masked by superficial muscles such as flexors and extensors [89]. Nielsen et al. [8] employed mirrored training to estimate the force in two DOF of the wrist (flexion-extension and abduction-adduction). This method was supervised as the force measured from the contralateral limb was used

as the training target for an ANN. The force estimation accuracy was high (R^2 > 90%). Similarly, Castellini et al. [90] successfully estimated grasp force (single DOF) using a support vector machine (SVM) with unilateral amputee subjects by employing mirrored training. The estimation error was found less than 10% for all users. Kamavuako et al. [91] used mirrored training with intramuscular EMG to estimate grasp force with ANNs. High estimation accuracy (mean R^2 =88%) was reported.

In unconstrained (position targeted) experiments, Artemiadis et al. [86] estimated position in four DOF of the shoulder and elbow joints for a robotic application. This work was on robotics and therefore the EMG and joint angles were measured from the same limb. A state-space model was used for mapping EMG to joint angle, and the mean correlation coefficient between estimated and measured angles was higher than 90%. For prosthesis control, using mirrored training, Sebelius et al. [92] employed ANNs to estimate finger joint angles with unilateral amputees with promising results (around 80% accuracy). Muceli et al. [93],[94] estimated joint angles for wrist DOF as well as hand close-open using mirrored training with around 80% estimation accuracy. Jiang et al. [89] successfully employed mirrored training to estimate joint angles in wrist DOF (flexion-extension, abduction-adduction, and pronation-supination) with healthy and transradial amputee subjects. The mean R^2 for able-bodied subjects was 72%, for long stump amputees 62.5%, and for short stump amputees 19.7%. Jiang et al. [89] pointed out that the striking difference between the performance of long and short residuum amputees highlights the paradox in myoelectric control: amputees with higher amputation levels have less signal sites available for EMG acquisition, while they require more functional restoration. Smith et al. [95] successfully estimated hand fingers joint angles

simultaneously with an able-bodied subject, where CyberGlove was used for joints measurement during mirrored training. The correlation coefficient between actual and estimated angle for different fingers ranged from 65% to 81%. ANNs were used to map EMG to joint angle in [89], [93]-[95].

Mirrored training however, is limited to unilateral amputees. For bilateral amputees, Choi et al. [96]-[98] proposed a training method that required the users to produce contractions according to a cursor on a screen. Subsequently, the cursor traces and corresponding EMG amplitudes were used to determine a non-negative synergy matrix, mapping EMG to motion intent. This system was evaluated in a real-time control test with promising results. Wrist flexion-extension, and abduction-adduction were investigated in this work.

In a recent study, Jiang et al. [99] proposed a control scheme based on non-negative matrix factorization with able-bodied and amputee subjects. The calibration (training) phase involved four repetitions of full motion range contractions for each DOF using single DOF contractions. A synergy matrix was estimated from the EMG data, using non-negative matrix factorization, to map EMG to user intent. The system was tested in a real-time control test with successful results. This work involved wrist flexion-extension and pronation-supination. This algorithm was also employed in other studies [100],[101].

As reviewed above, previous work has typically employed mirrored training for independent simultaneous estimation of multiple DOFs. However, only offline estimation for this approach has been evaluated in the literature, but its usability has yet to be determined during real-time control. This strategy may have the potential for clinical applications as suggested by previous studies with unilateral amputees [89]. It is not clear

however, whether a force or position targeted protocol for mirrored training can provide higher estimation accuracy and control performance. Mirrored training is limited to unilateral amputees, and it requires complex force or position sensing equipment. Therefore, more practical training paradigms are of particular interest.

2.9.5 Amputation Effects

After an amputation, extensive cortex reorganization occurs [102]. Studies on animals and humans show that within 24 hours after amputation a fast reorganization of the cortical hand/arm map may occur so that adjacent cortical areas spread into areas previously dedicated to the missing hand/arm. However, it has been suggested that the reorganization of the cortex areas is a reversible phenomenon [102].

A study of transradial amputees [102] showed that amputees were able to perform multiple movements with a virtual hand even 20 years after amputation. This suggests that the brain can relearn and experience plastic changes to command motions that had not been experienced for many years.

2.9.6 Real-time Myoelectric Control

A considerable amount of work has been performed in myoelectric control of prostheses [103], robot manipulators [104], and computer based avatars [105] or virtual limbs [106]. With this method, the motion intent is estimated from user contractions and subsequently translated into a control signal. Offline user intent estimation shows promising results,

but how well offline results translate to real-time control is not clear. Lock et al. [107] reported minimal correlation between classification accuracy and usability. Simon et al. [108] found that even with classification accuracy of higher than 90%, the users only were able to complete 69% of the targets in the target achievement test. This highlights the need for real-time tests in addition to offline tests to assess the performance. Hargrove et al. [109] reported that inclusion of the transient portions reduced the classification accuracy, but it improved the usability. Moreover, Hargrove et al. [109] found a weak correlation between classification accuracy and real-time performance, due to the narrow range of the classification accuracies (the classification accuracies were always higher than 90%).

In addition to the estimation accuracy, the ability of the user to interact with the control system is an important aspect of real-time control. Myoelectric prostheses typically use velocity control in which the intensity of effort regulates the speed of the device. Robot manipulators may use feedback control to implement a position control, in which the contraction intensity is mapped to position or joint angle. In computer based training tools, both velocity and position control have been employed [110],[111]. Sensinger et al. [112] conducted a comparison between velocity control and position control and found that velocity control provided faster control without increasing error. Also, in a study which was not on myoelectric control (and therefore it did not involve EMG measurement), Zhai and Milgram [113] compared velocity and position control modalities in a target reaching task. Two experiments including isometric and isotonic were performed in which a cursor was directly controlled using either measured force (in isometric experiment) or position (in isotonic experiment), respectively. They showed

that velocity control outperformed the position control in the isometric experiment, whereas position control outperformed the velocity control in the isotonic experiment.

Many studies have investigated real-time myoelectric control, and various test protocols have been employed to assess the performance. Hargrove et al. [72] conducted a virtual clothespin placement task with a pattern recognition based method, where hand and wrist movements were used to control a virtual limb. Kuiken et al. [114] designed a virtual arm control test to examine the clinical robustness of the pattern recognition based control in amputees that underwent targeted muscle reinnervation (TMR) surgery. Smith et al. [115] employed a real-time test where finger movement estimation from EMG was used to control a virtual hand.

Simon et al. [108] tested five transradial amputees in classification of wrist flexion-extension, forearm pronation-supination, hand open-close and no motion. The classified motions controlled a virtual arm to achieve a target posture. Choi et al. [116] designed a human computer interface to enable patients with motor disabilities to use a mouse with myoelectric control. Two DOFs of wrist were used to move the cursor on the screen, and the hand open motion was used for clicking the mouse. The performance was assessed through a target acquisition Fitts' law style test.

Williams et al. [117] employed EMG from face and neck muscles of tetraplegia patients to control a cursor during a Fitt's law test. Scheme et al. [118] conducted a Fitts' law test to assess the control performances of new pattern recognition based techniques. Wrist flexion-extension, pronation-supination, hand open-close, and no motion were used in this work. Also, Scheme et al. [119] performed a real-time Fitts' law style control test to

evaluate a confidence based rejection method for linear discriminant analysis (LDA) classifier. Moreover, Scheme et al. [120] employed a real-time Fitts' law test to assess different proportional control algorithms with classification based schemes.

As described in Section 2.9.4, Choi et al. [96]-[98] trained a non-negative synergy matrix (linear estimator) to estimate wrist motions in two DOFs. During the training, the users produced wrist motions according to a moving target on a computer screen. For real-time test, the motion intent was projected on the screen as a control cursor and the quality of tracking was assessed.

Castellini et al. [90] classified four hand/finger movements, and estimated the grasp force. The output controlled finger position and force of a robotic hand. Antfolk et al. [18] tested the ability of a trans-radial unilateral amputee to control a multi DOF prosthetic hand using a pattern recognition based system. Initial training was performed using a data glove fitted to the contralateral hand recording joint angle positions of the fingers during mirrored training. The myoelectric signal was obtained from seven possible grasps, and the finger joint angles were estimated to control the prosthetic hand. Sensory information recorded from the force sensors of the prosthesis was transmitted to actuators, continuously delivering force sensory stimulation to the amputee's stump. The amputee was reported to have learned to perform several dexterous hand movements after only two hours of training. Shenoy et al. [121] classified eight movements of hand and wrist to control a robotic arm. Artemiadis et al. [86] implemented myoelectric control of a robot arm in three DOFs of shoulder, elbow and wrist joints. Cipriani et al. [103] tested simultaneous real-time control of seven hand postures (finger movements) using trans-radial amputees. Khokhar et al. [122] investigated real-time control of a wrist exoskeleton

using classification methods and estimated the wrist torque. Momen et al. [123] implemented real-time classification of wrist flexion and extension movements with able bodied and amputee subjects. Ajiboye et al. [124] investigated real-time classification of wrist and hand motions with an able-bodied user.

As described in Section 2.9.4, Jiang et al. [99] and Muceli et al. [100] proposed an unsupervised approach for simultaneous control. Wrist flexion-extension and pronation-supination were investigated and the training involved single DOF contractions. For each trial, by applying non-negative matrix factorization to root mean square (RMS) values of EMG, a non-negative synergy matrix was derived. The matrices from both DOFs were incorporated to form a complete synergy matrix, which was used in a real-time test for simultaneous control.

There is limited literature on independent simultaneous real-time control of multiple DOFs. For simultaneous real-time control, to our knowledge, mirrored training has not been investigated previously. Mirrored training cannot be used by bilateral amputees, and the training protocol requires complex equipment for force or position sensing. Alternative methods for simultaneous control employed by Choi et al. [96]-[98], Jiang et al. [99] and Muceli et al. [100] are preferable, as they are applicable to both unilateral and bilateral amputees. Moreover, the implementation of these methods is simpler than the mirrored training approach as force or position sensing equipment is not required. In these studies, the training protocol involved only single DOF contractions. Also, a linear system was employed as the motor intent was estimated linearly from the EMG during the real-time control. To achieve possible performance improvement, a training paradigm can be investigated which includes combined motions as well as single DOF contractions,

as this has shown to enhance the offline simultaneous force estimation performance [125]. Moreover, nonlinear estimators may improve the control performance as due to the complexity of the musculoskeletal system the relationship between EMG and arm motion is highly nonlinear [126].

2.10 Performance Assessment

Surface EMG provides a non-invasive approach of capturing muscle activity, and has been widely used to control prosthetic devices. Decoding the EMG signals measured from forearm muscles of amputees who have lost their hands can help to restore part of the lost motor functionality in these individuals. An extensive amount of research has focused on the use of sophisticated signal processing methods to enhance the EMG decoding accuracy. Clinical investigations, however, show that for widespread acceptance, a prosthesis needs to be both accurate and intuitive to control. Furthermore, the usability of a myoelectric system cannot be determined by the accuracy of offline decoding alone; it must also be assessed based on its real-time control performance. Two different control schemes with similar offline decoding accuracies may provide completely different real-time control qualities.

Many real-time testing protocols have been proposed in the literature to assess the control quality. A widely accepted prosthetic control measure is the Assessment for Capacity of Myoelectric Control [127],[128], which requires controlling a physical prosthesis. For this assessment, a myoelectric prosthetic user performs daily bimanual tasks, while a clinician rates the user's capability to perform a grip on several items in 4 different areas:

gripping, holding, releasing and coordinating. Furthermore, the Upper Limb Prosthetics Outcome Measures Group (ULPOM) recommended several prosthesis control tests and identified numerous measures contributing to prosthesis usability [129]. They recognized several factors to assess such as control of the prosthesis, functional level, quality of life, and overuse of prostheses. It was pointed out that to evaluate "control of the prosthesis", a measurement tool is required which is sensitive enough to differentiate between control schemes and show variations of the control quality of the prosthesis over time. The tests described above, however, are largely qualitative and require subjective evaluation by trained clinicians.

As a compromise, it is often more practical to assess the performance of myoelectric control schemes in a virtual environment without a physical prosthesis, where a virtual arm or a cursor is controlled through user's contractions. Typically some form of target achievement tests have been employed in many studies during which users are prompted to move a cursor/virtual limb to a target position and remain there for a specific amount of time. Jiang et al. [99] and Muceli et al. [100] used a target acquisition test for simultaneous control of a feedback arrow using wrist flexion-extension and pronation-supination. In [99],[100], three metrics including *Completion time*, *path efficiency* and *completion rate* were used to assess control performance. Simon et al. [108] used similar metrics to evaluate a pattern recognition based system with a target acquisition test.

Several studies [116]-[120] employed a Fitts' law [44] style target acquisition test. As described earlier, Fitts' law [44] is a human movement model that predicts the time to rapidly move to a target as a function of the target distance and target size, and is based on Shannon's original work in information theory [130]. This exhibits a speed-accuracy

trade-off, so that the targets that are more distant and/or smaller are more difficult to achieve (Equation (2.1)). The results of repeated trials, using different target widths and distances are incorporated into a single parameter called *throughput* (*TP*), measured in bits per second and is defined as:

$$TP = \frac{1}{N}\sum_{i=1}^{N}\frac{ID_i}{MT_i} \tag{2.10}$$

where *N* is the total number of conditions, *i* is a particular movement condition, *ID* is the index of difficulty (Equation (2.2)) and *MT* is the time taken to complete the movement.

In previous myelectric control studies [117],[118], in addition to *throughput*, other metrics such as *path efficiency* and *completion rate*, and *overshoot* has been used to provide more comprehensive information about control performance.

Most multifunction myoelectric control research has been devoted to pattern classification methods in which the control is sequential. Most of the literature on simultaneous control of multiple DOFs for prosthetics, has used mirrored bilateral training, which cannot be applied to bilateral amputees. Therefore, there is a need for training methods which are applicable to these patients. Also previous work on mirrored training, has been limited to offline assessments using pre-recorded data, and has not included real-time control tests. Consequently, user's interaction with the system was absent.

In general, offline analysis and real-time control tests each have their own advantages and drawbacks. Offline assessment is popular because it is possible to test alternative signal processing approaches any time after the completion of the experiment. Offline analysis

also removes any inter-trial variability by allowing direct comparisons been algorithms using the same data. Real-time assessments, however, can provide more information regarding the system usability. The user interaction is included in an online test so that the user receives visual feedback of the output and can correct some erroneous movements. The drawbacks of real-time tests are that any modification of the decoding method requires repeating a complete test, and no direct comparisons can be made using like datasets. The disadvantage of offline evaluation is that high offline results can be a result of constrained conditions and do not guarantee satisfactory control performance. Other factors such as system processing delay, which are not considered in offline assessment, can greatly affect the control performance. Offline results show the potential ability of the system, but it is not obvious if the user is able to use this potential to complete a task in a natural and intuitive manner. Since offline and real-time results may provide different information with regard to the system performance, it is useful to employ both measures to assess a control scheme. Qualitative assessment from the user's point of view should also be considered and may add extra information in addition to the quantitative performance analyses.

Previous work on mirrored training has used force targeted and position targeted methods for simultaneous estimation of DOFs. However, the effect of different analytical approaches such as feature sets, estimators, feature projection and coordinate systems on the estimation performance must be investigated. There is limited literature on the real-time simultaneous myoelectric control. To our knowledge, no study has yet employed mirrored bilateral training for real-time control. With this method, it is of particular interest to compare force targeted and position targeted paradigms. Mirrored training has

the potential to be used for unilateral amputees, but it cannot be employed for bilateral amputees. Therefore, other approaches must also be investigated. The methods proposed by Jiang et al. [99], Muceli et al. [100] and Choi et al. [98] are promising as they are applicable to both unilateral and bilateral amputees. Since these methods employ linear estimations, it is desired to investigate a method with nonlinear estimators for possible performance improvements.

Chapter 3- Optimization of Analytical Methods

3.1 Introduction

In this chapter, force and position estimation in multiple DOFs from EMG during constrained and unconstrained contractions is investigated. A comparison between force and position estimation from EMG has not been conducted in previous studies. Consequently, this chapter and the next chapter intend to resolve the ambiguities in the literature on the relative performance of these approaches. Although this study was performed using able-bodied subjects, mirrored bilateral training was employed to make the approach applicable to unilateral amputees. It should be noted that in case of amputees, constrained and unconstrained setups will only apply to the contralateral (intact) limb, and the impaired limb have the same type of contractions between different protocols.

In this chapter, baseline results, established using methods based on previous work, are presented. Furthermore, offline data are used to optimize analytical approaches and explore novel methods, with the purpose of prescribing methods for the real-time investigations of the next chapters. It is difficult to perform the optimization process using real-time experiments while the user is interacting with the control system and the feedback mechanism, because it would necessitate repeating the experiment for each different analytical method. The chapter is organized as follows; Sections 3.2 and 3.3 are based on methods used in previous works. In Section 3.4, the optimization of existing methods and the application of novel techniques are investigated. Section 3.5 summarizes the chapter.

3.2 Methods

3.2.1 Experimental Design

In this study, performed with able-bodied subjects, the user intent estimation during *constrained* contractions (limb unable to move, joint force was measured) and *unconstrained* contractions (limb movement allowed, joint angle was measured) was investigated to facilitate a direct comparison between these two methods. Since the focus of this work is prosthesis control, *mirrored bilateral contractions* were employed to make the protocol applicable to unilateral amputees. Therefore, the joint force/angle was measured from the opposite (contralateral) limb. The experimental methods were designed to be directly comparable to those used in previous work.

Ten able-bodied subjects (ages: 24-39, all right handed) participated in this study (a power analysis (power=0.80) was also conducted using pilot data, and the minimum number of required subjects was found to be 5). The experimental protocol was approved by the University of New Brunswick's Research Ethics Board. The three DOF of the wrist; flexion-extension, abduction-adduction and forearm pronation-supination were investigated. Eight bipolar wireless surface electrodes (Delsys Inc.) were attached to each arm, equally spaced around the circumference of the forearm at approximately one-third of the forearm length, measured from the olecranon of the ulna. To prepare the skin, conducting gel was applied before the electrode attachment. The EMG data were sampled at 1 kHz using a 16 bit A/D converter (NI PCIe-6363). The real-time raw EMG signals were verified visually before the experiment to ensure the data quality. The protocol

involved both constrained and unconstrained experiments conducted in separate sessions in random order. Each session consisted of a training protocol, offline test, and the completion of a real-time tracking test, separated by sufficient amount of rest time based on the subject's request. Fourteen wrist contractions, consisted of individual and combined wrist actuations, were used in the experiments, as listed in Table 3.1. Pilot work showed that performing consistent contractions with combinations of all three DOFs was conceptually difficult for subjects (especially in *unconstrained* experiments). Therefore, these contractions were not included in the protocol. Signal acquisition and analysis was conducted using Matlab™ (Mathworks, Inc.) on a 3.30 GHz Intel Optiplex 990 workstation. The display adapter was an AMD Radeon HD 6670.

Table 3.1. The contractions of wrist and forearm included in the protocol

Index	Contraction
1	Flexion
2	Extension
3	Abduction
4	Adduction
5	Pronation
6	Supination
7	Simultaneous Flexion and Pronation
8	Simultaneous Flexion and Supination
9	Simultaneous Extension and Pronation
10	Simultaneous Extension and Supination
11	Simultaneous Abduction and Pronation
12	Simultaneous Abduction and Supination
13	Simultaneous Adduction and Pronation
14	Simultaneous Adduction and Supination

A. Constrained Experiment

Subjects sat in a chair, with arms secured to armrests. The hands were fixed in a neutral position with palms facing inward using two vertical handles attached to a steel frame mounted in front of the chair (Figure 3.1). A 3-axis force/torque transducer (Gamma FT-130-10, ATI Industries) was mounted between the left handle and the steel frame, so that the x-axis corresponded to wrist flexion-extension, y-axis to abduction-adduction and z-axis to pronation-supination. The torque exerted on the force/torque transducer was recorded at 1 KHz using a 12 bit A/D converter (NI PCI-6024E). The force/torque transducer resolution was approximately 0.001 Nm, so the measurement error was assumed to be negligible in the range of wrist forces.

(a)

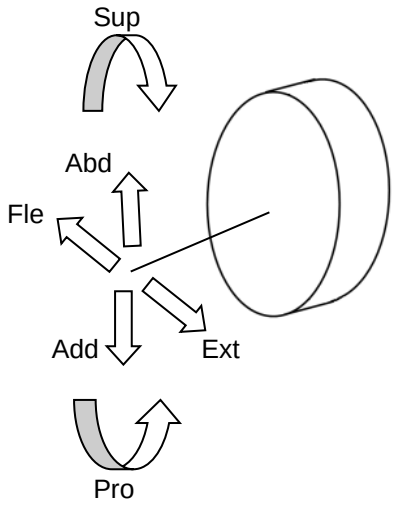

(b)

Figure 3.1. (a) *Constrained* experiment apparatus, (b) The force/torque transducer was positioned between the left handle and steel frame such that its three axes were aligned to wrist flexion-extension, abduction-adduction, and pronation-supination. The torque exerted on the force/torque transducer was measured.

To provide subjects with real-time force feedback, the force transducer output was displayed on a computer screen using a cursor with orientation. The flexion-extension DOF was mapped to the horizontal displacement of the cursor, while abduction-adduction was mapped to the vertical displacement. The orientation angle of the cursor was determined by pronation-supination. The system was calibrated before each trial, which located the cursor to the screen center with vertical orientation when a user performed the neutral *zero force* contraction. With the calibration, the bias force (the

measured force during neutral contraction) was saved, so that net force was obtained by subtracting the bias force from the measured force. The EMG from both arms and the force of the left (non-dominant) upper limb were recorded concurrently.

The protocol involved fourteen trials associated with the fourteen contractions listed in Table 3.1. The subjects were asked to perform mirrored bilateral contractions within the constraints. In each trial, a picture of the requested contraction was displayed. To standardize the maximum applied force between the subjects, a fixed target representing a medium force level (of constant magnitude for all subjects and directions) corresponding to the requested contraction was highlighted on the screen. Each movement was 6 seconds in duration and included approximately 1 second of initial *zero force*, 1 second of movement towards the target, 2 seconds of holding the target contraction, 1 second of returning to zero force, followed by sustaining zero force for the remaining time. Each trial involved four repetitions of a movement.

B. Unconstrained Experiment

Two experimental methods were conducted in random order in the *unconstrained* experiment. The first experiment was performed without restraints (*unconstrained* protocol). In the second setup, the subjects were fitted with a pair of flexible wrist braces (Figure 3.2 (a)) used to provide nominal resistance during wrist movements (*resisted unconstrained* protocol). Adjustable straps were tightened to provide a moderate resistance to movement during the experiment. The reduction in range of motion caused by the wrist braces was negligible.

The inclusion of the *resisted unconstrained* protocol was motivated by the observation that EMG levels were low during pilot *unconstrained* experiments. Previously, Muceli et al. [93],[94] acknowledged this issue and attempted to accommodate it by using arm orientation to employ gravity as an opposing force to wrist movement. The use of wrist braces in this experiment was intended to provide roughly uniform resistance in all DOFs. Empirical observation during pilot work indicated that the wrist braces elevated EMG magnitude to levels similar to those elicited during the *constrained* protocol.

The subjects sat in a chair with armrests supporting both arms. In a neutral state (*no motion*), the subjects rested their forearms with palms facing inward. Six reflective ball shaped markers with a diameter of 15 mm were attached to the left (non-dominant) upper limb at the medial and lateral epicondyles of the humerus, the styloid processes of the radius and ulna, the radial head of the second metacarpal bone and the ulnar head of the fifth metacarpal bone, as shown in Figure 3.2 (b). The positions of the markers were captured by a Vicon 512 system using 8 infrared video cameras recording at 60 Hz. The motion capture system resolution is approximately 2 mm, so the measurement error was assumed to be negligible in the range of wrist movements (the angle measurement accuracy however, for abduction-adduction is lower than other DOFs, because it has lower motion range). The motion capture system was synchronized with the EMG collection system using a digital trigger through a PC serial port. The EMG from both arms and the position of the left (non-dominant) limb were recorded simultaneously. Table 3.2 summarizes the experimental setup for each protocol.

(a)

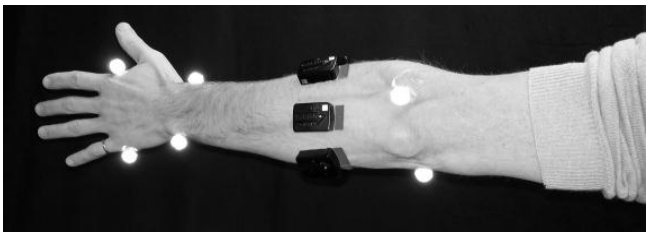

(b)

Figure 3.2 (a) The wrist brace used in the *resisted unconstrained* experiment, (b) Marker locations in the *unconstrained* experiments.

Table 3.2. Experimental setup for each protocol.

	Constrained	*Unconstrained*	*Resisted unconstrained*
Training target	joint force	joint angle	joint angle
Wrist setup	fixed with handles	Free	wrist braces

3.2.2 Data Processing

As previously stated, the first objective was to reproduce the constrained and unconstrained experiments previously reported, to serve as a baseline for comparison with new methods investigated in this work. The EMG data were bandpass filtered using a third order Butterworth filter between 10-450 Hz, after which the time domain (TD) features (comprised of mean absolute value, zero crossings, slope signs changes and waveform length) were extracted using a 200 ms window length with an increment of 50 ms (this increment was used for offline analysis, but for real-time tests in next chapters, the increment rate was equal to the screen update rate). The EMG TD features have been shown to be effective in representing surface EMG for pattern recognition [73] and outperform the mean absolute value alone [8] in force estimation.

In the *unconstrained* experiments, the joint angles were calculated as follows [93], with respect to the resting position. In Figure 3.3, marker locations are shown using the points *M, L, P, Q, R,* and *U*. It was assumed that:

- Origin (*O*) is the midpoint between *P* and *Q*.
- *E* is the midpoint between *M* and *L*.
- *H* is the midpoint between *R* and *C*.
- *x*-axis is the line *O*-*E* pointing toward *O*.
- *y*-axis is the line perpendicular to the plane *P, Q, E* that passes through *O*, pointing posteriorly.
- *z*-axis is the cross product of *z* and *y* axes using the right hand rule.

The flexion-extension angle was computed as the angular displacement of the projection of the vector *O-H* on the plane *x-y* (with positive values used for flexion), and the abduction-adduction angle was calculated as the angular displacement of the projection of the vector *O-H* on the plane *x-z* (with positive values used for abduction). The pronation-supination angle was computed using the projections of the lines *P-Q* and *L-M* on a plane perpendicular to the line *O-E* (with positive values used for pronation).

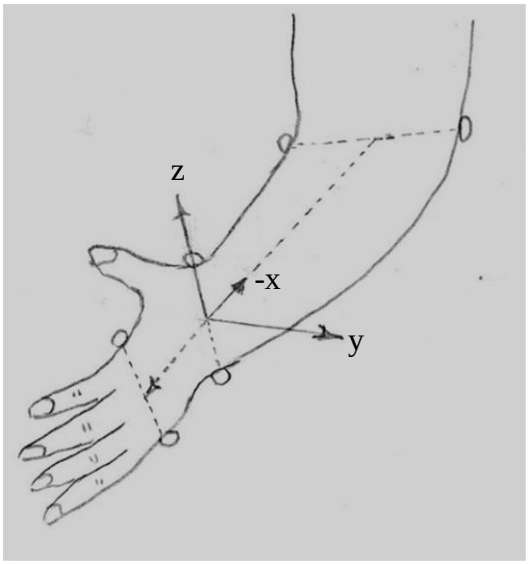

Figure 3.3. *Unconstrained* experiment; the marker locations and the *x, y* and *z* coordinates for calculation of the joint angles are shown.

The measured force and position were lowpass filtered using a third order Butterworth filter with a cutoff frequency of 1 Hz [131]. Subsequently, the average value of the force/position over the 200 ms window was used so as to match the time resolution of the EMG TD features.

For modeling the relationship between EMG and joint force/angle, multilayer perceptron feedforward artificial neural networks (ANN) were used. A separate ANN was used for

each DOF, as this was shown in pilot work to outperform a single ANN. For each limb, a separate set of ANNs was trained with the limb's EMG TD features as the inputs and the left limb force (*constrained* experiment) or joint angle (*unconstrained* experiments) as the target. The case in which the EMG and force/position were acquired from the same limb (*ipsilateral*) was expected to be the best case scenario for force/position mapping as it is not degraded by imperfections in the bilateral mirroring process. It should be noted that for applications such as prosthesis control, however, force/position would have to be acquired from the opposite (contralateral) limb.

A four-fold cross-validation procedure was used to evaluate the performance, where three out of four movement repetitions in each trial were used as the training set and the remaining repetition was used as the test set (training: 75%, testing: 25%). All data containing both static and dynamic segments were included. The training set was divided randomly into 80% training and 20% validation set. The ANN structure, which was determined empirically using the validation set, included one hidden layer of five neurons, with the hidden and output layers having tan-sigmoid and linear activation functions, respectively. Levenberg-Marquardt back-propagation was used as the ANN training method. The estimated output was lowpass filtered (cutoff = 1 Hz) to match the target frequency content. Figure 3.4 illustrates the training and testing procedure.

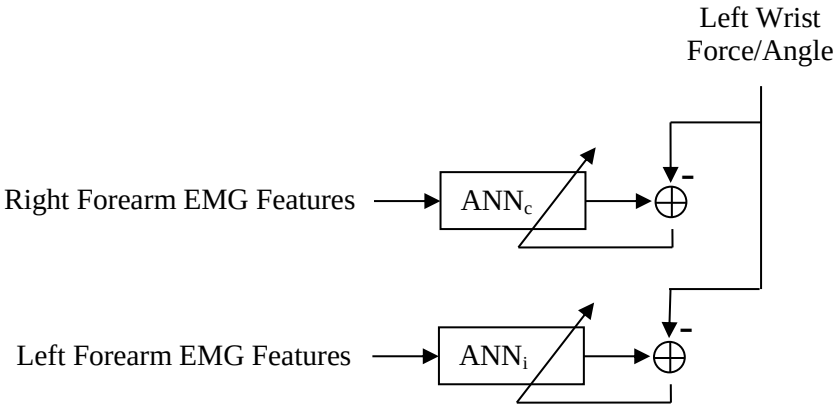

(a)

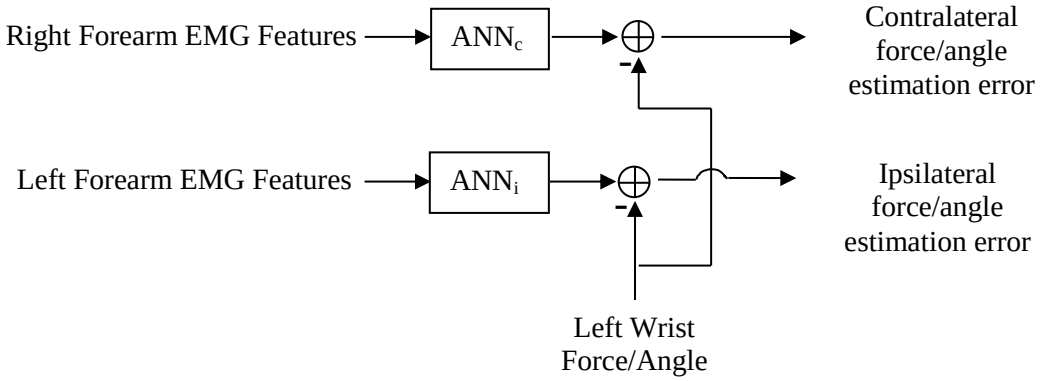

(b)

Figure 3.4. (a) Training: the contralateral and ipsilateral ANNs (ANN_c, ANN_i) were trained using the right and left arms EMG, respectively as the ANNs input and the left wrist joint force/angle as the target. (b) Testing: Using a new data set, the estimated output of ANN_c and ANN_i were compared with the corresponding left wrist joint force/angle to obtain the estimation accuracy.

3.2.3 Performance Metrics

The performance of each DOF was assessed using the widely used coefficient of determination (R^2) [71], [8], [94].

$$R_k^2 = 1 - \frac{\sum_{t=0}^{N}\left(\widehat{f_k(t)} - f_k(t)\right)^2}{\sum_{t=0}^{N}(f_k(t) - \overline{f_k(t)})^2} \tag{3.1}$$

where $f_k(t)$ is the force/angle of the k^{th} DOF, $\widehat{f_k(t)}$ is the corresponding estimate from the ANN, $\overline{f_k(t)}$ is the temporal average of $f_k(t)$, N is the number of data samples, and R_k^2 is the coefficient of determination of the k^{th} DOF.

The overall (mean across all DOFs) contralateral estimation accuracies (R^2) were compared between the three protocols (*isometric, unconstrained, resisted unconstrained*) using a one-way repeated-measures analysis of variance (ANOVA) test followed by a *Bonferroni* post-hoc test. Also for each DOF, the contralateral R^2 values were compared between the three protocols using the same tests. The significance level was set to 0.05.

3.3 Baseline Results

The estimated outputs for a representative subject in the *constrained, resisted unconstrained,* and *unconstrained* experiments (using EMG from the right limb) are plotted in Figure 3.5 (a), (b), (c) respectively. The results averaged across all subjects showed that the mean of all DOFs contralateral estimation accuracy (R^2) values were 89.7 ± 0.5 %, 89.5 ± 0.4 %, and 85.5 ± 0.9 %, for the *constrained, resisted unconstrained,* and *unconstrained* experiments, respectively (the corresponding values for the ipsilateral case were 91.2 ± 0.4 %, 90.7 ± 0.6 %, and 87.3 ± 0.7 %). As was expected, the performance of the ipsilateral case was higher than that of the contralateral case, and is consistent with the previous work [8].

Based on the results from all subjects, for the overall contralateral R^2, no significant difference was observed between the *constrained* and *resisted unconstrained* protocols (p>0.1), while the *constrained* overall R^2 was statistically higher (p=0.001) than that of the *unconstrained* protocol. This was expected because the EMG levels in the unconstrained experiment were lower than those of the constrained experiment, which resulted in lower estimation accuracy. The contralateral R^2 results in each DOF from all subjects using mean ± standard error are listed in Table 3.3. The statistical analysis results for the R^2 values of each DOF are listed in Table 3.4. The R^2 results showed that no significant difference (p>0.01) was found between the constrained and resisted unconstrained methods in any DOF. However, the constrained experiment outperformed the unconstrained experiment in the abduction-adduction (p=0.01) and pronation-supination (p=0.02), but no appreciable difference (p>0.01) was observed in flexion-extension.

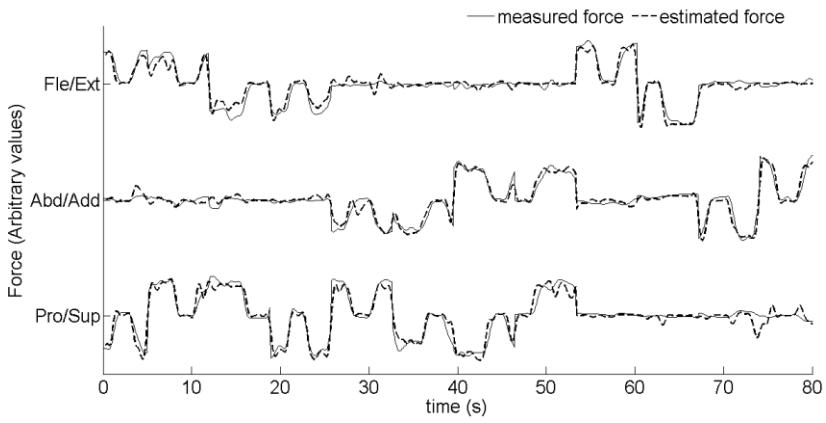

(a)

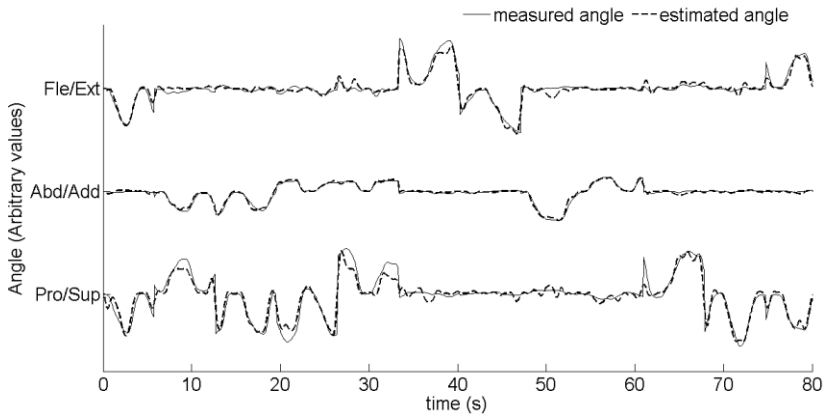

(b)

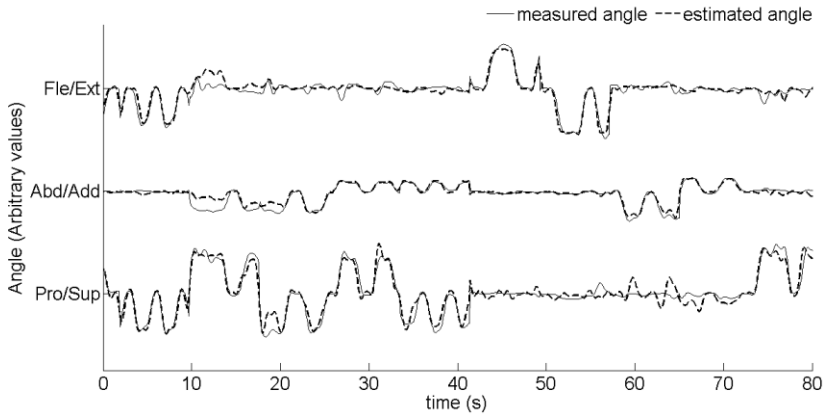

(c)

Figure 3.5. (a) *Constrained* experiment; the estimated and measured forces are plotted for a representative subject in the contralateral case. In this example the R^2 were 95.0% for flexion-extension, 93.0% for abduction, and 83.3% for pronation-supination. Medium force levels were used in the *constrained* experiment, (b) *Resisted unconstrained* experiment; the estimated and measured angles are plotted for a representative subject in the contralateral case. In this example the R^2 were 87.0% for flexion-extension, 87.6% for abduction, and 90.4% for pronation-supination. A comfortable full range of joint angles was used in this experiment, (c) *Unconstrained* experiment; the estimated and measured angles in each DOF are plotted for a representative subject in the contralateral case. In this example the R^2 were 84.9% for flexion-extension, 86.3% for abduction, and 87.5% for pronation-supination. A comfortable full range of joint angles was used in this experiment.

Table 3.3. The estimation accuracies R^2 (%) of each DOF for the contralateral case, averaged across all subjects, using mean ± standard error.

	Constrained (Force)	*Unconstrained (Position)*	*Resisted unconstrained (Position)*
Fle/Ext	89.8 ± 0.9	88.7 ± 0.9	89.3 ± 0.6
Abd/Add	90.8 ± 0.6	85.6 ± 1.6	90.3 ± 0.5
Pro/Sup	88.5 ± 0.9	82.3 ± 1.6	88.8 ± 1.2

Table 3.4. Statistical analysis results of the offline contralateral R^2 values of each DOF. Significant comparisons are marked with *.

	Constrained vs. Unconstrained	*Constrained vs. Resisted unconstrained*
Fle/Ext	$p>0.1$	$p>0.1$
Abd/Add	$p=0.01$*	$p>0.1$
Pro/Sup	$p=0.02$*	$p>0.1$

The results showed that the *constrained* and *unconstrained* experiments estimation accuracies (R^2) were comparable to those reported in previous studies [71], [94], [125].

The wrist braces in the *resisted constrained* protocol were used to increase the level of muscle activity during contractions. The wrist braces were selected such that the observed EMG levels were similar to those of the *constrained* experiment in the pilot work. This made it possible to make a more fair comparison between the *constrained* and *unconstrained* protocols. The overall R^2 in the *unconstrained* experiment was significantly lower than that of *constrained* experiment, while that of the *resisted constrained* protocol was not. As mentioned above, this may be due to the low level of effort (and EMG) with no external resistance which may reduce the usable information

content of the EMG signals at the surface. Using wrist braces in the *resisted constrained* experiment increased the EMG level, so that the estimation accuracies improved to a level similar to those of the *constrained* protocol. These results suggest that the *constrained* and *unconstrained* based myoelectric schemes exhibit similar performance when using similar EMG levels (loading conditions).

In a clinical scenario, the EMG levels produced by different amputees may be widely different, but they are expected to be less than those elicited by intact constrained limbs during this experiment. The amputee EMG levels are estimated to be around or slightly higher than those of intact unconstrained limb contractions, although greatly depends on the amputee.

3.4 Exploring Analytical Methods

In this section, the optimization of the existing methods and exploring novel analytical approaches are investigated.

3.4.1 Feature Set

As described in Section 3.2, in the baseline configuration, TD features were used. The analysis window length was set as 200 ms. However, employing other feature sets may improve the user intent estimation performance. Adding these features may enhance the intent estimation by adding extra information to the current feature set. A number of

well-known feature sets were investigated to determine the best configuration. The investigated feature sets are listed below.

1. The Mean absolute value, referred to as MAV.
2. The TD features.
3. The TD features combined with the Willison amplitude (described in [132]), referred to as TDWA.
4. The TD features combined with the root-mean square value and six autoregressive coefficients, as used in [75], referred to as TDAR.
5. The TD features combined with five wavelet marginals using discrete decomposition by the Daubechies wavelet, as used in [76], referred to as TDWV.
6. The TD features combined with median frequency (described in [132]), referred to as TDMF.

Figure 3.6 depicts the estimation accuracies using each feature set.

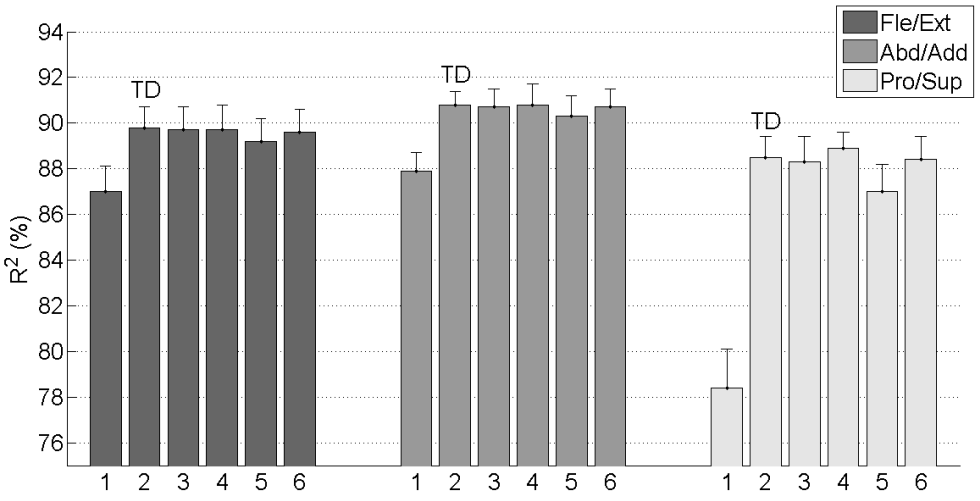
Fle/Ext
Abd/Add
Pro/Sup
R2 (%)
94
92
90
88
86
84
82
80
78
76
TD
TD
TD
1 2 3 4 5 6 1 2 3 4 5 6 1 2 3 4 5 6

(a)

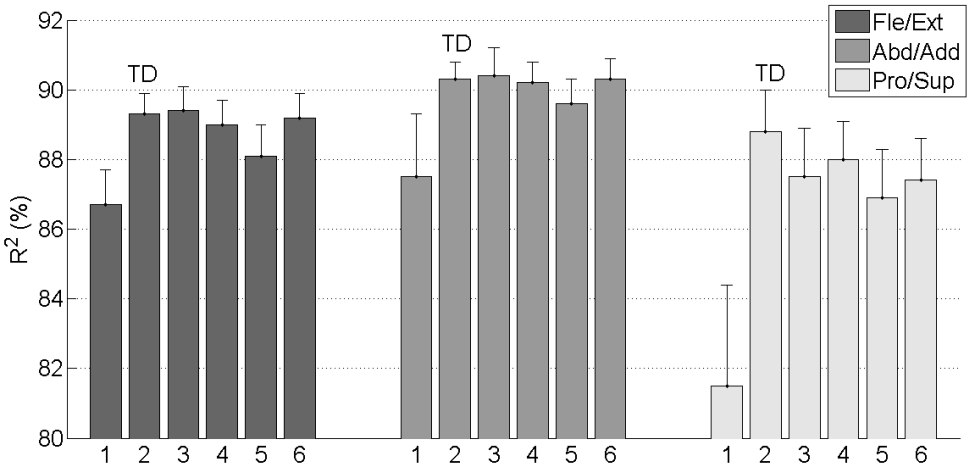
Fle/Ext
Abd/Add
Pro/Sup
R2 (%)
92
90
88
86
84
82
80
TD
TD
TD
1 2 3 4 5 6 1 2 3 4 5 6 1 2 3 4 5 6

(b)

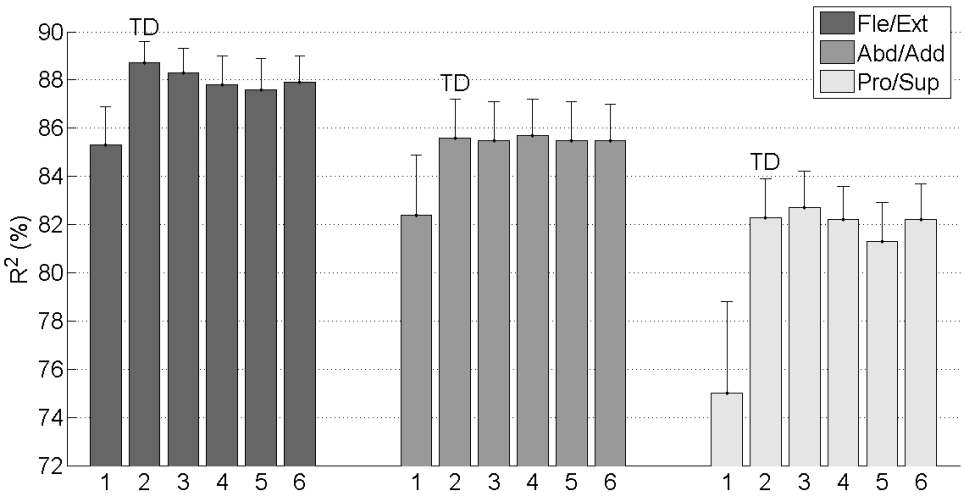

(c)

Figure 3.6. The estimation accuracies (R^2) averaged across all subjects using different feature sets in the (a) constrained, (b) resisted unconstrained, and (c) unconstrained experiments are plotted using mean ± standard error. Each feature set is shown using the representative number from the list above. The baseline case (TD features) is distinguished for comparison.

To compare the performances of the feature sets, a one way repeated measures ANOVA followed by a *Bonferroni* post hoc test was conducted for each experiment and DOF. In all cases, the MAV had lower performance (R^2) compared to other feature sets (p<0.05). However, the R^2 values were not appreciably different (p>0.1) between other feature sets including the TD, TDWA, TDAR, TDWV, and TDMF. Therefore, the TD feature set was chosen to represent EMG signals and was used for the rest of this thesis.

3.4.2 Estimators

As described in Section 3.2, multilayer perceptron ANNs were employed for the baseline configuration. ANNs are known for their ability to learn highly nonlinear modeling. In

this section, several estimators were investigated for modelling the relationship between EMG and joint force/kinematics. The results in each case were compared with those of the baseline estimator (ANNs). The motivation was to find the model with the highest estimation accuracy. The TD features were employed for EMG representation.

3.4.2.1 ANN Optimization

In this section, the effect of the multilayer perceptron ANNs number of hidden neurons on the estimation performance (R^2) is studied. The hidden and output layers had tan-sigmoid and linear activation functions, respectively, based upon optimization in previous work [8]. Levenberg-Marquardt back-propagation was used as the ANN training method. The effect on performance when varying the number of hidden layer neurons is shown in Figure 3.7.

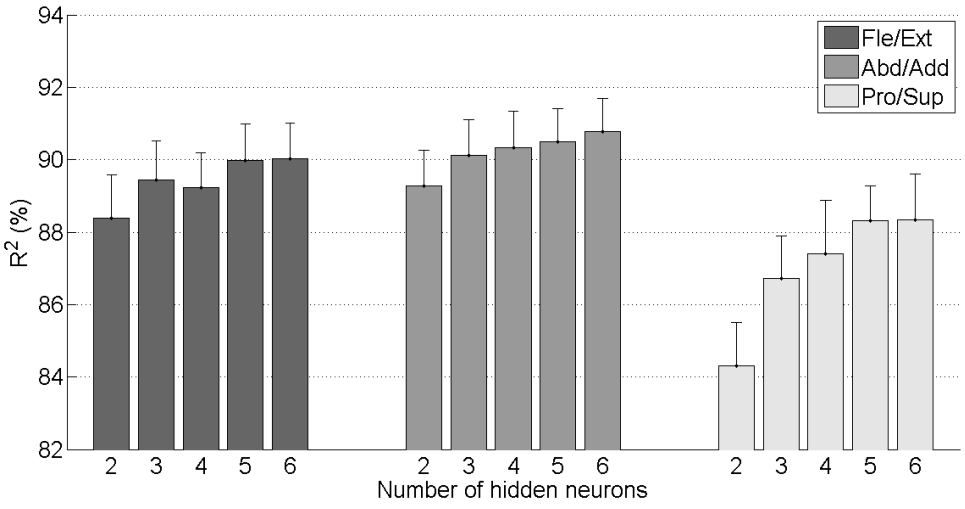

(a)

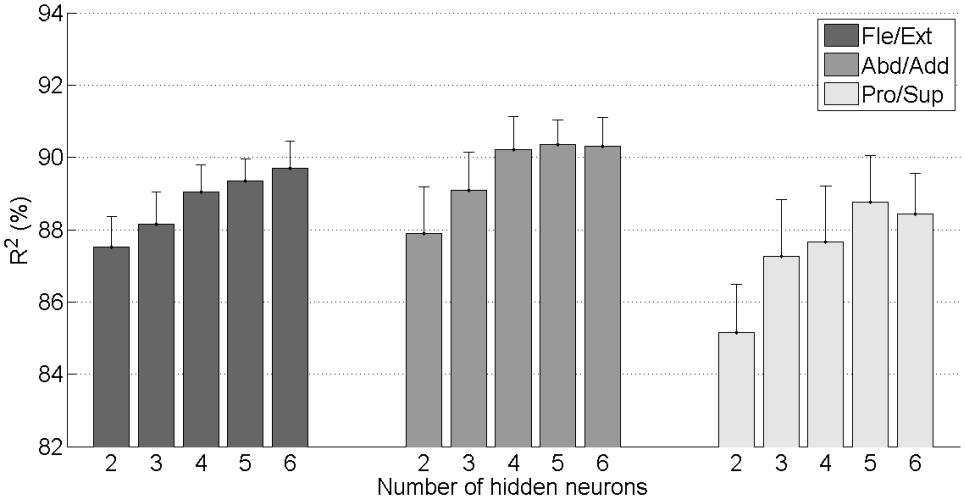

(b)

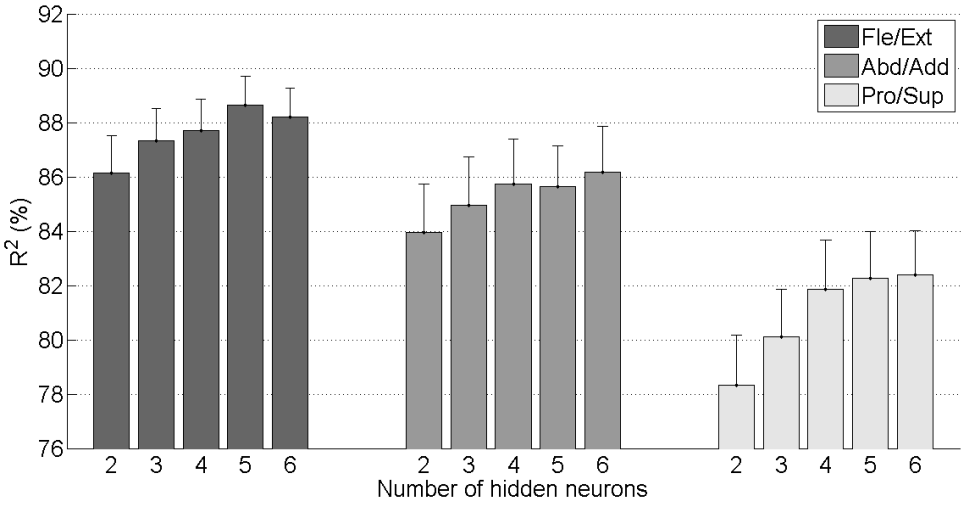

(c)

Figure 3.7. The effect of number of hidden neurons on the estimation accuracy is shown using mean ± standard error in the (a) *constrained*, (b) *resisted unconstrained*, and (c) *unconstrained* experiments.

Based on the results, increasing the number of hidden neurons greater than five did not cause performance improvement (p>0.1). Therefore, the number of neurons was set as five to avoid overfitting.

Also, the performance using a single ANN (with three outputs) estimating all three DOFs, was compared to that of using three ANNs with one output (one ANN for each DOF). Figure 3.8 shows the R^2 values for one vs. three ANNs. For all DOFs, the R^2 of three ANNs were higher than those of a single ANNs (p<0.05). The p-values are listed in Table 3.5.

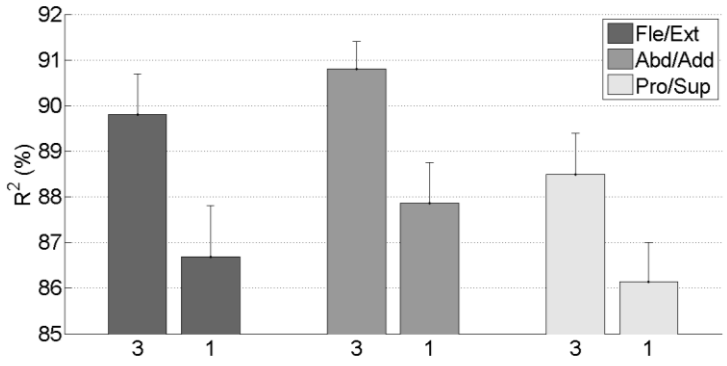

(a)

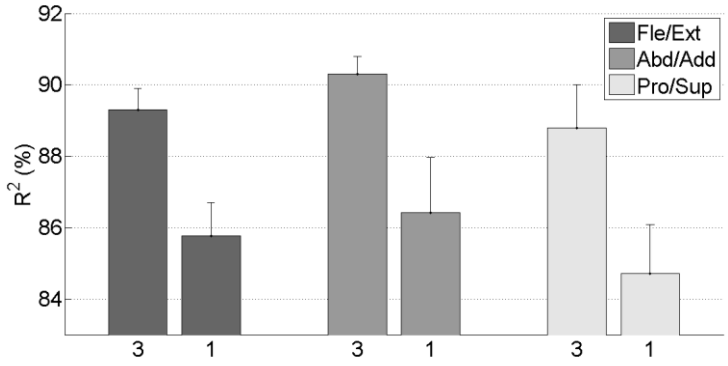

(b)

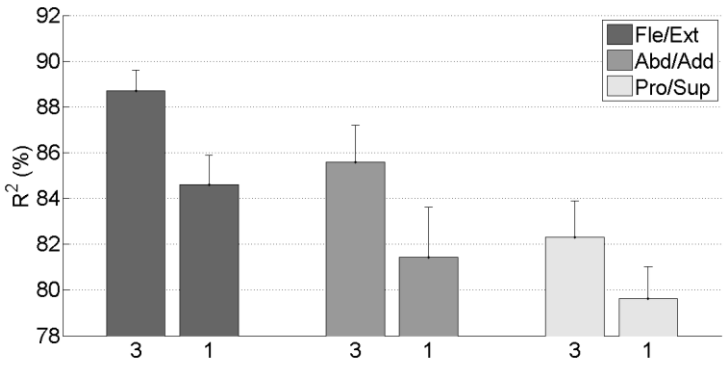

(c)

Figure 3.8. The estimation accuracies (R^2) using one vs. three ANNs are shown using mean ± standard error in the (a) *constrained*, (b) *resisted unconstrained*, and (c) *unconstrained* experiments.

Table 3.5. The *p*-values for comparison of one vs. three ANNs.

	Constrained	*Resisted unconstrained*	*Unconstrained*
Fle/Ext	$p<0.001$*	$p<0.001$*	*$p<0.001$**
Abd/Add	$P<0.001$*	$p=0.04$*	$P=0.003$*
Pro/Sup	$P=0.001$*	$p<0.001$*	*$p<0.001$**

Moreover, to achieve possible improvements, applying two ANNs for each DOF (1 ANN for each direction, or six ANNs for three DOFs) was compared to that of one ANN for each DOF (three ANNs for three DOFs). Figure 3.9 illustrates the results for one vs. two ANNs for each DOF (the results of both one and two ANNs cases were compared using one fold of the four-fold cross validation to reduce the processing time).

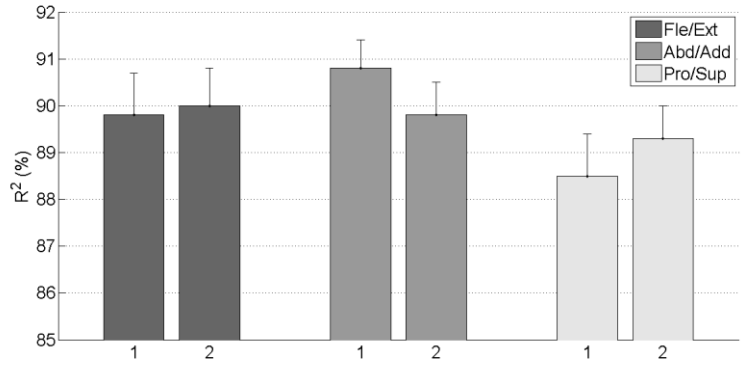

(a)

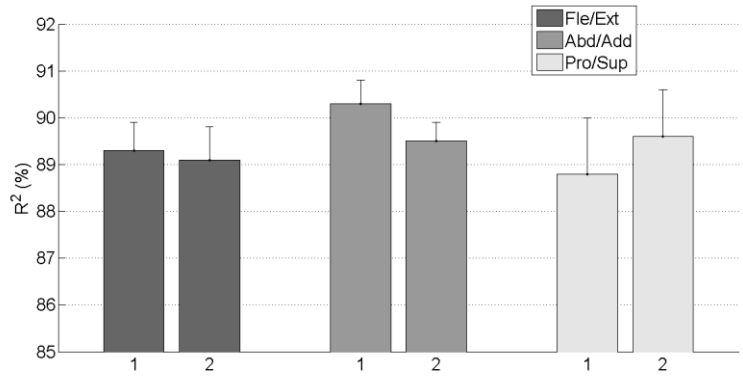

(b)

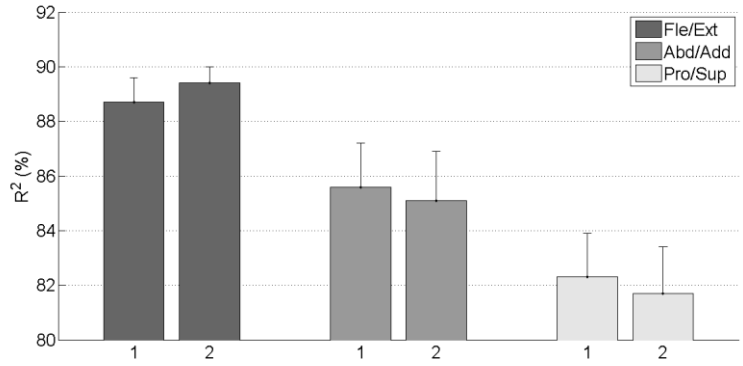

(c)

Figure 3.9. The estimation accuracies (R^2) using one vs. two ANNs for each DOF are shown using mean ± standard error in the (a) *constrained*, (b) *resisted unconstrained*, and (c) *unconstrained* experiments.

Based on the results for each experiment, using two ANNs in each DOF did not significantly change the estimation accuracy (p>0.1).

3.4.2.2 Polynomial Estimator

The relationship between EMG and joint force/angle may be estimated using polynomial models. The first order polynomial model is a linear estimator and can be formulated as

$$f = A_1 \times X + a_0 \tag{3.2}$$

where f is the force/angle, and X is the EMG feature vector. The coefficient matrix A_1 and a_0 are the model constants. The second order polynomial model is written as:

$$f = A_2 \times X^2 + A_1 \times X + a_0 \tag{3.3}$$

Similarly, the nth order polynomial model can be written as:

$$f = \sum_{i=1}^{N} A_i \times X^i + a_0 \tag{3.4}$$

The coefficients A_i and a_0 can be estimated using an iterative least squares approach. The R^2 results using the first to the fourth order polynomial models are plotted in Figure 3.10. The ANNs estimation accuracy is also shown for comparison.

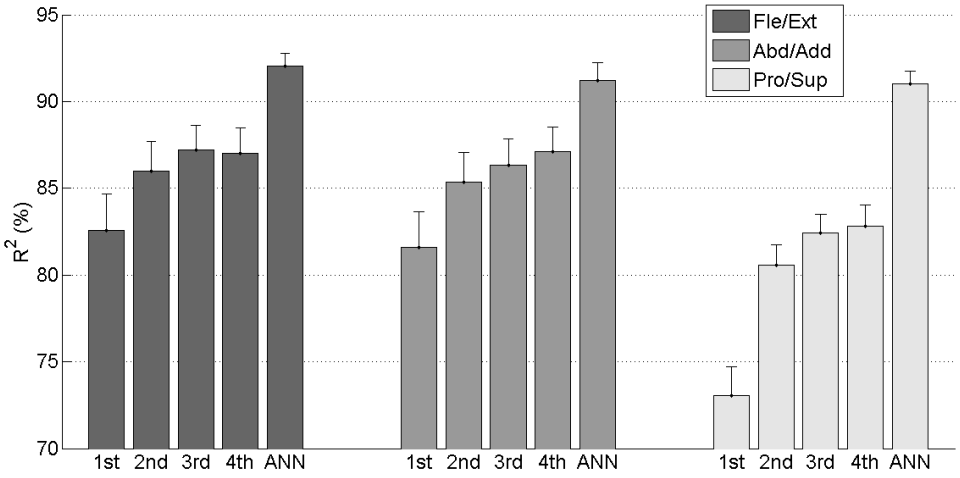
Fle/Ext
Abd/Add
Pro/Sup
R^2 (%)
95
90
85
80
75
70
1st 2nd 3rd 4th ANN
1st 2nd 3rd 4th ANN
1st 2nd 3rd 4th ANN

(a)

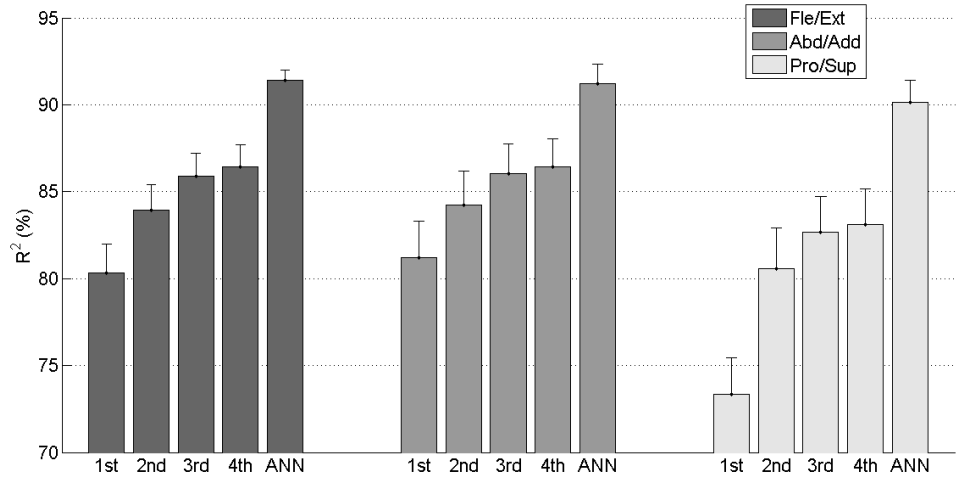
Fle/Ext
Abd/Add
Pro/Sup
R^2 (%)
95
90
85
80
75
70
1st 2nd 3rd 4th ANN
1st 2nd 3rd 4th ANN
1st 2nd 3rd 4th ANN

(b)

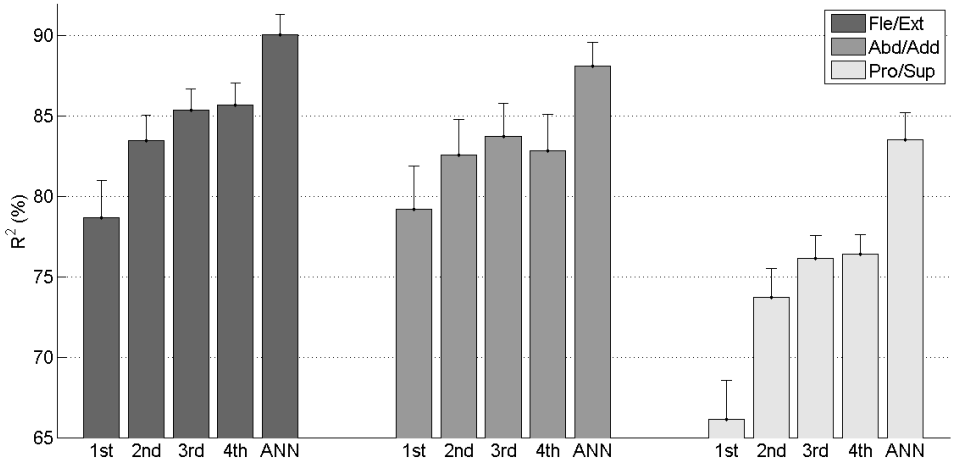

(c)

Figure 3.10. The estimation accuracies (R^2) using the first, second, third, and fourth order polynomial models, and a comparison with the ANN in the (a) *constrained*, (b) *resisted unconstrained*, and (c) *unconstrained* experiments, are shown using mean ± standard error.

The results show that the polynomial model performance was inferior to that of the ANNs in each DOF (p<0.001) in each experiment. This shows that the nonlinear hidden layer nodes allowed the ANN to outperform the polynomial models in capturing the system nonlinearities. However, an advantage of the polynomial models is that the estimation of a test sample is performed more than 100 times faster than that of ANN, which may be useful in real-time implementations.

3.4.2.3 Time-delayed ANN

Time-delayed networks are dynamic networks that are similar to feedforward networks, except that a tap delay line is associated with the input weight. The time-delayed network

was investigated to determine if including previous input data improves the estimation performance. Figure 3.11 depicts the estimation accuracies (R^2) for the time-delayed networks. A delay of *N* samples corresponds to the inclusion of the last *N* samples as the inputs. The distance between samples is equal to the increment rate (50ms).

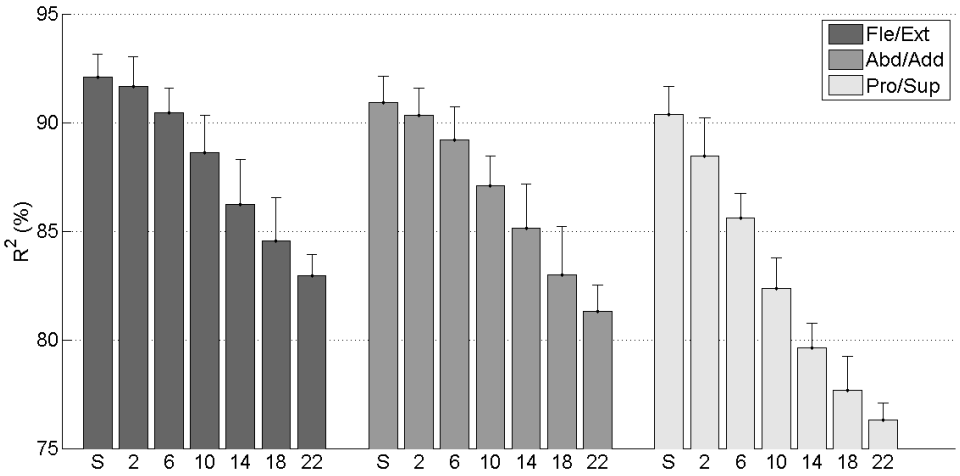

(a)

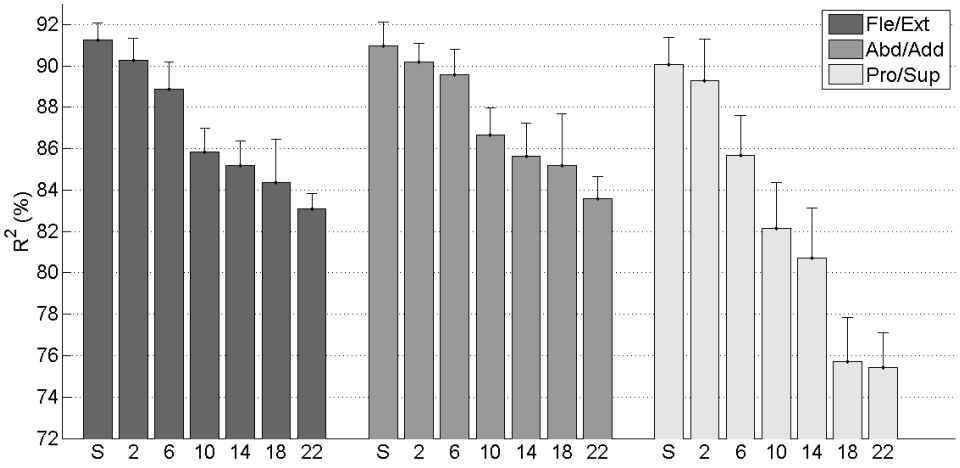

(b)

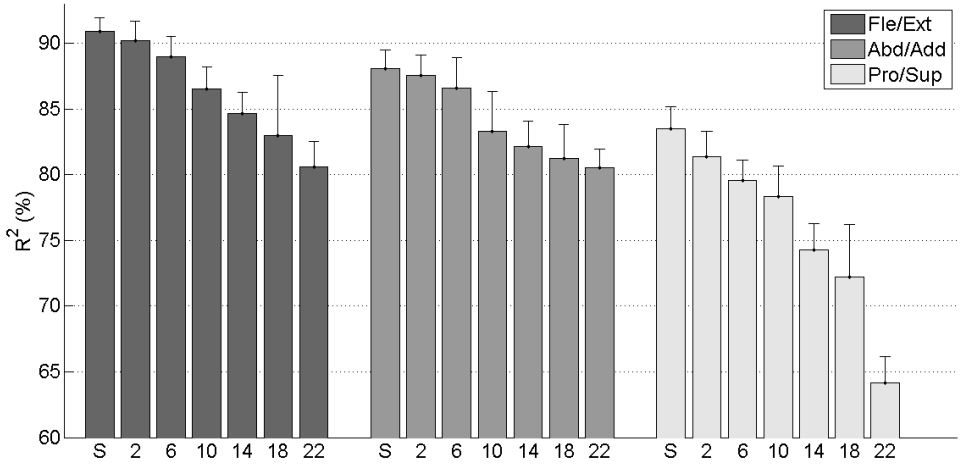

(c)

Figure 3.11. The estimation accuracies (R^2) using time delayed ANNs, and comparison with the static ANN in the (a) *constrained*, (b) *resisted unconstrained*, and (c) *unconstrained* experiments. The results are shown using mean ± standard error. The numbers on the *x*-axis for each bar represents the number of delayed samples, and *S* represents the static ANN.

As shown in the plots above, adding delayed inputs reduced the estimation performance in comparison with the static networks. This suggests that the system is memoryless as increasing the input delay reduced the R^2. This is because the EMG patterns' relevance to the target (joint force/angle) diminishes with increasing the EMG delay. Also, with increasing delay, the percentage of the useful data (the non-delayed input) in all input data reduces.

3.4.2.4 Radial Basis Function ANN

To achieve possible estimation improvements by changing the estimator, an alternative neural network model, radial basis function network, was also investigated. Radial basis

function (RBF) networks are artificial neural networks that use a radial basis function (Equation (3.5)) as the activation function.

$$\rho(n) = e^{-n^2} \tag{3.5}$$

Radial basis function networks have three layers including an input layer, a hidden layer with an RBF activation function, and a linear output layer. The network output is a linear combination of radial basis functions of the inputs and neuron parameters.

The estimation accuracies using RBF networks are plotted in Figure 3.12. For comparison, the multilayer perceptron ANNs results are also shown. As described earlier the baseline multilayer perceptron ANNs had one hidden layer of five neurons, with the hidden and output layers having tan-sigmoid and linear activation functions, respectively. Levenberg-Marquardt back-propagation was used as with the multilayer perceptron ANNs training method.

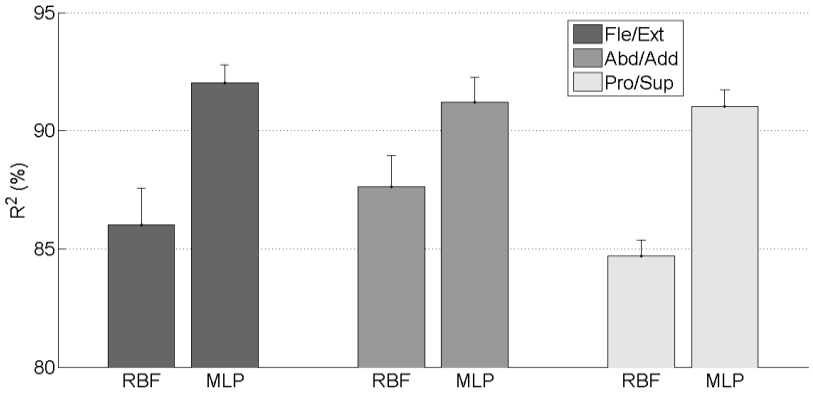

(a)

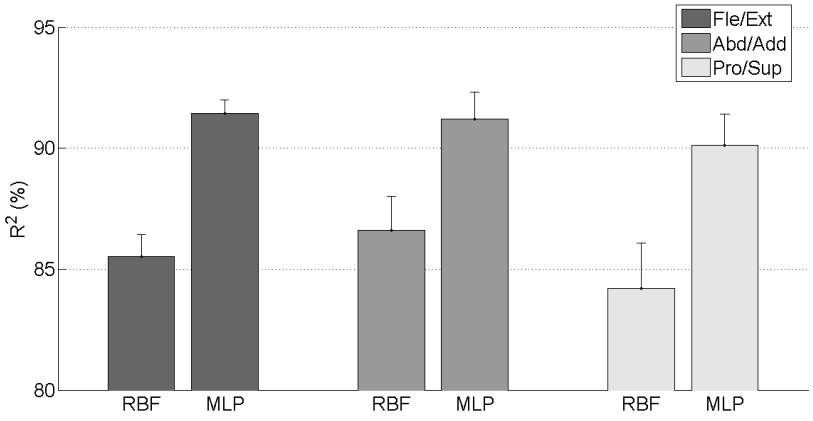

(b)

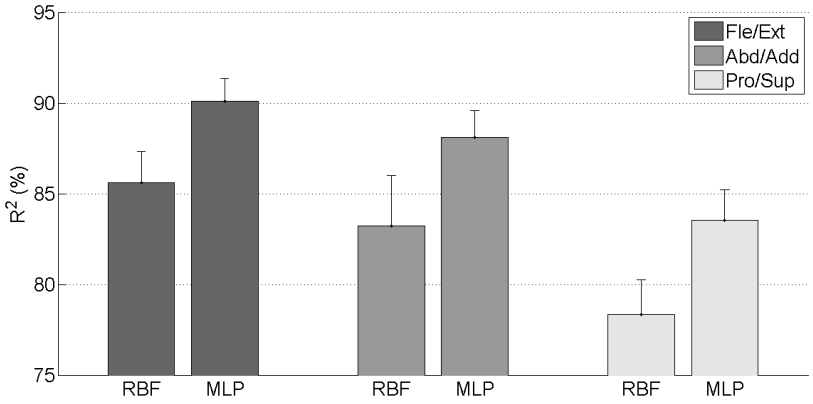

(c)

Figure 3.12. The estimation accuracies using radial basis function networks in the (a) *constrained*, (b) *resisted unconstrained*, and (c) *unconstrained* experiments. For comparison, the results of the multilayer perceptron ANNs are also plotted. The results are shown using mean ± standard error.

As seen in the results above, the MLP outperformed the RBF networks in all experiments and DOFs (p<0.05). It should also be noted that the RBF networks processing time for the training was significantly longer than that of the MLP.

3.4.2.5 Ensemble of Bagged Decision Trees

Although ensembles of bagged trees have been used in other areas (e.g. [133],[134]), their application in myoelectric signal estimation is, to our knowledge, novel. A decision tree is a supervised learning method which creates an estimation model based on a multivariate input [135]. To estimate a response, the decisions in the tree from the root (beginning) node down to a leaf node are followed. The leaf node contains the estimated outcome. Each step in estimation involves checking the value of one input variable and asking a binary question which splits the node into two child nodes. Figure 3.13 illustrates a simple decision tree.

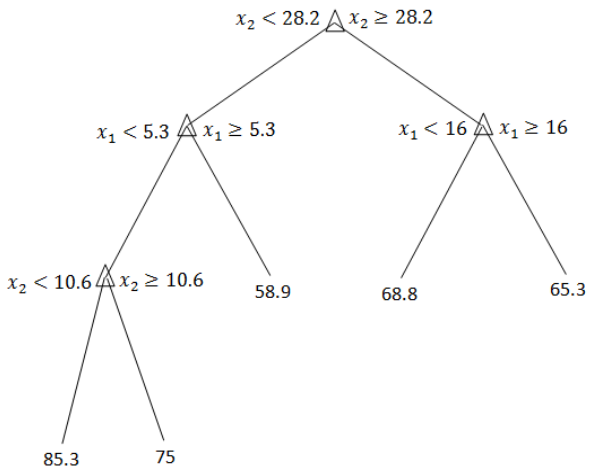

Figure 3.13. An example of a regression decision tree with two inputs (x_1 and x_2)

To create a decision tree, starting with input data, all possible binary splits on every input variable are examined. Then a split with best optimization criterion is selected and the split is imposed. This procedure is repeated recursively for the two child nodes. The

splitting is stopped when the node is *pure*, (a node is pure if the mean squared error (MSE) for the observed response in this node drops below a desired threshold). A split is chosen to minimize the MSE of estimations.

Several decision trees can be combined in a process called ensemble learning to generate a more robust estimator. Decision trees are typically combined using *bootstrapping aggregating* (*bagging*) approach [136] to form a stronger estimator. *Bagging* trains multiple (*m*) models on different samples (data splits) and creates an estimate by averaging the results of *m* models (Figure 3.14). Given a training set of *n* observations, *bagging* generates *m* new training sets by selecting *n* out of *n* samples uniformly with replacement from the original training set. It can be shown that with large *n*, each set will contain $(1-^{1}/e) = 63.2\%$ of the unique examples and the rest are replicates. In other words, around 37% of the training samples will be left out from a single set. Each model is fitted using its own data set (bootstrap set). For testing, the models are combined by averaging the output. In general, *bagging* decreases error by decreasing the variance in the results due to unstable learners such as decision trees whose output can change significantly when the training data is slightly changed [136].

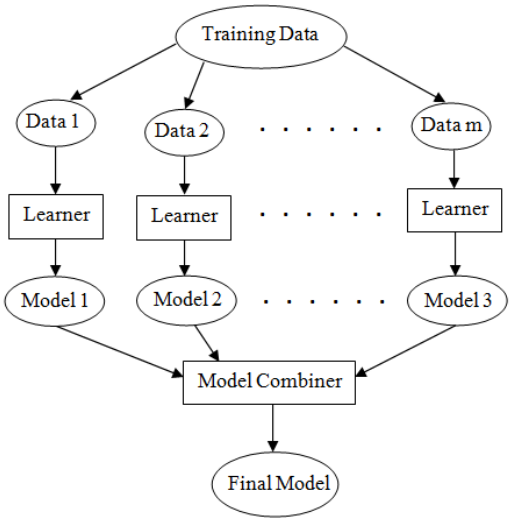

Figure 3.14. The *Bagging* training procedure; multiple models (usually with the same type of learner) are trained using different training sets. For testing, the final output is obtained by averaging all models outputs.

To map the EMG TD features to force/position using *bagged trees* modeling, a separate ensemble for each DOF was used. Figure 3.15 illustrates the estimation results using different numbers of trees in each ensemble. The results of ANNs are also shown for comparison. It should be noted that one of the advantages of the *bagging* method is that increasing the ensemble size does not cause over-fitting [136].

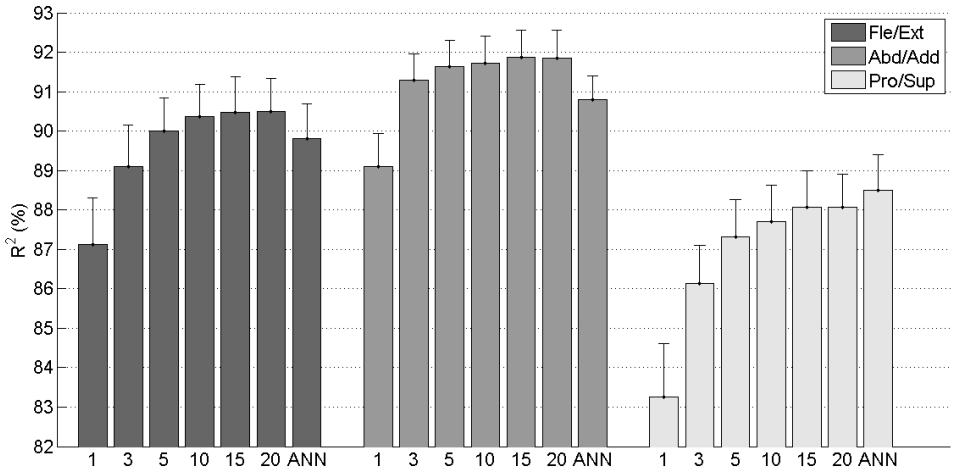
Fle/Ext
Abd/Add
Pro/Sup
R2 (%)
93
92
91
90
89
88
87
86
85
84
83
82
1 3 5 10 15 20 ANN 1 3 5 10 15 20 ANN 1 3 5 10 15 20 ANN

(a)

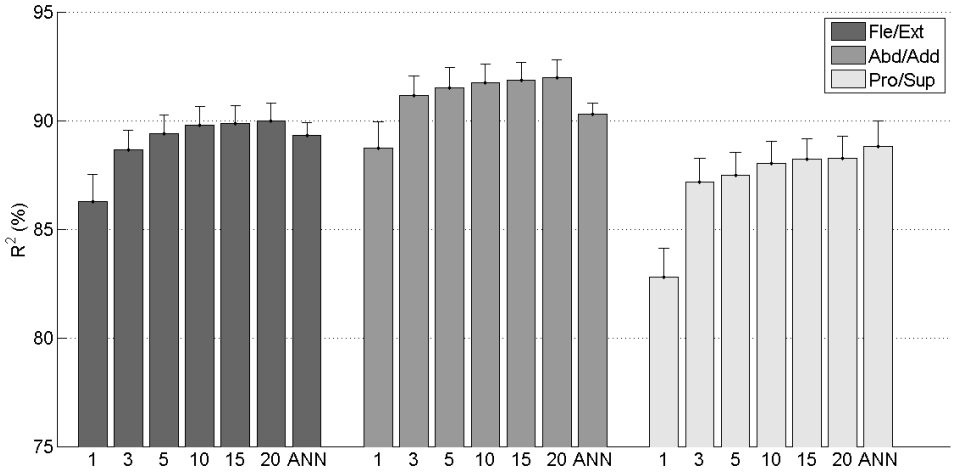
Fle/Ext
Abd/Add
Pro/Sup
R2 (%)
95
90
85
80
75
1 3 5 10 15 20 ANN 1 3 5 10 15 20 ANN 1 3 5 10 15 20 ANN

(b)

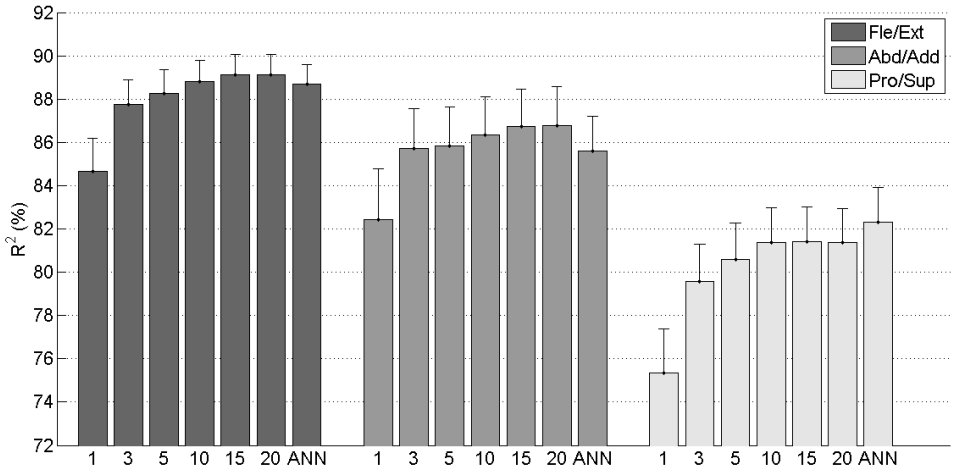

(c)

Figure 3.15. The effect of ensemble size on the estimation accuracies (R^2) of *bagged trees* in the (a) *constrained*, (b) *resisted unconstrained*, and (c) *unconstrained* experiments. The ANNs results are also plotted for comparison. The results are shown using mean ± standard error

When using five trees in each ensemble, one-way repeated-measures ANOVA tests showed that for each DOF and each experiment, the R^2 results were not statistically different (p>0.1) between bagged trees and those of the ANNs (except that in the *resisted unconstrained* experiment in abduction-adduction, bagged trees outperformed ANNs with p=0.01). When using ensemble sizes of more than five trees (more than ten trees in case of *unconstrained* experiment), bagged trees outperformed ANNs in abduction-adduction (p<0.05). An advantage of *bagged trees* over ANNs is its lower processing time. When using ensembles of five trees, the estimation processing time of a test sample using bagged trees (each DOF: 6 ms) was approximately one third of that of the ANNs (each DOF: 20 ms) for the computer used in this work.

3.4.2.6 Support Vector Machine

SVMs, first introduced by Vapnik and colleagues [137],[138] are supervised learning algorithms that can be used for both classification and regression. Assuming a set of training data, $\{(\boldsymbol{x_1}, y_1), \ldots, (\boldsymbol{x_n}, y_n)\}$, where each $\boldsymbol{x_i} \in R^N$, and $y_i \in R$, and n is the number of training examples, the goal is to find a regression function $f(\boldsymbol{x})$ that has at most a deviation of ε from the target (y) for all training data. Since choosing appropriate ε may be difficult, v-SVM was proposed in 1999 [139] for both classification and regression. With this method, an intuitive tunable parameter $0<v<1$ is employed which gives a lower bound on the fraction of support vectors and an upper bound on the fraction of margin errors. For support vector regression (SVR), the input data ($\boldsymbol{x}$) is mapped to a higher dimension space by performing a nonlinear projection, in order to linearly estimate the regression function $f(\boldsymbol{x})$ from

$$f(\boldsymbol{x}) = \boldsymbol{w^T}\Phi(\boldsymbol{x}) + b \tag{3.6}$$

where $\Phi(\boldsymbol{x})$ is the nonlinear projection of the input data to the high dimensional feature space. SVR seeks the flattest function in the high dimensional space, or equivalently a small $\boldsymbol{w}$ in Eq. (1), which is ensured by minimizing the norm, i.e. $\| \boldsymbol{w} \|^2$. By constructing a Lagrange function and solving a quadratic programming problem, $f(\boldsymbol{x})$ can be written in the following final form.

$$f(\boldsymbol{x}) = \sum_{i=1}^{n} \{(\alpha_i - \hat{\alpha}_i) K(\boldsymbol{x_i}, \boldsymbol{x}) + b\} \tag{3.7}$$

where $K(\boldsymbol{x_i}, \boldsymbol{x})$ is a kernel function that replaces the product $\Phi^T(\boldsymbol{x_i})\Phi(\boldsymbol{x})$, and enables using low dimensional space data without knowing the transformation. The coefficients

$\alpha_i, \hat{\alpha}_i$ are Lagrange multipliers, and b is the bias constant that is determined using Karush–Kuhn–Tucker (KKT) conditions [140],[141]. The radial basis function is typically used as the kernel for regression.

$$K(\boldsymbol{x_i}, \boldsymbol{x}) = exp(\frac{\| \boldsymbol{x_i} - \boldsymbol{x} \|^2}{2\sigma^2}) \tag{3.8}$$

For all training examples that $|f(\boldsymbol{x_i}) - y_i| < \varepsilon$, the Lagrange multipliers $\alpha_i, \hat{\alpha}_i$ are equal to zero. Only for training data that $|f(\boldsymbol{x_i}) - y_i| \geq \varepsilon$, the Lagrange multipliers may be nonzero. The examples with nonzero coefficients are called *support vectors* and contribute in the regression function $f(\boldsymbol{x})$. Detailed descriptions of ν-SVR algorithm are provided in [142],[143].

In this work, ν-support vector regression (ν-SVR) was employed for modeling the relationship between the EMG TD features and wrist force/angle data. A separate SVM was used for each DOF. The SVM configuration was determined empirically and consisted of a radial basis function kernel type, a ν of 0.5, cost of 0.2, and kernel function degree of 3. The libsvm Matlab package [144] was used for simulation. SVM estimators are sensitive to training data scaling [145], therefor, each feature (attribute) of the training data must be normalized, so that all features have the same scaling. The normalization coefficients were saved and applied to new test data. The estimation results using the SVMs are depicted in Figure 3.16. The baseline estimator (ANNs) results are also plotted for comparison.

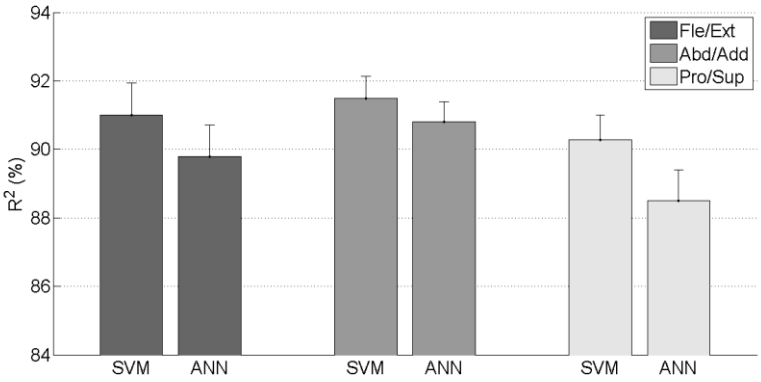

(a) ***Constrained***

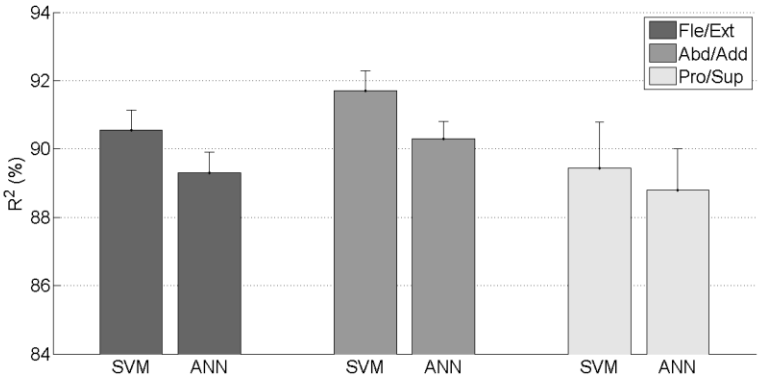

(b) ***Resisted unconstrained***

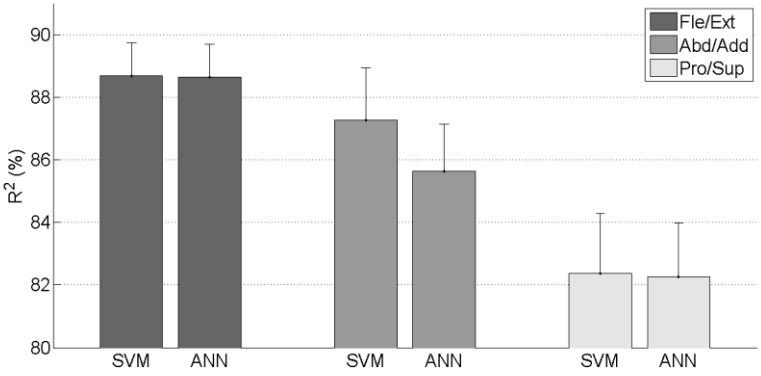

(c) ***Unconstrained***

Figure 3.16. The estimation accuracy (R^2) results for SVM and ANN averaged across all subjects are shown using mean ± standard error in (a) ***constrained,*** **(b)** ***resisted unconstrained*** **(c)** ***unconstrained*** **experiments.**

The R^2 results were compared between the SVM and ANN in each protocol. In the *constrained* experiment, the SVM outperformed the ANN in flexion-extension (p=0.006) and pronation-supination (p=0.01), but no difference between the SVM and ANN was observed in abduction-adduction (p>0.1). In the *resisted unconstrained* experiment, the SVM outperformed the ANN in flexion-extension (p<0.001) and abduction-adduction (p=0.003), but no difference between the two estimators was found in pronation-supination (p>0.1). In the *unconstrained* experiment, the SVM results were higher than those of the ANN in abduction-adduction (p=0.003), but no difference between the two estimators was found in flexion-extension (p>0.1) and pronation-supination (p>0.1).

The processing time of the SVM was significantly lower than that of the ANN in both training and testing. The average processing time (using a Dell Optiplex 185 990 workstation with a 3.30 GHz Intel processor) for estimation (one DOF) of one sample using the SVM was 2 ms, while 20 ms was taken with the ANN.

When using the SVM, a comparison between the R^2 values of the three protocols (*constrained*, *resisted unconstrained*, and *unconstrained*) was also conducted. A one-way repeated measures ANOVA followed by a *Bonferoni* post-hoc test was used. No significant difference was found between the R^2 of the *constrained* and *resisted unconstrained* experiments in any DOF (p>0.1 in all cases). The R^2 value of the *constrained* method was found to be significantly better than that of the *unconstrained* method for the abduction-adduction (p=0.04) and pronation-supination DOF (p=0.006), but no significant difference was found in the flexion-extension DOF (p>0.1). These results are consistent with those obtained using the ANN.

Also, the R^2 results of the SVM were compared to those of the bagged trees (with ten trees in each ensemble). In the constrained experiment, the SVM outperformed the bagged trees in flexion-extension (p=0.01) and in pronation-supination (p=0.003), while no significant difference was found in abduction-adduction (p>0.1). In the resisted unconstrained experiment, the SVM outperformed the bagged trees in pronation-supination (p=0.03), while no significant difference was found between the SVM and bagged trees in flexion-extension (p=0.07) and abduction-adduction (p>0.1). In the unconstrained experiment, the SVM outperformed the bagged trees in abduction-adduction (p=0.007), but no appreciable difference was found between them in flexion-extension (p>0.1) and pronation-supination (p>0.1). Also, the processing time of the SVM was faster than that of the bagged trees. The estimation of one sample for each DOF using SVM was 2 ms, while it was 10 ms for bagged trees (with size of 10).

3.4.3 Feature Projection

Feature projection methods map the data to a new (usually lower dimensionality) space. It is hypothesized that some projection methods may eliminate spurious information and, in a lower-dimensional feature space, provide improved estimation performance. Previous work [86] has demonstrated that a lower dimensional feature space may make the relationship between EMG and the corresponding force/angle simpler, and consequently enhance the estimation accuracy. To investigate this possibility, this section describes the effect of feature projection on the estimation accuracy. Previously used

principal components analysis [8] and non-negative matrix factorization [100] and a novel method of canonical correlation analysis were investigated.

3.4.3.1 Principal Component Analysis (PCA)

Principal component analysis (PCA) is a linear transformation that converts a set of possibly correlated variables into a set of linearly uncorrelated (orthogonal) variables. The first principal component has the largest possible variance, accounting for as much of the variability in the data as possible, and each subsequent component has the highest possible variance with the constraint that it must be uncorrelated to the previous components. The goal of PCA is to decrease the dimensionality of the data while describing as much of the variance of the original dataset as possible.

Assuming $X \in R^{m \times N}$ represents the data sample set, where m is the total number of variables and N is the total number of observations (samples), first each variable is subtracted by its mean and then the $m \times m$ covariance matrix is computed. The principal components S are given in terms of unit-length eigenvectors of C_x, where the projection matrix (W) contain the eigenvectors ($e_1 ... e_m$).

$$S = W \times X \tag{3.9}$$

Dimensionality reduction is performed by selecting a subset consisting of the larger principal components. Figure 3.17 illustrates the effect of PCA feature projection on the estimation performance.

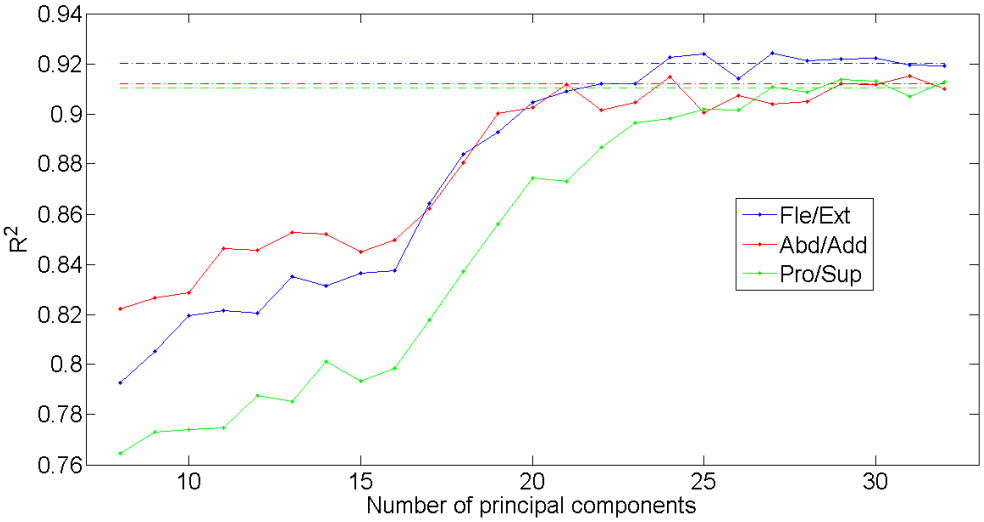
0.94
0.92
0.9
0.88
0.86
0.84
0.82
0.8
0.78
0.76
R2
10
15
20
25
30
Number of principal components
Fle/Ext
Abd/Add
Pro/Sup

(a)

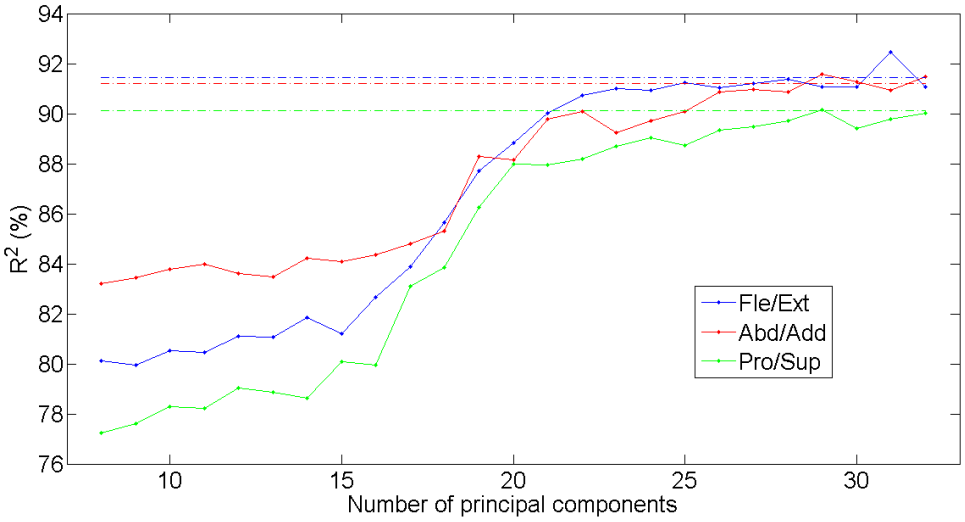
94
92
90
88
86
84
82
80
78
76
R2 (%)
10
15
20
25
30
Number of principal components
Fle/Ext
Abd/Add
Pro/Sup

(b)

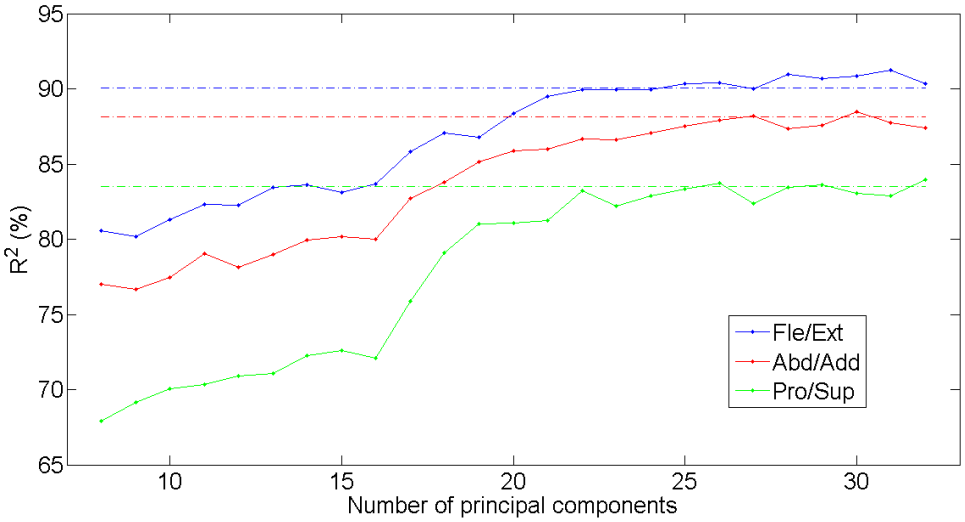

(c)

Figure 3.17. The effect of dimensionality reduction using PCA on the R^2 values in the (a) *constrained*, (b) *resisted unconstrained*, and (c) *unconstrained* experiments. The original feature set results are shown using dashed lines.

Based on the results, using equal to or greater than 21, 24, and 24 principal components in the constrained, resisted unconstrained, and unconstrained experiments, respectively, the R^2 values in each DOF were not different (p>0.1) than those of the original feature set.

3.4.3.2 Non-Negative Matrix Factorization (NNMF)

Non-negative matrix factorization (NNMF) is a group of algorithms in multivariate analysis and linear algebra that decompose a nonnegative data matrix as the product of two matrices with only nonnegative elements. In general, NNMF results in a dimensionally reduced representation of the original data, and therefore can be used for dimensionality reduction purposes.

Let's assume the nonnegative matrix $X \in R^{m \times N}$ represents the data sample set, where m is the total number of variables and N is the total number of samples. Let k denote the dimension of the desired dimension reduced projection space, the task of data factorization is to derive a nonnegative basis matrix $W \in R^{m \times k}$ and a nonnegative encoding coefficient matrix $H \in R^{k \times N}$ (reduced dimension matrix) such that the data matrix X can be approximated as the product of these two matrices.

$$X \approx W \times H \tag{3.10}$$

Letting y denote the original vector of the new testing sample and h_y represent the encoding coefficient vector to derive, each testing observation y is projected into the linear space spanned by the column vectors of the basis matrix W. A method widely used by previous works [146]-[148] uses the pseudo-inverse of matrix W to reconstruct the projection of the test data, namely,

$$h_y \approx W^{\dagger} \times y \tag{3.11}$$

where $W^{\dagger}$ indicates the pseudo-inverse of matrix W.

Since the TD features are nonnegative, NNMF can be applied for the feature projection. Figure 3.18 depicts the effect of NNMF feature projection using different reduced dimensions of the projected space on the estimation performance.

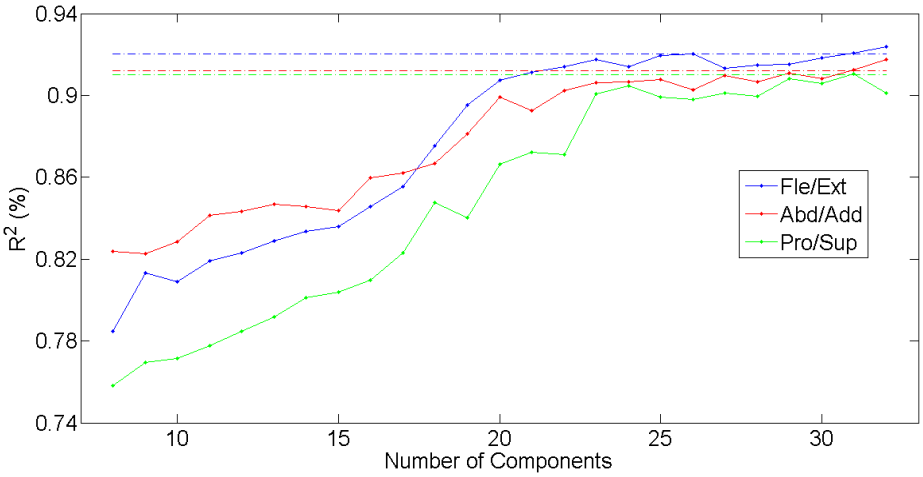
0.94
0.9
0.86
0.82
0.78
0.74
R2 (%)
10
15
20
25
30
Number of Components
Fle/Ext
Abd/Add
Pro/Sup

(a)

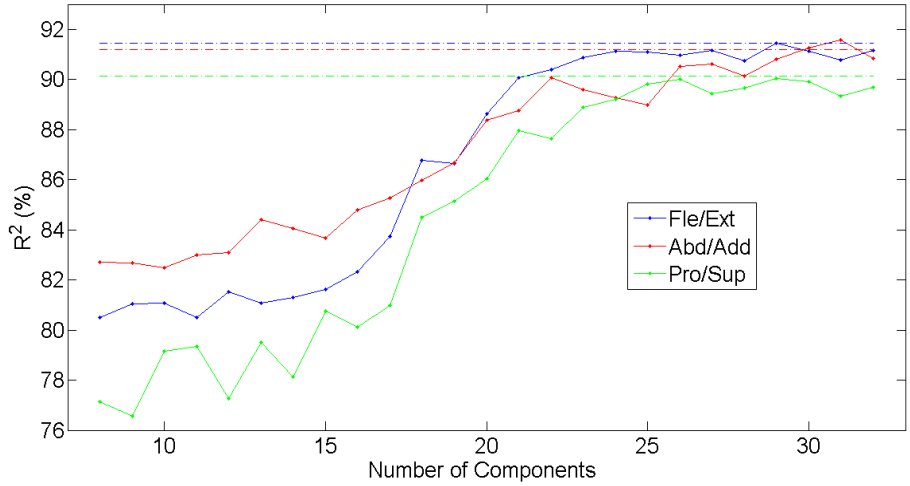
92
90
88
86
84
82
80
78
76
R2 (%)
10
15
20
25
30
Number of Components
Fle/Ext
Abd/Add
Pro/Sup

(b)

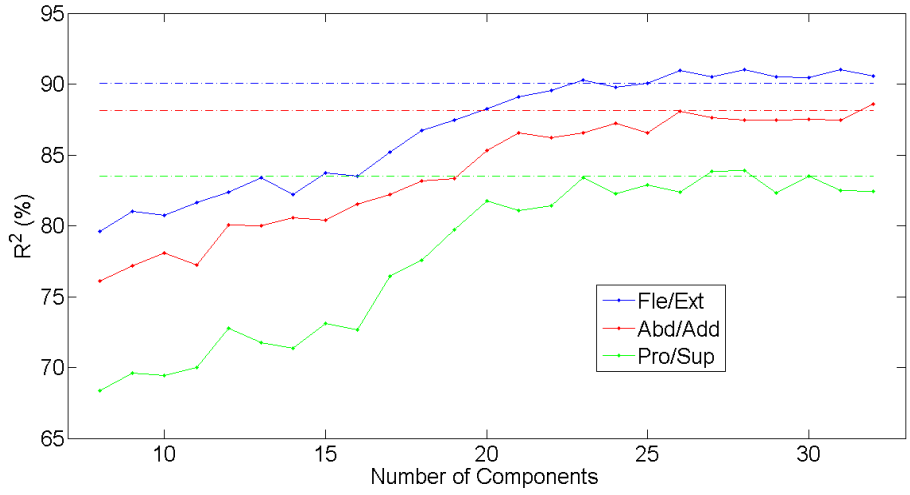

(c)

Figure 3.18. The effect of dimensionality reduction using NNMF on the R^2 values in the (a) *constrained*, (b) *resisted unconstrained*, and (c) *unconstrained* experiments. The original feature set results are shown using dashed lines.

The results showed that for reduced sizes equal or greater than 23, 26, and 26 in the constrained, resisted unconstrained, and unconstrained experiments, respectively, the R^2 values in each DOF were similar to those of the original feature sets (p>0.1).

3.4.3.3 Canonical Correlation Analysis (CCA)

Another means of decomposing a multivariate signal (X) into uncorrelated signals is by using canonical correlation analysis (CCA) as proposed in [149]. The decomposed signals are uncorrelated with each other, but within each signal there is maximum temporal correlation between a sample and a linear combination of a neighboring (but not

overlapping) region. The uncorrelated components S can be estimated using the decomposing matrix W:

$$S = W \times X \tag{3.12}$$

Similar to the PCA, the dimensionality reduction is performed by selecting the first components which have the highest variance. Figure 3.19 depicts the effect of CCA features projection using different reduced dimensions of the projected space on the estimation performance.

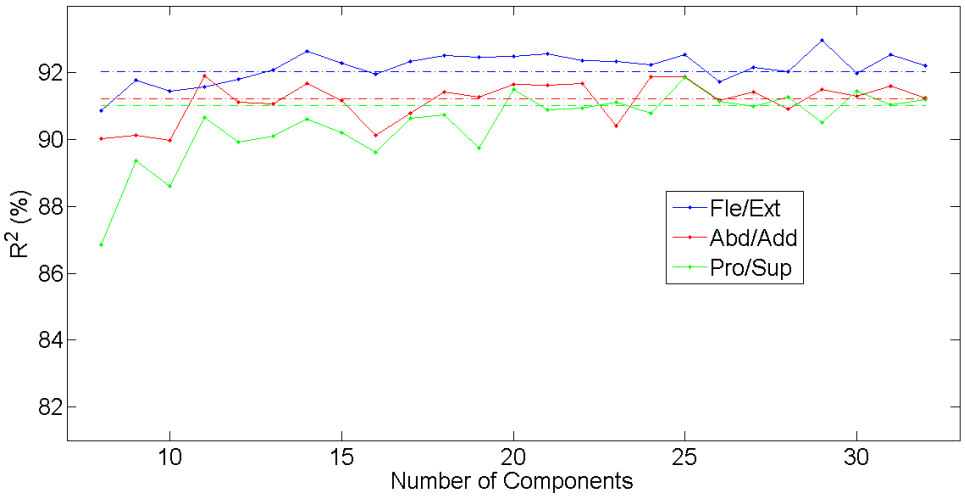

(a)

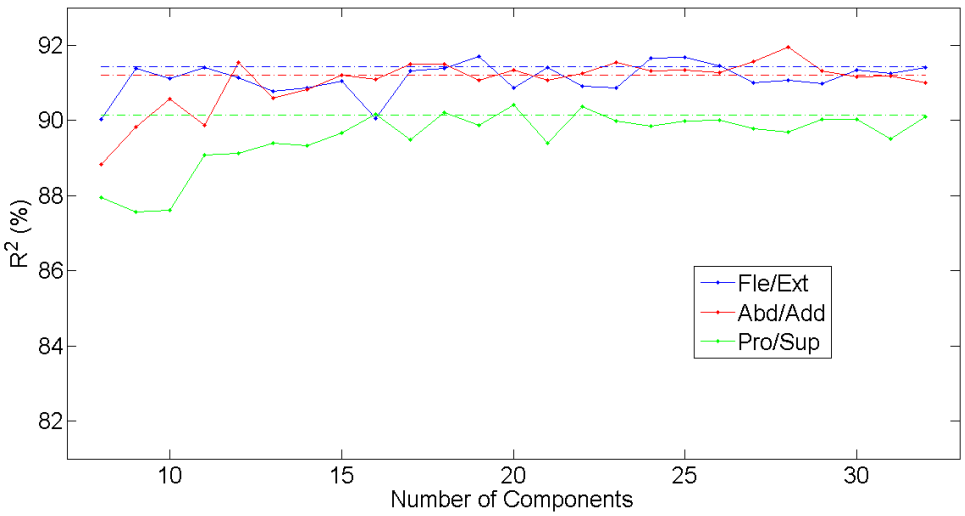

(b)

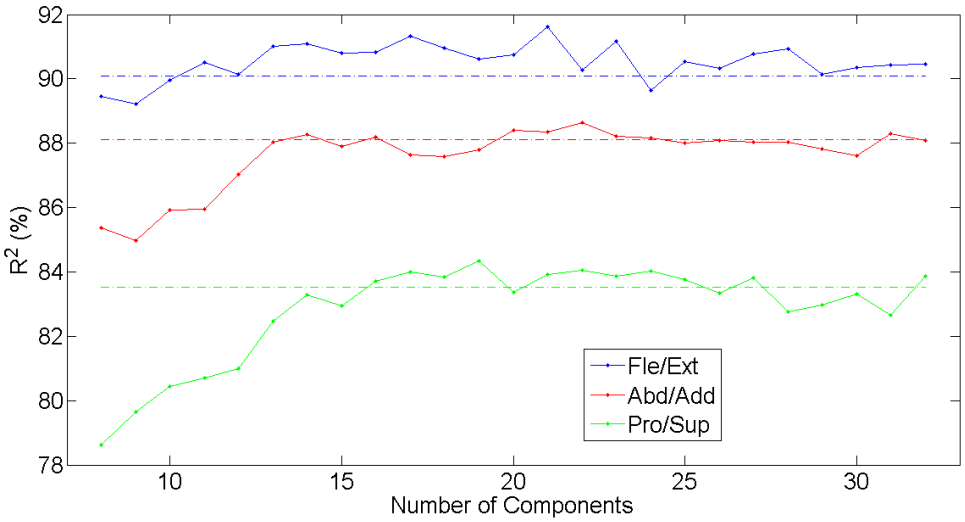

(c)

Figure 3.19. The effect of dimensionality reduction using CCA on the R^2 values in the (a) *constrained*, (b) *resisted unconstrained*, and (c) *unconstrained* experiments. The original feature set results are shown using dashed lines.

Based on the results of the feature projection using CCA, for projections with sizes equal or greater than 9, 9, and 12 components, in the constrained, resisted unconstrained, and unconstrained experiments, respectively, the R^2 values in each DOF were similar to those of the original feature sets (p>0.1).

3.4.3.4 Comparison of the Feature Projection Methods

Figure 3.20 illustrates a comparison of the aforementioned feature projection methods on the overall R^2. The plot shows that, compared to PCA and NNMF, the CCA is capable of providing substantially better dimensionality reduction with similar estimation performance to that of the original feature set.

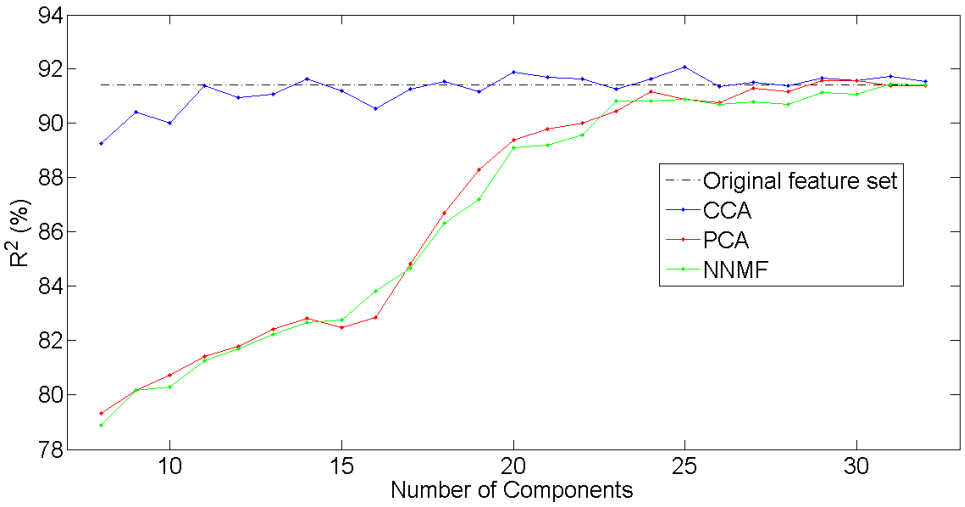

(a)

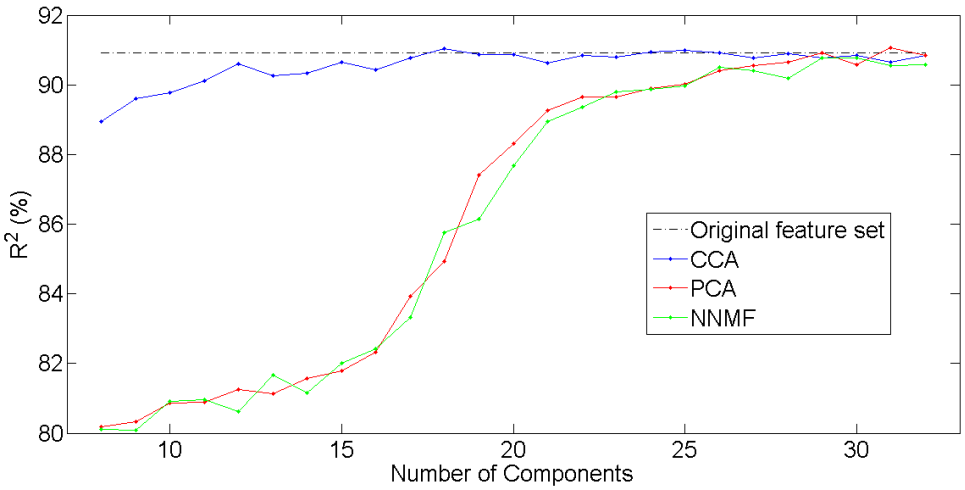

(b)

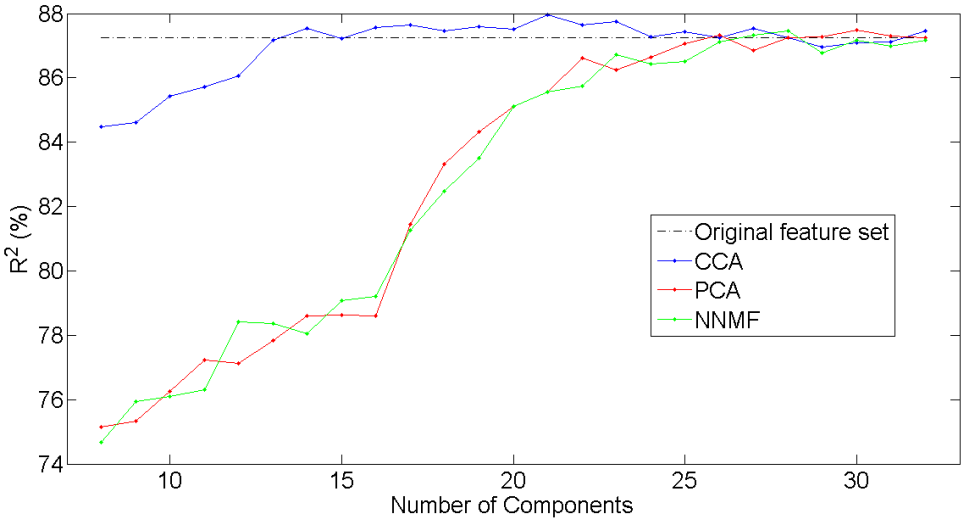

(c)

Figure 3.20. The overall R^2 values using feature projection techniques: PCA, NNMF, CCA in the (a) *constrained*, (b) *resisted unconstrained*, and (c) *unconstrained* experiments. The original feature set overall R^2 is shown using dashed line.

The results suggest that the feature projection methods of PCA, NMF and CCA are able to provide a lower dimensional representation of the EMG features that yields similar

user intent estimation performance. These methods improve the computer processing time for both training and estimation. However, no significant increase of the estimation accuracy over that of the original feature set was observed. There are a few reasons why this may be the case.

1. Projecting features to another space, does not add extra useful information for estimators.
2. Feature projection methods cannot distinguish the irrelevant data to remove and enhance the estimation performance. Another possibility is that there is not any conflicting information to remove.
3. It may be that the estimators have sufficient capacity to learn the mapping relationships in high dimensional space, and do not benefit from a lower dimensional mapping (e.g. SVM is trained by transforming data to a high dimensional space).

Although in some applications a lower dimensional representation may be appealing for computational efficiency, it is not of particular concern here. Furthermore, dimensionality reduction may result in over-tuning which may compromise the robustness of the control system during real-time control. Consequently, no projection methods were used in the following work.

3.4.4 Alternative Coordinate Systems

It was hypothesized that some coordinate systems may have higher estimation performances by simplifying the relationship between EMG and user intent. Data from the *unconstrained* experiment was used in this section. In the baseline configuration, the EMG was mapped to the flexion-extension, abduction-adduction and pronation-supination angles. Herein, changing the targets by employing alternative coordinate systems is studied for possible estimation enhancements.

This analysis did not include *constrained* (force) experiment, as the force transducer was designed to measure force in the conventional coordinate system, i.e. flexion-extension, abduction-adduction and pronation-supination. Therefore, changing the coordinate system will not affect the performance as it requires using target data from the baseline coordinate system.

3.4.4.1 Spherical Coordinate System

A spherical coordinate system was considered as being possibly more innate, as the wrist articulation motor planning task may resemble positioning the wrist at a point on a bounded sphere of fixed radius. When using the spherical coordinate system, the pronation-supination angle is the same as it is used in the conventional system, and therefore it is excluded from this analysis.

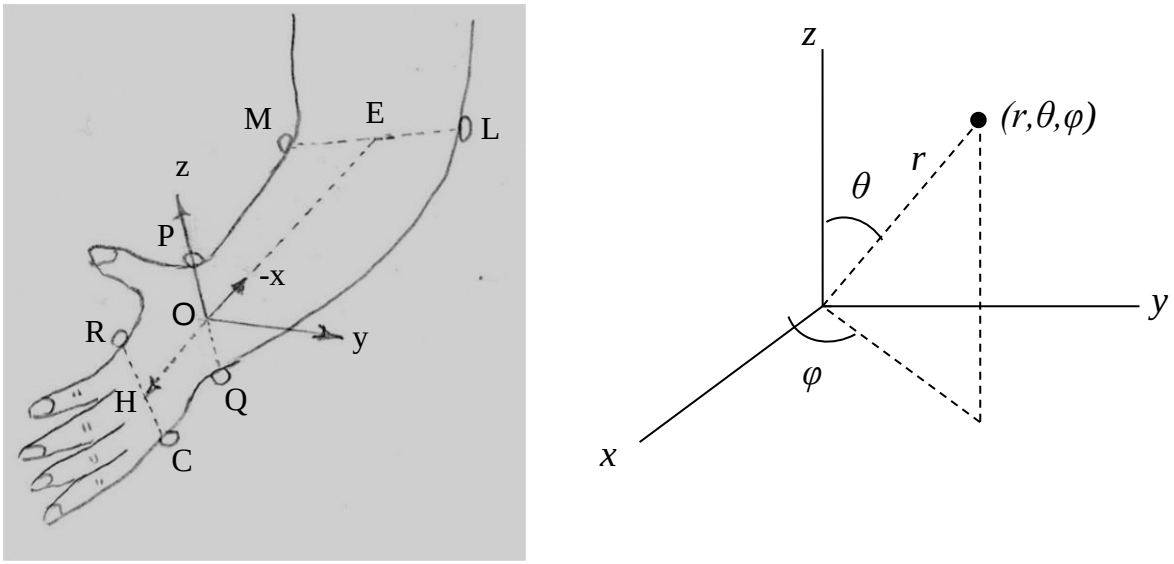

(a) **(b)**

Figure 3.21. (a) The marker locations for calculation of the joint angles are shown. (b) The spherical coordinate system representation.

As described earlier, the flexion-extension (or abduction-adduction) angle is calculated as angular displacement of the projection of the vector *O*-*H*, *H* being the midpoint between *P* and *Q*, on the plane *x*-*y* (*x*-*z*) (Figure 3.21 (a)). Using the definition above, the flexion-extension angle is equal to the azimuthal angle (φ) of the spherical coordinate system, (*H* in Figure 3.21 (a) corresponds to the end-point in the spherical coordinate system (Figure 3.21 (b)). However, the abduction-adduction angle ($\pi/2-\beta$) is different from the polar angle (θ) of the spherical coordinate system (Figure 3.22).

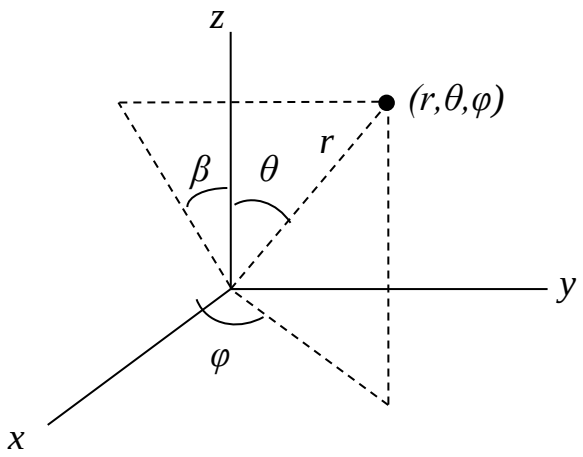

Figure 3.22. The spherical coordinates and the abduction-adduction angle (π/2− β) is shown.

Assuming the end-point Cartesian coordinates in Figure 3.22 are *x*, *y*, and *z*, we have

$$Cos\ \varphi = \frac{x}{\sqrt{x^2 + y^2}} \tag{3.13}$$

$$z = \frac{x}{tg\ \beta} \tag{3.14}$$

$$\theta = \frac{\pi}{2} - tg^{-1}\left(\frac{z}{\sqrt{x^2 + y^2}}\right) \tag{3.15}$$

Replacing (1) and (2) in (3) we have

$$\theta = \frac{\pi}{2} - tg^{-1}\left(\frac{Cos\ \varphi}{tg\ \beta}\right) \tag{3.16}$$

In Equation (3.16), φ and ($\pi/2-\beta$) are flexion-extension and abduction-adduction angles, respectively. Therefore,

$$\theta = \frac{\pi}{2} - tg^{-1}\left(\frac{Cos\,(FE)}{Cotg(AA)}\right) \tag{3.17}$$

where *FE* represents the flexion-extension angle and *AA* is the abduction-adduction angle.

In summary, when using the spherical coordinate system, the pronation-supination angle is the same as that in the conventional system. Also, the azimuthal angle (φ) is equal to the flexion-extension angle. The polar angle (θ) can be derived from the flexion-extension and abduction-adduction angle using the Equation (3.17).

Since the only difference between the spherical coordinate system and the conventional system is using the polar angle instead of abduction-adduction angle, only the results of this DOF are compared. The polar angle computed using the flexion-extension and abduction-adduction angles form the Equation (3.17), was used as target for estimation. The polar angle estimation accuracies were compared to those of abduction-adduction angle (the *unconstrained* experiment data were used). The results are listed in Table 3.6.

Table 3.6. The estimation accuracies R^2 (%) of the abduction-adduction and polar angles

	Abd/Add angle	*Polar angle*
Mean of all subjects	86	86
Su 1	86	88
Su 2	87	88
Su 3	76	74
Su 4	78	77
Su 5	89	88
Su 6	88	85
Su 7	90	91
Su 8	89	90
Su 9	84	84
Su 10	89	90

A one-way repeated measures ANOVA showed that the R^2 results of abduction-adduction angle were not different (p>0.1) from those of the polar angle. This may suggest that the ANN is able to learn the coordinate system transformations, as the polar angle is simply a function of the flexion-extension and abduction-adduction angles.

3.4.4.2 Two-Dimensional Motion Projection

In this section, the coordinate system transformation by motion projection on the vertical plane (y-z in Figure 3.22) is investigated. Again, the pronation-supination angle remains the same in this transformation. However, for the other two DOFs, instead of flexion-extension angle (φ) and abduction-adduction angle ($\frac{\pi}{2} - \beta$) in Figure 3.22, the y and z Cartesian coordinates of the end-point position are used.

The *y* and *z* coordinates can be computed from the azimuthal (φ) and polar θ angles as

$$y = r.Sin\,\theta.Sin\,\varphi \tag{3.18}$$

$$z = r.Cos\theta \tag{3.19}$$

The azimuthal angle (φ) is the same as flexion-extension angle and the polar angle (θ) can be derived from flexion-extension (*FE*) and abduction-adduction (*AA*) angles using the Equation (3.17).

The *y* and *z* coordinates were calculated using flexion-extension and abduction-adduction angles. A separate ANN was trained to map EMG features to each new coordinate. The estimation accuracy (R^2) of each DOF was compared with those of the conventional coordinate system (the pronation-supination results were not included as this DOF was the same in both coordinate systems). The results are listed in Table 3.7.

Table 3.7. The estimation accuracy R^2 (%) of the conventional and 2D projection coordinates

	Fle/Ext angle	*y-coordinate*
Mean of all subjects	89	88
Su 1	85	86
Su 2	89	89
Su 3	90	88
Su 4	84	81
Su 5	88	88
Su 6	92	91
Su 7	89	90
Su 8	84	87
Su 9	93	92
Su 10	92	92

	Abd/Add angle	*z-coordinate*
Mean of all subjects	86	86
Su 1	86	86
Su 2	87	88
Su 3	76	76
Su 4	78	77
Su 5	89	88
Su 6	88	86
Su 7	90	91
Su 8	89	88
Su 9	84	86
Su 10	89	91

For each DOF, a one way repeated measures ANOVA test showed that, the R^2 results were not different (p>0.1) between the two coordinate systems. This again suggests that the ANNs can learn the nonlinear relationships, so that coordinate transformation does not facilitate mapping EMG features to force or position.

3.5 Summary

In the first part of this chapter, constrained and unconstrained experiments were compared. The force and position based methods have been investigated individually in the literature. However, no study has yet directly compared these approaches. In this

work, a comparison between force and position based paradigms was conducted to assess their relative performance.

Although the constrained (force-based) method outperformed the unconstrained (position-based) method, the difference was largely attributed to a difference in activation levels. Upon introducing a resistance to the unconstrained case to equalize EMG levels, no significant difference was found between the estimation of constrained and unconstrained contractions. It should be noted that in case of amputees, the EMG levels between different protocols are not different as the constrained or unconstrained setup is only applied to the contralateral (intact) limb, whereas EMG is only measured from the affected limb. These protocols were designed to determine the relative efficacy of force and position based estimation paradigms from EMG. Based on the results with able-bodied subjects, these strategies yield similar results with able-bodied subjects when using similar EMG levels. Therefore, similar performance between these paradigms is also expected with amputees, as the EMG levels are not different between constrained and unconstrained methods. However, the results may be influenced by the specific structure of the residual muscles for an amputee, as this may affect the correlation between contractions of the intact and affected limbs.

The second part of the chapter described alternative analytical approaches to achieve possible estimation enhancements over the baseline configuration. Employing other EMG feature sets including autoregressive features, wavelet marginals, Willison amplitude, and median frequency did not provide significant performance improvement over that of the TD features. Therefore, the TD features will be used for the rest of this work.

Various estimators were studied to model the relationship between EMG and joint force/angle. The results in each case were compared to those of the baseline estimator (multilayer perceptron ANNs). The linear model results were shown to be lower than that of the ANNs, which suggests a nonlinear relationship between EMG features and force/position. Modeling using polynomial models outperformed the linear estimator but their performance was still inferior to those of the ANNs.

In general, time-delayed ANNs estimation accuracies were worse than those of the static ANNs, and including further delayed inputs resulted in degradation of estimation. This implies that force/angle estimation does not depend on time-delayed EMG features for the frame increment used in this work. The radial basis function ANNs performance was also lower than that of the multilayer perceptron ANNs. Ensembles of bagged trees outperformed the baseline (ANNs) in abduction-adduction, with no significant difference in the other DOFs, while reducing the processing time. Support vector machines significantly outperformed the baseline (ANNs) in multiple DOFs (depending on the experiment), while having substantially faster processing time in both training and estimation. For 3 DOFs, the SVMs average estimation time was 6 ms, where that of the ANNs was 60 ms. This faster processing time may potentially improve the responsiveness and in a real-time usability scenario.

Feature projection techniques which transform data to a new, lower dimensional, space were investigated. PCA, NNMF and CCA were all able to reduce the size of feature sets with similar estimation accuracies to those of the original feature set. The CCA, however, was able to maintain the same performance with fewer features than the PCA and NNMF.

Because no benefit was gained in estimation accuracy, no projection methods will be used in the remaining work.

Alternative coordinate systems were also explored. It was postulated that new coordinate systems may improve the results by transforming the joint angle data to another space, which possibly facilitates its mapping to EMG. The *Spherical coordinates* and *2D projection onto a vertical plane* were examined. However, the estimation accuracies using the new coordinate systems were similar (no significant difference) to those of the conventional coordinate system. These results suggest that the ANNs can learn the coordinate transformations, as the performance did not change significantly when using different coordinate systems. Future work can investigate the effect of using feedback in different coordinate systems during real-time control test.

Based on the results of this chapter, the myoelectric system configuration for real-time tests of Chapters 4 and 5 was determined. It was decided not to use coordinate transformations as they did not increase the estimation performance. The TD features were chosen as the feature set to represent the EMG data since other features did not provide performance improvement. In Chapters 4 and 5, ANN estimators are employed, as the use of SVMs was only investigated after the completion of these studies. In Chapter 6, a comparison between the usability of the ANN and SVM is conducted.

Chapter 4- Target Acquisition Test

This chapter describes a real-time *target acquisition* experiment to assess myoelectric control of mirrored bilateral training methods using *constrained* (force targeted) and *unconstrained* (position targeted) contractions. Previous work [71], [94], [8] investigated these methods using pre-recorded data, and consequently the interaction of the user with the control system was absent. The correlation (R^2) between the actual and estimated joint force/angle of offline data was used to assess the estimation accuracy. The novelty of this chapter is that it compares for the first time, control strategies based on *constrained* (force-based) and *unconstrained* (position-based) contractions in a real-time target acquisition paradigm with user feedback. This which offers much greater insight regarding the suitability of the two approaches for functional user intent estimation.

The intent of the user can be estimated from the surface EMG, as illustrated in Figure 4.1. Once the user intent has been estimated, this must be translated into some functional manifestation by using an appropriate control scheme. For myoelectric prostheses, the control scheme typically employs *velocity control*, in which the intensity of effort is proportional to the angular velocity of a device. Robot manipulators can afford greater complexity, and consequently often use feedback control to implement a *position control* scheme. Computer based training and rehabilitation tools have employed both *velocity* and *position control* [110], [111].

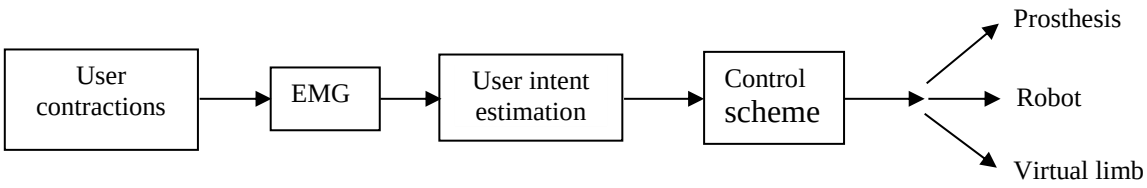

Figure 4.1. The hierarchical levels of real-time myoelectric control; control scheme can use position or velocity control.

Although the focus of this work is prosthesis control, the process of intent estimation is relevant to other applications (such as robotic control and human computer interfaces). Therefore, for generality and to enable quantitative comparisons, the user intent was mapped to the *position* of a cursor on a computer screen. The *position* modality was selected instead of *velocity control* (as is often used in prosthetics) because it allows a more direct evaluation of control quality. In this case, acquisition of targets with different amplitudes evaluates the output magnitude, while targets with combinations of DOF assess the efficacy of simultaneous control. Position control is often used in commercial myoelectric training software [111]. It should be noted however that, while often slower, velocity control is easier to control for a user as the cursor movements are smoother (because the cursor displacements are the integrals of the estimated outputs, so the fluctuations in the estimated outputs are less apparent in the cursor displacements). Also, maintaining the cursor on a target requires the user to stop contracting (the *no motion* command*)* in *velocity control*, whereas in a *position* modality, a user has to continuously contract in order to keep the cursor on a target. The level of effort in a target acquisition task is therefore higher during position control, but it allows a direct comparison of simultaneous motion performance. Another reason for using the position control was that it enables detecting smaller differences between the constrained and unconstrained

methods. This is because estimation inaccuracies may be partially masked by smoothing effect of the velocity control, because the velocity is the integral of the estimated outputs.

The target acquisition test in this experiment was not designed as a Fitts' law style test. This was because due to jitter, small target widths were not possible, whereas Fitts' law test requires targets with different widths. Usually with velocity control, the control is smoother and therefore smaller target widths can be acquired. Sensinger et al. [112] also found that velocity control outperformed the position control.

4.1 Experimental Design

As described in the previous chapter, this experiment was performed using ten able-bodied subjects. A power analysis test (power=0.80) was conducted using pilot data and the minimum number of required subjects was determined to be 5. For each experimental protocol (*constrained, resisted unconstrained,* and *unconstrained*), a target acquisition test was conducted to evaluate the system usability. For each protocol, the training and real-time test was performed in the same session and were separated by sufficient rest time to minimize fatigue. Additional rest periods were given during the experiment, when fatigue was subjectively reported.

Before the real-time test, the collected data were used to train the ANNs (as described in Chapter 3) using the right (dominant) forearm EMG as the input and left wrist force/angle as the target. The configuration of the myoelectric intent estimation process was determined by the offline analyses explained in Chapter 3. In addition, the TD features

were lowpass filtered (cutoff=1 Hz) [131],[94],[100], as this was empirically found to improve the cursor control. The TD features were used as inputs to the ANNs, so smoothing the features ultimately smoothed the output. The output was also lowpass filtered as in offline assessment in Chapter 3.

The real-time raw EMG signals were visually inspected before the data collection to ensure the data quality. Prior to the tests, the subjects were fully familiarized with the protocol, and allowed to practice until they felt comfortable to proceed. A MATLAB^{TM} based graphical user interface was designed for the target acquisition protocol. The test was performed using the right upper limb, where the estimated joint force/angle in the three DOFs was estimated from the right forearm EMG. The output was mapped to the position and orientation of a control cursor; the flexion-extension DOF was mapped to the horizontal displacement of the cursor, while abduction-adduction was mapped to the vertical displacement. The orientation angle of the cursor was determined by pronation-supination.

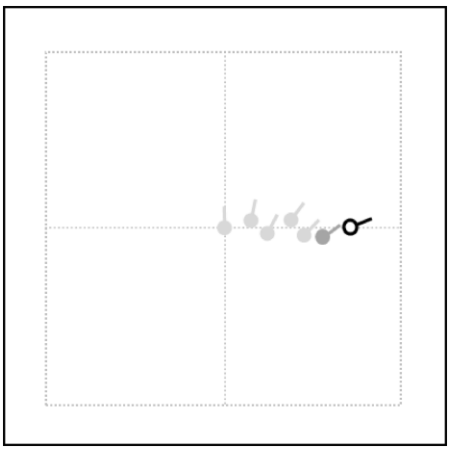

Figure 4.2. The trace of the cursor (filled) movement towards a target (black, not filled) is shown during a target acquisition test. The target in this example case corresponds to simultaneous wrist extension and supination.

The estimated angles in each direction (two directions for each DOF) were normalized by the subject's maximum joint angles in that direction in the training experiment. Similarly, the estimated forces in each direction were normalized using the maximum force target magnitude (constant) in the training to correspond to the percent deviation from rest.

Performing *no motion* resulted in the cursor being positioned at the screen center with vertical orientation. A normalized estimated force/angle with unity magnitude (corresponding to maximum deflection) in flexion-extension or abduction-adduction DOF positioned the cursor at the 100% location (full range) of the screen (the inner square shown in Figure 4.2), whereas in pronation/supination it resulted in a 90 degree rotation of the cursor. The estimations and screen rendering were updated every 100 ms, limited by numerical processing and graphics rendering delays.

To begin each test, a fixed target was displayed on the screen and the subjects were prompted to reach the target as quickly as possible. A picture of the required

contraction(s) was also presented. A target was considered to be successfully acquired when the user kept the location and orientation of the cursor within a specified tolerance for a full second (*dwell time*). The tolerance region was defined as a three dimensional distance from the target of less than 15% of full range (determined empirically to yield a reasonable difficulty usable for all subjects). The 3D distance between the cursor and target was stated in percentage of full range as the cursor displacements were normalized. Consequently, the accuracy of each direction was assessed using relative error as in offline estimation accuracies (this is important because in unconstrained experiments, for example, the ranges of flexion and abduction are substantially different). As feedback, the cursor color changed if the cursor was within the target tolerance.

If the task was not completed within 10 seconds, the target timed out and was considered unsuccessful (10 seconds was chosen to not tire the user during unsuccessful tasks). Each trial included fourteen consecutive targets corresponding to the contractions of Table 4.1 with randomized order (the same contractions used in the training protocol). A two second rest time was provided between successive targets by prompting the subjects to return to the neutral position. The test included four trials, with target magnitudes of 90%, 70%, 50%, and 30% of full range.

Table 4.1. Each Target corresponded to one of the following practical contractions of wrist and forearm.

Index	Contraction
1	Flexion
2	Extension
3	Abduction
4	Adduction
5	Pronation
6	Supination
7	Simultaneous Flexion and Pronation
8	Simultaneous Flexion and Supination
9	Simultaneous Extension and Pronation
10	Simultaneous Extension and Supination
11	Simultaneous Abduction and Pronation
12	Simultaneous Abduction and Supination
13	Simultaneous Adduction and Pronation
14	Simultaneous Adduction and Supination

A similar target acquisition test was also conducted using the force transducer to control the cursor directly. The output was lowpass filtered with the same filter used in other protocols to have comparable results. This test was included to provide a baseline for the force estimation protocol. Since the position data recorded by the motion capture system (Vicon 512) were not accessible in real-time, a similar dynamic test was unfeasible.

During the experiment, the subjects were observed to ensure they did not make excessive contractions causing fatigue and frustration. After the experiment and during the breaks, the subjects were encouraged to comment about the control quality details.

4.2 Performance Metrics

A set of performance metrics (*completion rate*, *completion time, path efficiency*, and *overshoot*) used in [108],[117],[118] was employed as described in Table 4.2. These measures provide information about various aspects of the control quality.

Table 4.2. The Target acquisition test performance metrics

Metric	*Description*
Completion Rate	Task success; a ratio between the number of acquired targets and the total number of targets.
Completion Time	Overall performance; the time to reach the target without the inclusion of the dwell time.
Path Efficiency	Quality of control; a ratio between the shortest 3D distance to the target and the actual 3D distance travelled.
Overshoot	Target acquisition; the number of times the target was acquired and then lost before completing the *dwell time*.

A one-way repeated-measures ANOVA test followed by a *Bonferroni* post-hoc test was used to compare each real-time performance metric between the protocols. The significance level was set to 0.05.

4.3 Results

Figure 4.3 (a) and (b) depict a three dimensional representation (with cursor orientation shown in the *Z*-direction for visualization purposes) of path traces in the target acquisition test for a representative subject in the *constrained* and *unconstrained* experiments (only the first eight acquired targets are shown for clarity).

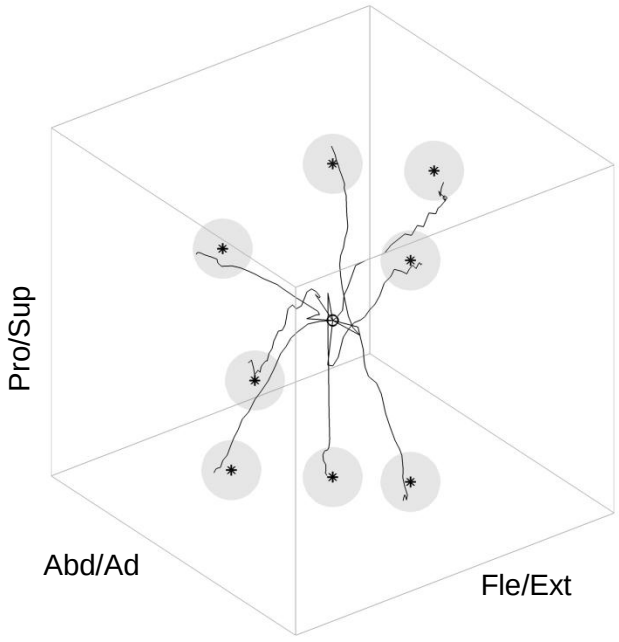

(a)

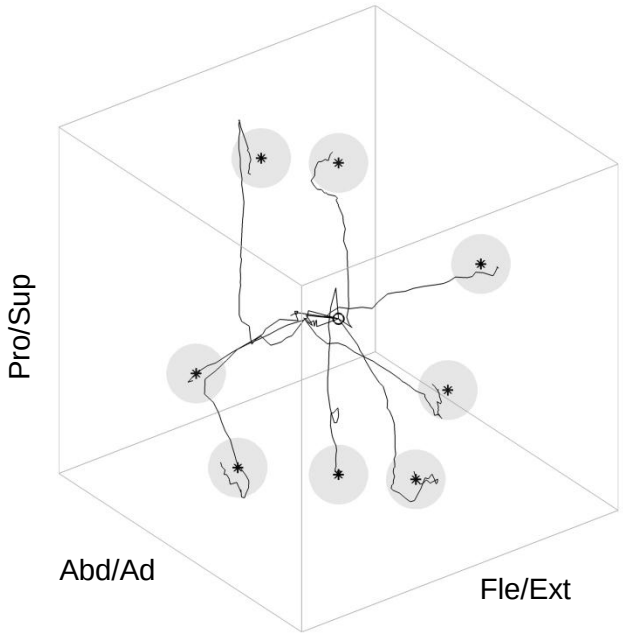

(b)

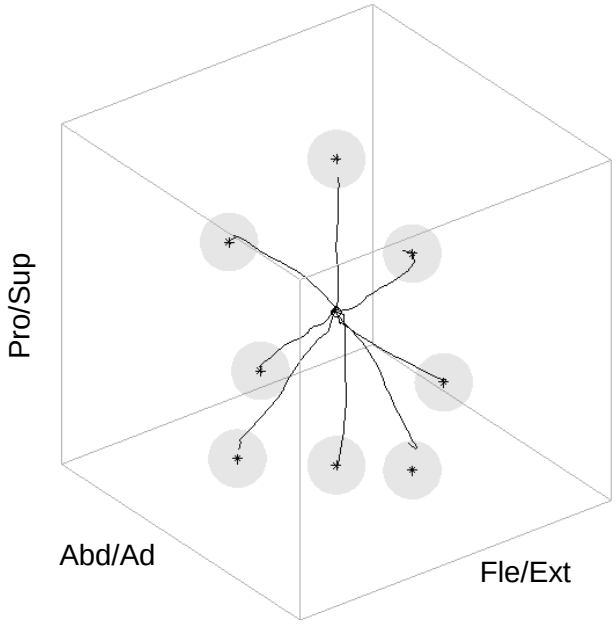

(c)

Figure 4.3. A 3D representation of path traces for a representative subject in the target acquisition test; the first eight acquired targets are shown for clarity: (a) *Constrained* experiment, (b) *Unconstrained* experiment, and (c) the force sensor experiment.

The target acquisition test results averaged across all subjects are shown in Table 4.3 using mean ± standard error for *constrained*, *unconstrained* and *resisted unconstrained* protocols as well as the test where the cursor was controlled directly by the force transducer. The statistical analysis results for each performance metric are listed in Table 4.4.

Table 4.3. The target acquisition test results averaged across all subjects are shown using mean ± standard error.

	Constrained	*Unconstrained*	*Resisted unconstrained*	*Force transducer*
Completion rate (%)	84.4 ± 2.9	80.9 ± 2.6	81.2 ± 2.8	97.1 ± 0.9
Completion time (s)	4.23 ± 0.27	4.94 ± 0.29	4.43 ± 0.28	2.94 ± 0.21
Overshoot	0.72 ± 0.07	0.91 ± 0.06	0.81 ± 0.07	0.30 ± 0.06
Path Efficiency (%)	59.3 ± 4.0	50.1 ± 4.1	54.5 ± 4.7	78.1 ± 1.3

Table 4.4. Statistical analysis results of the target acquisition test metrics. Significant comparisons are marked with *.

	Constrained vs. Unconstrained	*Constrained vs. Resisted unconstrained*
Completion rate	$p>0.1$	$p>0.1$
Completion time	$p=0.03$*	$p>0.1$
Overshoot	$p>0.1$	$p>0.1$
Path Efficiency	$p=0.02$*	$p>0.1$

The results show that the *constrained* and *resisted unconstrained* protocols results were not different for any real-time metric. As well, the results of the *constrained* experiment in *completion rate* and *overshoot* were not different from those of the *unconstrained* protocol. However the *constrained* experiment *completion time* and p*ath efficiency* outperformed those of the *unconstrained* experiment.

During combined DOF targets, the users were encouraged to move the cursor in the corresponding directions, simultaneously. To quantitatively evaluate this, a metric β was defined as the ratio between the number of times that the cursor speeds in multiple DOFs were greater than a threshold *TH* (found empirically as 25% of full range per second) and number of times that the cursor speed in only one DOF was larger than *TH*. The β values averaged across all subjects computed for single and combined DOF targets are listed in Table 4.5. As expected, the β values for combined DOF targets were significantly higher (p<0.001) than those of the single DOF targets. This shows that the users chose to move in multiple directions (DOFs), simultaneously during combined DOF targets. The difference between the results of the force transducer experiment and those of other control schemes indicates the estimation errors with EMG based systems.

It should be noted that successful acquisition of targets did not require simultaneous movement towards the target. Therefore, encouragement played an important role to improve simultaneous movements of the cursor.

Table 4.5. The β values averaged across all subjects for single and combined DOF targets are shown using mean ± standard error. The significant comparisons are marked with *.

	Single DOF targets	*Combined DOF targets*	*p-value*
Constrained	0.31 ± 0.04	2.42 ± 0.25	<0.001*
Unconstrained	0.35 ± 0.07	2.27 ± 0.21	<0.001*
Resisted Unconstrained	0.36 ± 0.05	2.35 ± 0.26	<0.001*
Force Transducer	0.14 ± 0.02	3.04 ± 0.34	<0.001*

Tables 4.6, 4.7 and 4.8 list each subject's offline R^2 (from the training data) and real-time target acquisition metrics in the *constrained*, *resisted unconstrained*, and *unconstrained* experiments.

Table 4.6. The offline R^2 value and real-time performance metrics for each subject in the *constrained* experiment.

	R^2 *(%)*	*Completion rate (%)*	*Completion Time (s)*	*Path efficiency (%)*	*Overshoot*
S1	90	96	3.66	65	0.59
S2	89	93	3.47	64	0.65
S3	90	74	5.69	39	0.87
S4	93	96	3.41	76	0.65
S5	88	84	4.53	60	0.43
S6	91	87	3.54	71	0.43
S7	91	88	3.34	72	0.61
S8	91	79	4.76	55	1.06
S9	88	70	5.04	42	0.91
S10	88	78	4.90	49	1.01

Table 4.7. The offline R^2 value and real-time performance metrics for each subject in the *resisted unconstrained* experiment.

	R^2 (%)	*Completion rate (%)*	*Completion Time (s)*	*Path efficiency (%)*	*Overshoot*
S1	88	82	4.15	60	0.52
S2	91	96	3.74	63	0.72
S3	90	73	5.56	43	0.62
S4	87	86	3.90	58	0.62
S5	90	84	4.18	65	0.80
S6	91	89	3.05	74	0.68
S7	90	86	3.81	67	0.93
S8	88	75	5.35	33	1.22
S9	89	66	5.73	29	1.04
S10	91	75	4.79	53	0.86

Table 4.8. The offline R^2 value and real-time performance metrics for each subject in the *unconstrained* experiment.

	R^2 (%)	*Completion rate (%)*	*Completion Time (s)*	*Path efficiency (%)*	*Overshoot*
S1	86	79	4.56	57	0.56
S2	88	96	3.85	64	0.72
S3	81	79	5.98	37	0.79
S4	87	84	4.12	58	1.19
S5	85	82	4.62	53	0.96
S6	86	76	5.97	48	0.98
S7	87	91	3.92	63	0.77
S8	81	79	5.69	38	1.16
S9	84	65	6.11	25	0.98
S10	89	79	4.54	59	1.02

To investigate the relationship between the performance metrics, their scatter plots versus completion time are plotted in Figure 4.4, which shows that there is an inverse relationship between *completion time* and either *completion rate* or *path efficiency*. However, no relationship was observed between the *completion time* and *overshoot*. Figure 4.5 shows the performance metrics for each protocol versus subject.

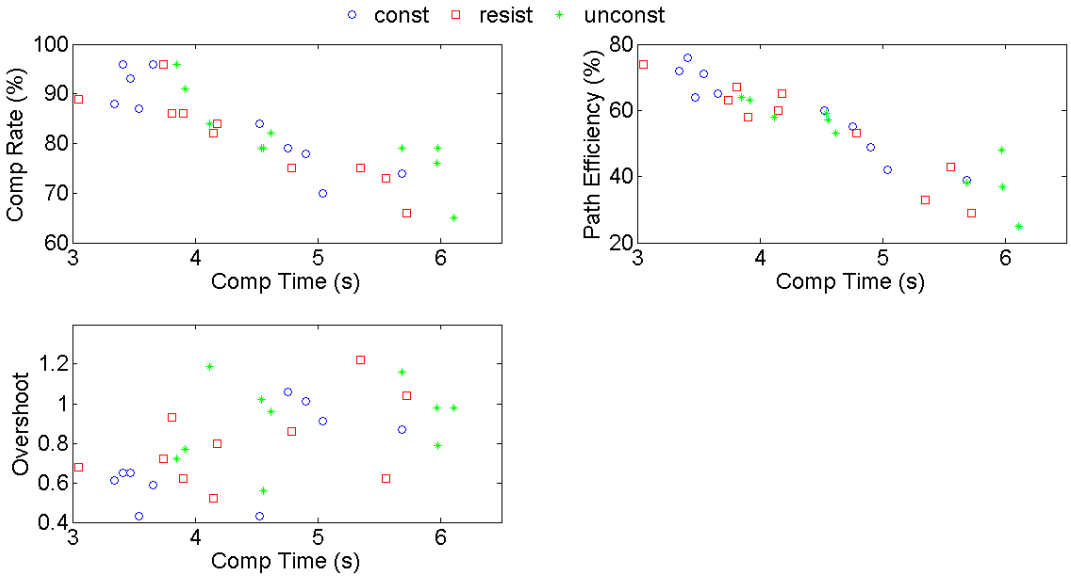

Figure 4.4. The scatter plots of real-time performance metrics versus completion time are plotted.

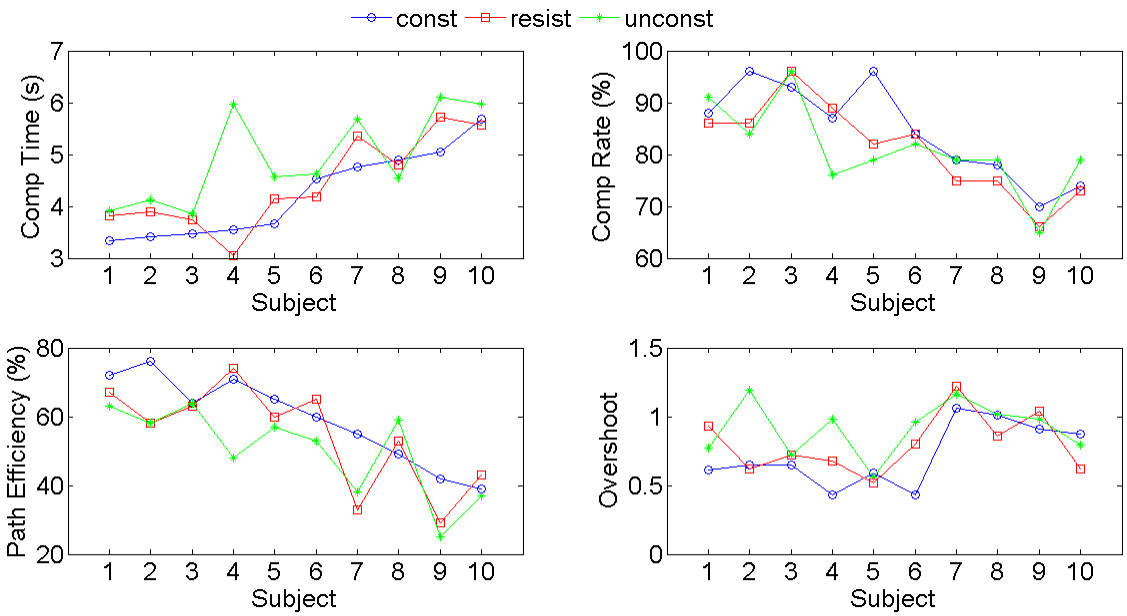

Figure 4.5. The real-time performance metrics for each protocol is plotted versus subject (the subjects in this figure are sorted based on the completion times of the constrained experiment).

As shown in Figure 4.5, the metrics were highly subject-dependent, but for most subjects, *completion time* and *path efficiency* of the unconstrained experiment were inferior to those of other protocols. In Figure 4.6, the performance metrics averaged across all subjects are plotted versus experiment.

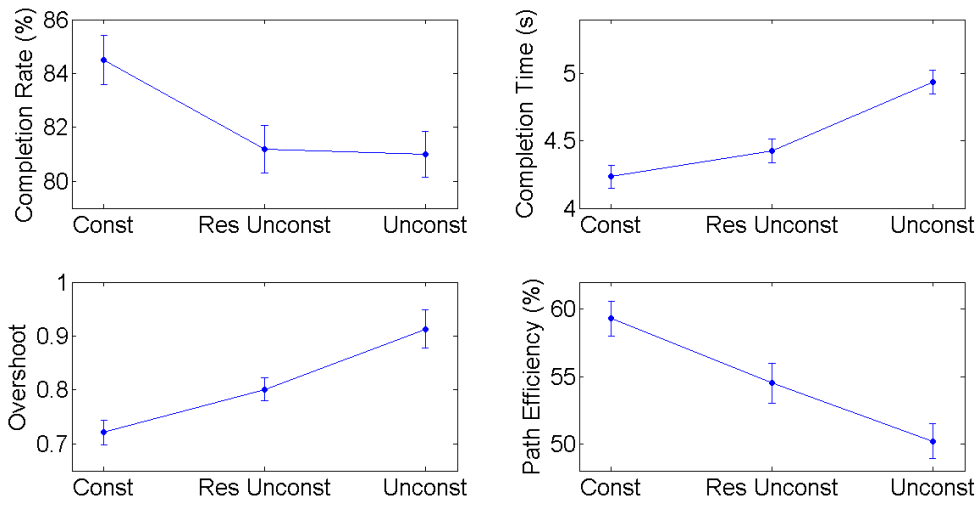

Figure 4.6. The real-time performance metrics averaged across all subjects are plotted versus experiment.

4.4 Discussion

As described in chapter 3, the wrist braces in the *resisted unconstrained* protocol were used to increase the level of EMG activity during contractions. The *unconstrained* protocol performance was inferior to that of the *constrained* experiment in the *completion time* and *path efficiency*. This, again, may be attributed to the limited range of EMG level in the *unconstrained* experiment that caused estimation accuracy degradation. However, the *resisted unconstrained* experiment results were similar to those of the *constrained* experiment in both offline and real-time test metrics. As such, it can be concluded that *constrained* and *unconstrained* based myoelectric control schemes perform similarly when compared using similar contraction intensities (EMG level). This is likely due to similarities of constrained and unconstrained cases. In unconstrained contractions, force and position are proportional, and therefore force is in fact the training target. Also, the

same muscles are responsible for constrained and unconstrained contractions. Therefore the main difference between the *constrained* and *unconstrained* protocols is the surface EMG recording method. Muscle displacement during contractions changes the relative location of the electrodes in the bipole. Larger displacements occur in *unconstrained* contractions due to changes in muscle length. The effect of muscle displacement is mixed with that of varying force/position, but this can be learned by ANNs.

It should be noted however, that in case of amputees, the EMG levels from the affected limb are similar between the constrained and unconstrained protocols. Moreover, muscle displacements beneath the electrodes (in the impaired limb) are not different between constrained and unconstrained contractions.

Although the target acquisition test was not designed as a Fitts'a law style test (becasue only one target width was used), the results were found to obey Fitts' law in the sense that the R^2 of linear regression between *completion times* and *indices of difficulty* was higher than 0.95 for each protocol as shown in Figure 4.7. Different indices of difficulty were due to different target distances, as only one target width was used. The index of difficulty (*ID*) is determined using Equation (4.1), where *D* is the target distance, and *W* is the target width.

$$ID = log_2(1 + \frac{D}{W}) \tag{4.1}$$

However, as it is shown in Figure 4.7, the Y-intercept was higher than 1 s, which does not match the recommended intercepts in Fitts' law tests (close to zero), and therefore this test was not called a Fitts' law test.

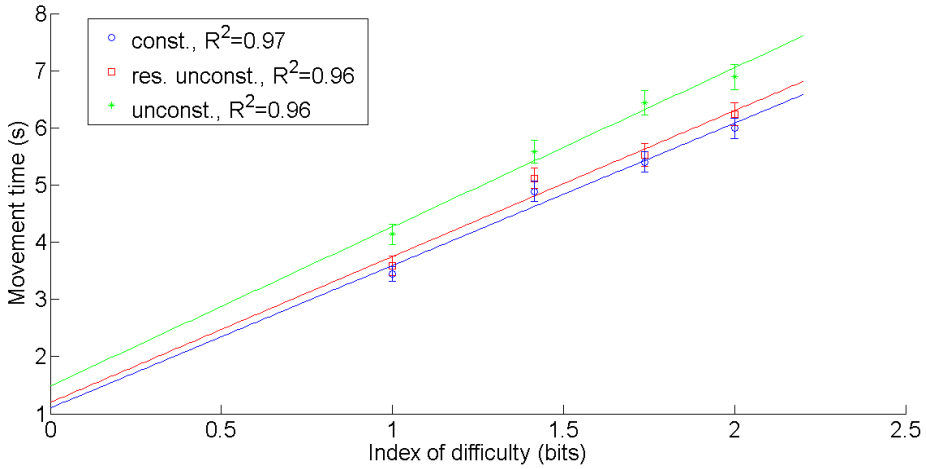

Figure 4.7. The relationship between the average completion time and index of difficulty was strongly linear (R^2>0.95).

Although three wrist DOFs were investigated in this work, there is currently no commercially available prosthesis capable of active wrist abduction-adduction. Therefore, inclusion of a more practical DOF such as hand open-close might be preferred. This however, was not feasible due to hardware (force transducer) limitations.

All subjects could perceive and use simultaneous control as they were able to acquire targets with combined motions. The subjects were able to generate comfortable contractions to reach the full range cursor deviation in each DOF.

The performance in all three protocols was subject-dependent. This is indicated by the relatively high inter-subject variability in usability metrics as shown in Tables 4.6, 4.7 and 4.8. Seven out of ten subjects reported that they felt that the *constrained* protocol provided better control than the *unconstrained* protocol, since they had a wider range of contraction intensities available for cursor control which enabled improved selection of desired intensity (apparent resolution). Higher estimation accuracies in constrained experiment also resulted in smoother cursor movements. Three subjects reported no perceivable difference between these two protocols. Two out of ten subjects preferred the constrained control over the *resisted unconstrained* control, while the others were indifferent between these two protocols. The qualitative results were closely consistent with the quantitative performance.

The majority of subjects found that, sometimes during single or combined DOF motions, special care must be taken to ensure that non-target DOFs do not move due to inadvertent cursor motions in these DOF(s). For example, when trying to achieve combined DOF targets (i.e. combination of two DOFs), the user had to make sure to keep the third DOF zero. This required extra mental effort and was related to estimation errors of inactive DOF(s) when other DOF(s) were active. Another origin of this issue is that it is not easy to naturally move the wrist DOFs completely independently of each other. Also, clinical experience suggests that patients were not able to control more than 2 DOFs, simultaneously [150].

All ten subjects found that acquisition of closer targets (requiring lower contraction levels) were easier, which was expected and was supported by the experimental results. The majority of subjects found that a subset of the targets were difficult to achieve. These

targets were different for different users and included both single and combined motion targets. These cases were consistent with poor estimation accuracy of the corresponding motions in those experiments. Eight out of ten subjects found no difference between the single and combined DOF targets difficulties. Two subjects, however, found that combined motion targets were more challenging than single DOF targets to achieve.

All subjects felt that controlling the cursor using the direct force transducer was easiest, which was expected as no estimation error is incurred. Moreover, the myoelectric intent estimation delay (due to the feature extraction window of length 200 ms), which may degrade usability, does not exist when using the force transducer control. It should be noted, however, that the screen update rate was common between the EMG and force-transducer experiments.

The total time to complete the entire experiment (training and usability test) was about 45 minutes for each protocol (*constrained*, *resisted unconstrained*, and *unconstrained*). Over the course of the experiment, no performance degradation was noted, qualitatively (quantitative results also did not show performance reduction). This suggests that fatigue, electrode shift or impedance change did not occur, or did not cause adverse effects, during the experiment.

4.5 Relationship between offline R^2 and real-time performance

The relationship between the offline estimation accuracy (R^2) and real-time metrics was investigated. Scatter plots of real-time metrics with respect to the offline R^2 are illustrated

in Figure 4.8, showing small correlation between the offline and real-time results. To quantitatively investigate the relationship between the offline and real-time performance, the *correlation coefficient* was used. The correlation coefficient (ρ) between two variables *X* and *Y*, is defined as the covariance of the two variables divided by the product of their standard deviations (Equation (4.2)). The correlation coefficient is between -1 and 1 inclusive.

$$\rho = \frac{cov(X,Y)}{\sigma_X \sigma_Y} \tag{4.2}$$

Table 4.9 shows the correlation coefficients between the offline R^2 and each real-time performance metric.

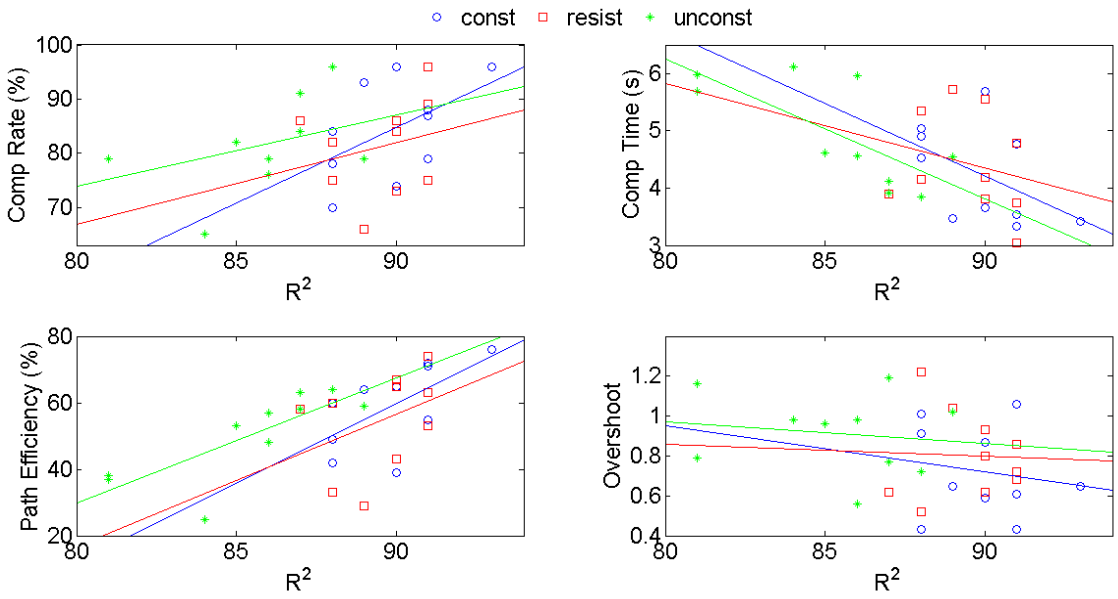

Figure 4.8. Scatter plots of the real-time performance metrics versus the offline R^2 values in the *constrained*, *resisted unconstrained*, and *unconstrained* experiment. The regression lines are also plotted.

Table 4.9. The correlation coefficients between the offline R^2 values and real-time performance metrics.

	Constrained	*Resisted unconstrained*	*Unconstrained*
Completion rate	0.38	0.11	0.42
Completion time	-0.27	-0.05	-0.70
Overshoot	0.02	0.02	-0.30
Path Efficiency	0.38	0.26	0.79

Table 4.9 shows that, in general, higher offline R^2 corresponded to improved real-time performance, as the ρ signs were as expected (except for *overshoot* in the *constrained* and *resisted unconstrained* cases, which approximately no correlation was found). However, the magnitude of correlations between offline and real-time results were not strong.

The correlations were stronger in the *unconstrained* case. The reason might be the wider range of offline R^2 with the *unconstrained* experiment. A better understanding of the relationship between the offline and real-time results would require a higher number of sample points (more subjects), and a wider range of estimation accuracies (especially in the *constrained* and *resisted unconstrained* experiments, where the R^2 range is limited). The offline estimation accuracy (R^2) was calculated without the presence of feedback, whereas the user in a real-time test is able to correct erroneous estimations using feedback. The user's ability to interact with the control system is not considered in offline

estimation and so the real-time results provide a more meaningful evaluation of the estimation performance. Low correlation between offline estimation accuracy and real-time control is also reported by Lock et al. [107].

4.6 Summary

This chapter described a target acquisition protocol used to assess the usability of control paradigms based on *constrained* and *unconstrained* contractions. Three protocols, using constrained, *resisted unconstrained*, and *unconstrained* contractions were investigated. Offline estimation accuracy investigations (described in Chapter 3) and real-time target acquisition test results showed that the *constrained* based control method outperformed the *unconstrained* protocol without added resistance. However, when nominal resistance was added to the *unconstrained* protocol, no significant difference from that of the constrained protocol was found (both offline and online metrics resulted in $p>0.1$). These results suggest that the constrained and *unconstrained* based control schemes exhibit similar control performance when using similar EMG levels.

It is not obvious whether an *constrained* or *unconstrained* experiment is best suited for the case of an amputee user of a myoelectric control system. Using *unconstrained* based mirrored bilateral contractions of an intact limb to represent an impaired limb as in [93]-[89] may not be appropriate because much of the EMG modulation with position is due to the change in the muscle geometry through the excursion of joint angle. The action of a muscle changing length across a joint may not exist in the context of an amputee. In fact, in some surgical outcomes, the remaining muscle or tendon is sutured to the bone or

other muscle. In this scenario, an amputee's case may more closely resemble constrained contractions that occur in normally limbed individuals. In amputees with muscles that are not tied down, the muscle shortens, but not against a load; instead it can sometimes retreat with significant movement. Although this bears some similarity to the changing length in an intact limb, it does so without the resistance of a terminal point. Ultimately, amputated limb articulations likely differ from both *constrained* and *unconstrained* contractions of an intact limb and vary greatly from one amputee to another. Generalizable conclusions will therefore require an extensive investigation and access to many amputees. Nonetheless, it is an essential next step, and is the focus of our ongoing clinical research.

One of the limitations of the real-time test was the system processing delays. The processing times were bench tested using MATLAB^{TM} on a 3.30 GHz Intel Optiplex 990 workstation. The display adapter was a AMD Radeon HD 6670. The average time taken to extract the EMG features was 4 ms. The average estimation time for each ANN was 20 ms, resulting in 60 ms using the three ANNs (one ANN for each DOF). The average time taken for other processing and to render the movement in the interface was around 20 ms, resulting in total processing delay of roughly 85 ms. A margin of 15 ms was used and consequently, the screen was updated every 100 ms, to ensure that the processing time does not exceed the update time (the processing time was variable).

In a real scenario, when using a prosthetic limb, the processing will be faster with embedded implementation, and rendering times will be irrelevant. Faster processing time can potentially improve the completion time metric due to improved responsiveness of the system.

Chapter 5- Training Using Visual Targets

This chapter describes a training strategy based on visual targets, for simultaneous and proportional myoelectric control of multiple DOFs. *Mirrored bilateral training* is limited to unilateral amputees and requires additional apparatus to measure joint force or position from the intact limb. Moreover, the upper limb asymmetry in unilateral amputees can potentially reduce the estimation performance of the affected limb trained using the intact limb's force/position target. To address these issues, a training paradigm is proposed that can be applied to both unilateral and bilateral amputees without requiring force or position sensing equipment. This method removes the need for *mirrored bilateral training*.

In the proposed training paradigm, the subjects are prompted to elicit contractions according to displacements of a moving cursor on a computer display. Consequently, the cursor displacements are used as targets to train the system. In comparison of the proposed method with *mirrored training*, the goal is to show whether the correlations between the user contractions and a visual prompt are as strong as the correlations between bilateral contractions. The use of target cursor is similar to the method proposed by Choi et al. [96]-[98], and therefore, it can be regarded as an extension of this approach. The training protocol in [96]-[98] only included single DOF contractions, and a linear estimator was trained to map EMG to user intent. To achieve potential improvements, the proposed training paradigm includes combined motions in training and employs nonlinear estimation of user intent from EMG for test. Also, pronation-supination is added to the DOFs used in [96]-[98].

5.1 Experimental Design

The experiment was performed in the same session as the *mirrored training - constrained* experiment (described in Chapters 3 and 4) using the same group of subjects (ten able-bodied subjects, age range: 24-39 years, all right handed). The order of the two experiments in the session was randomized across the subjects. The same three DOFs (wrist flexion-extension, abduction-adduction and forearm pronation-supination) were used. As described previously, eight bipolar wireless surface electrodes (Delsys Inc.) were attached, equally spaced, around the circumference of subjects' dominant forearm. The electrodes were placed at approximately one-third of the forearm length, proximal to the elbow. To prepare the skin, conducting gel was applied before the electrode attachment. The EMG data were sampled at 1 KHz using a 16 bit A/D converter (NI PCIe-6363). The real-time raw EMG signals were visually inspected before the data collection to ensure the data quality. During the experiment, rest intervals were periodically provided based on the subject's preference to avoid fatigue.

5.1.1 Training Protocol

During the training, a cursor with orientation was presented on a computer display, while the subjects were prompted to elicit contractions according to the cursor displacement on the screen. The horizontal, vertical and orientation displacement of the cursor corresponded to flexion-extension, abduction-adduction, and pronation-supination, respectively.

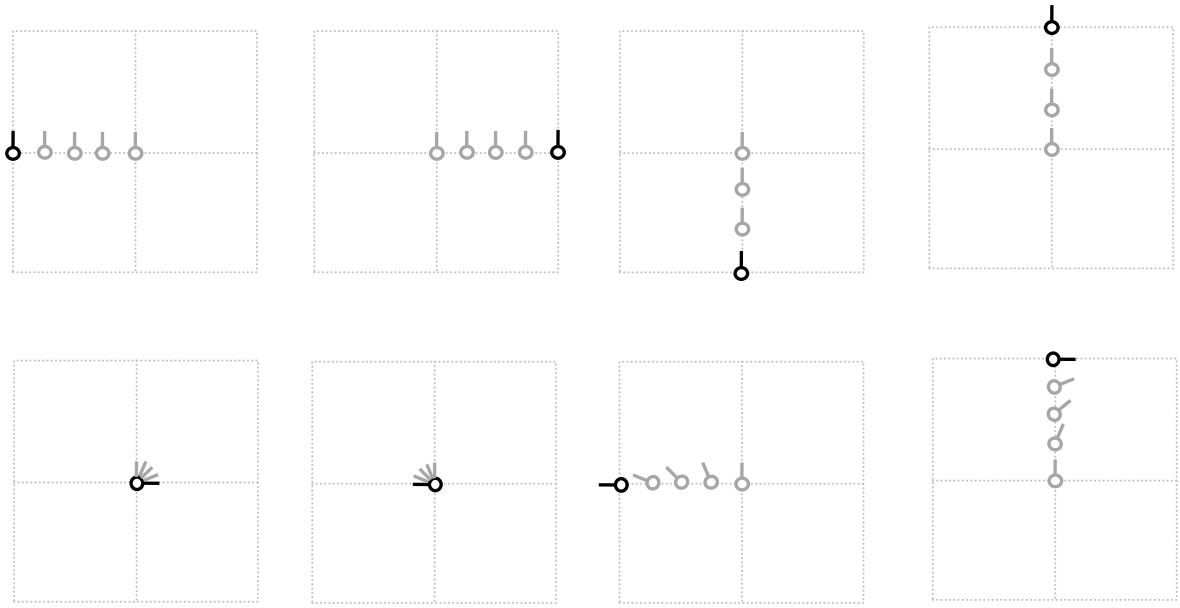

Figure 5.1. Training protocol: eight examples (trials) of the cursor movements displayed on the screen. From the top left to bottom right figure, the transition shown from the neutral position towards the target corresponds to 1-flexion, 2-extesion, 3-adduction, 4- abduction, 5-supination, 6-pronation, 7- simultaneous flexion and pronation, 8- simultaneous abduction and supination.

The training protocol is illustrated in Figure 5.1. The protocol involved fourteen trials, each corresponding to one of the fourteen contractions listed in Table 5.1. A two dimensional target with orientation (in a different color than the user's cursor) corresponding to the trial-specific contraction from Table 5.1 was displayed. Note that these are the same contractions as in Chapters 3 and 4. Also, a picture of the corresponding contraction was shown. The subjects were instructed to follow the target cursor movements in each DOF by producing contractions with intensities proportional to the dynamic cursor displacement. Each movement was 6 s in duration and included approximately 1 s of initial *no motion* (cursor at the neutral position i.e. screen center

with vertical orientation), 1 s of movement towards the target (cursor moving towards the target), 2 s of holding the target contraction (cursor on the target), 1 s of returning to *no motion* (cursor returning towards the neutral position), followed by holding *no motion* for the remaining time (cursor at the neutral position). Each trial involved four repetitions of a movement. The subjects were instructed to use a comfortable and sustainable range of contraction intensities. In case of trials with combined motions, according to the cursor movements, the subjects were instructed to elicit the active DOFs simultaneously. The EMG data and cursor traces were recorded.

Table 5.1. The practical contractions of wrist and forearm included in the protocol.

Index	Contraction
1	Flexion
2	Extension
3	Abduction
4	Adduction
5	Pronation
6	Supination
7	Simultaneous Flexion and Pronation
8	Simultaneous Flexion and Supination
9	Simultaneous Extension and Pronation
10	Simultaneous Extension and
11	Simultaneous Abduction and Pronation
12	Simultaneous Abduction and
13	Simultaneous Adduction and Pronation
14	Simultaneous Adduction and

5.1.2 Data Processing

Data processing was conducted offline. The EMG data were bandpass filtered between 10-450 Hz using a third order Butterworth filter. Subsequently, the EMG TD features

were calculated using a window size of 200 ms and an increment of 50 ms. The cursor displacement data were normalized to the range [-1,1] in each DOF and were used as the targets for training the estimators. Multilayer perceptron ANNs were employed for intent estimation. A separate ANN for each DOF was used as this has been shown to outperform a single ANN in force/position estimation in Figure 3.8. In each DOF, the ANN was trained using the EMG TD features as the inputs, and the cursor horizontal (in case of flexion-extension), vertical (in case of abduction-adduction) and orientation (in case of pronation-supination) displacement, as the target. The ANN structure was as described in Chapter 3; one hidden layer of five neurons, with the hidden and output layers having tan-sigmoid and linear activation functions, respectively. Levenberg-Marquardt back-propagation was set as the training method.

A four-fold cross-validation procedure was used to evaluate the offline cursor displacement estimation, where three out of four movement repetitions in each trial were used as the training set and the remaining repetition was used as the test set (training: 75%, testing: 25%). The offline cursor displacement estimation performance of each DOF was assessed using the coefficient of determination R^2 (as employed in Chapters 3 and 4).

$$R_k^2 = 1 - \frac{\sum_{t=0}^{N}\left(\widehat{f_k(t)} - f_k(t)\right)^2}{\sum_{t=0}^{N}(f_k(t) - \overline{f_k(t)})^2} \tag{5.1}$$

where $f_k(t)$ is the cursor displacement corresponding to the k^{th} DOF (e.g. for flexion-extension, the horizontal displacement is used), $\widehat{f_k(t)}$ is the corresponding estimate of the ANN, $\overline{f_k(t)}$ is the temporal average of $f_k(t)$, N is the number of data samples, and R_k^2 is the coefficient of determination of the k^{th} DOF. The offline estimation accuracies (R^2) of

each DOF were compared to those of the *mirrored training* (the *constrained experiment*, described in Chapter 3 and 4, was used for comparison as it had the highest results) using a one-way repeated-measures ANOVA test.

5.1.3 Target Acquisition Test

After completion of the training protocol, a target acquisition test (the same as that described in Chapter 4) was used to evaluate the system in a real-time control scenario with visual feedback. As in Chapter 4, the task was not designed as a Fitts' law style test.

Sufficient rest time, based on subject's preference, was provided between the training and real-time test. The control performance was quantified using the same metrics described in Chapter 4. For each performance metric, the results were compared to those of the *constrained mirrored training* using a one-way repeated-measures ANOVA test. The significance level was set to 0.05.

5.2 Results

The offline estimated cursor displacements for a representative subject are plotted in Figure 5.2(a). Figure 5.2 (b) shows the corresponding estimation error. The offline estimation accuracies (R^2) averaged across all subjects using mean ± standard error are listed in Table 5.2. The statistical analyses results are also presented in Table 5.2. The corresponding R^2 results of the *constrained mirrored training* are also shown for comparison. Based on the results, the offline estimation accuracy of the *constrained*

mirrored training were statistically higher than those of the proposed *visual training* approach in abduction-adduction and pronation-supination, but there was no difference between the two protocols in flexion-extension.

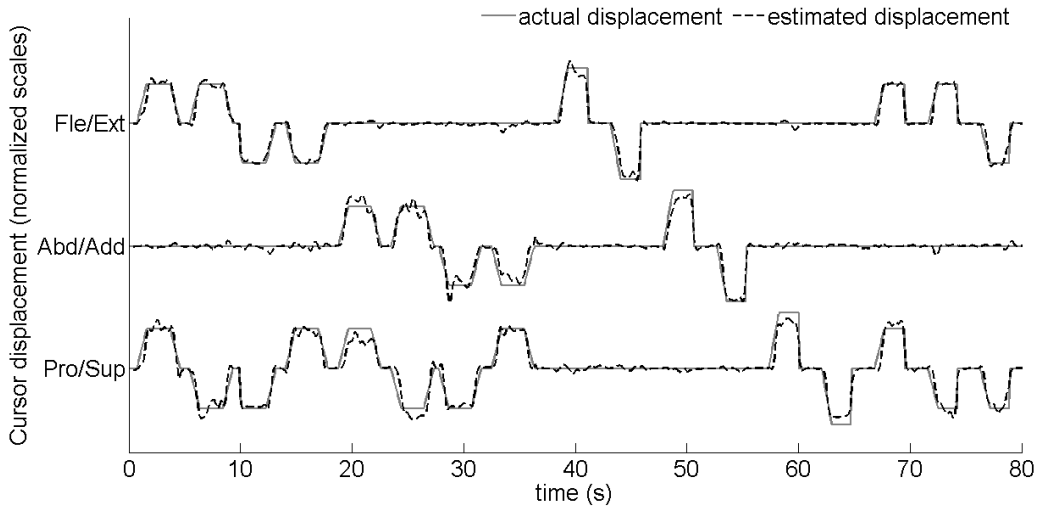

(a)

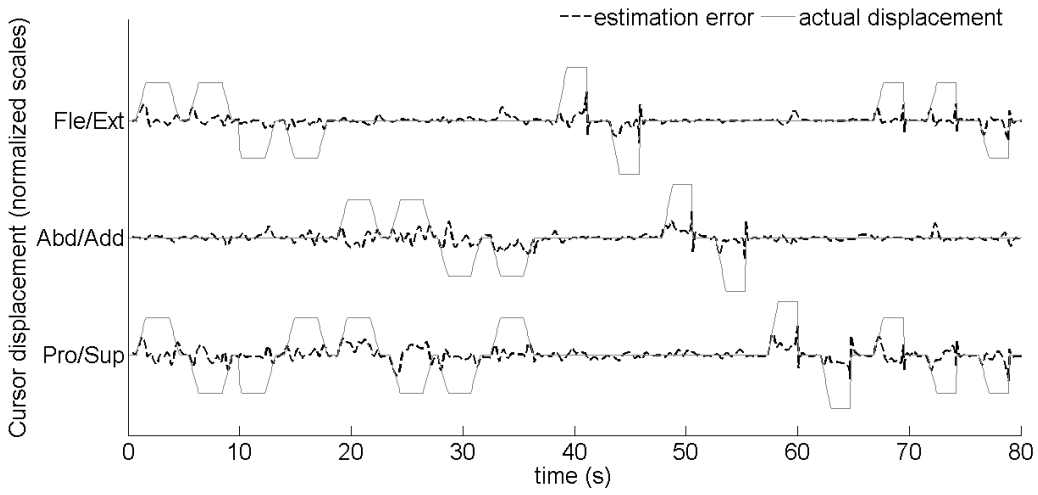

(b)

Figure 5.2. (a) The offline estimated cursor displacements are plotted for a representative subject. In this example, the offline R^2 values were 91% for flexion-extension, 87% for abduction-adduction, and 88% for pronation-supination. (b) The corresponding estimation error for Fig (a) is plotted.

Table 5.2. The offline estimation accuracies (R^2), averaged across all subjects, are shown using mean ± standard error for the *visual training* and constrained *mirrored training* experiments. The statistical analyses results are also included. The significant comparisons are marked by *.

	Visual Training	*Mirrored (Constrained)*	*p-value*
Fle/Ext	91.8 ± 0.4	89.8 ± 0.9	>0.01
Abd/Add	82.3 ± 1.0	90.8 ± 0.6	<0.001*
Pro/Sup	85.0 ± 0.6	88.5 ± 0.9	0.02*

Figure 5.3 depicts a three dimensional representation (where cursor orientation is shown in the Z-direction for visualization purposes) of cursor path traces in the target acquisition test for a representative subject in (a) *visual training* experiment and (b) *constrained mirrored training* experiment (only the first eight achieved targets were shown for clarity). Two-dimensional plots of path traces for all subjects in the target acquisition test are demonstrated in Figure 5.4, where only targets with the highest distance (90% of full range) are shown for clarity. The target acquisition test results averaged across all subjects are listed using mean ± standard error in Table 5.3.

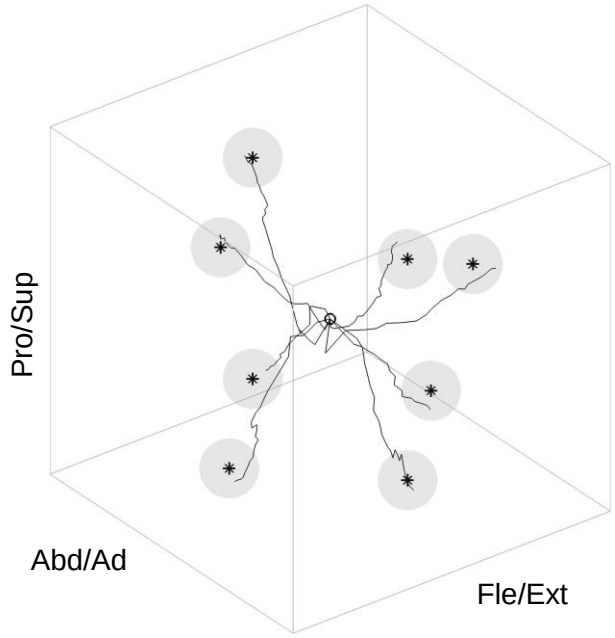

(a)

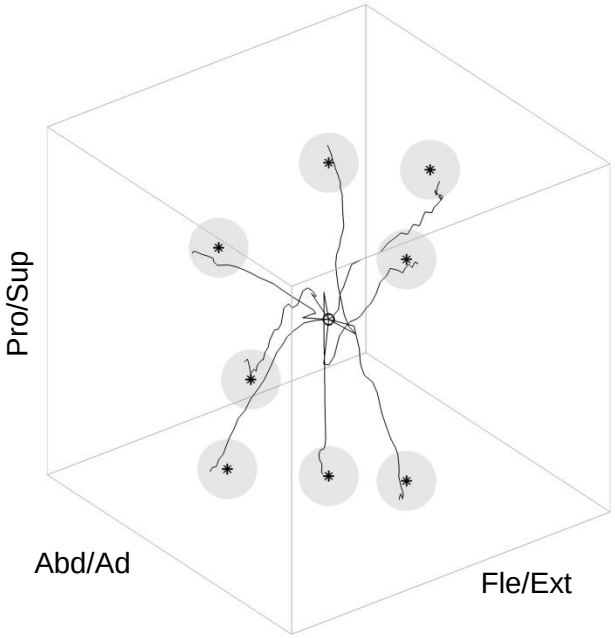

(b)

Figure 5.3. A 3D representation of path traces for a representative subject in the target acquisition test; the first eight acquired targets are shown for clarity: (a) *visual training* experiment, (b) *constrained mirrored training* experiment.

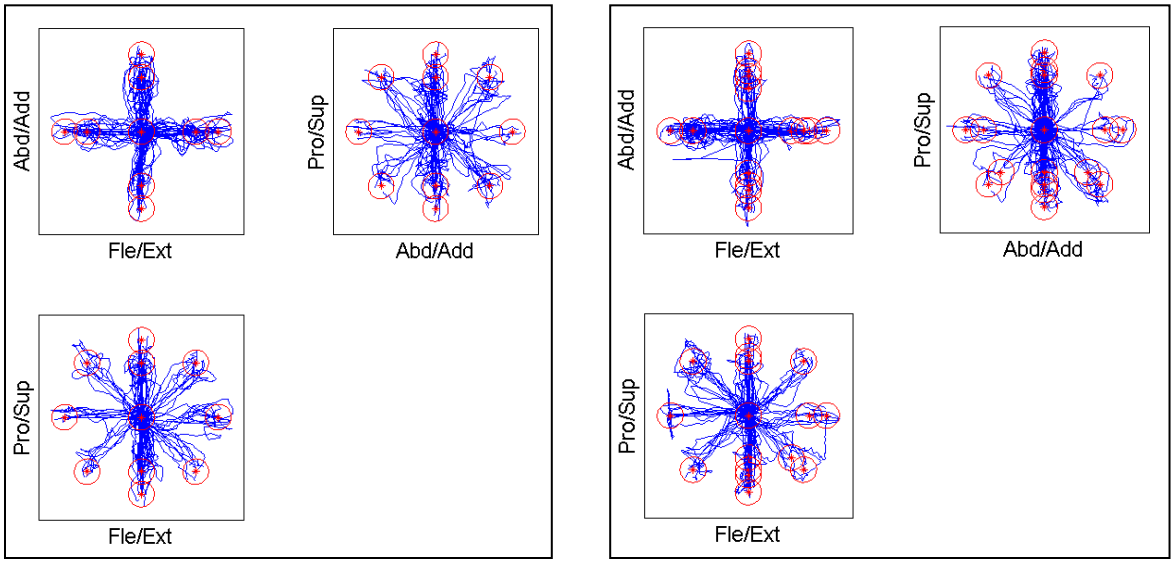

(a) Visual training experiment **(b) Constrained mirrored training experiment**

Figure 5.4. Two-dimensional plots of path traces for all subjects in the target acquisition test. Only targets with the highest distance (90% of full range) are shown for clarity for: (a) *visual training* experiment, (b) *constrained mirrored training* experiment.

Table 5.3. The target acquisition test results averaged across all subjects are shown using mean ± standard error for the *visual training* and *constrained mirrored training* experiments. The statistical analyses results are also included.

	Visual Training	*Mirrored (Constrained)*	*p-value*
Completion rate (%)	82.7 ± 2.4	84.4 ± 2.9	>0.1
Completion time (s)	4.37 ± 0.28	4.23 ± 0.27	>0.1
Overshoot	0.67 ± 0.07	0.72 ± 0.06	>0.1
Path Efficiency (%)	56.4 ± 4.2	59.3 ± 4.0	>0.1

During combined DOF targets, the users were encouraged to move the cursor in the corresponding directions, simultaneously. To assess this, the metric β was used, which is defined (as in Chapter 4) as the ratio between the number of times that the cursor speed in multiple DOFs were greater than the threshold *TH* (found empirically as 25% of full range per second) and number of times that the cursor speed in only one DOF was larger than *TH*. The β values averaged across all subjects calculated for single and combined DOF targets are shown in Table 5.4. As expected, the β values for combined DOF targets were significantly higher ($p<0.001$) than those of the single DOF targets. This shows that the subjects chose to move in multiple directions (DOFs), simultaneously during combined DOF targets. It should be noted that successful acquisition of targets did not require simultaneous movement towards the target. Therefore, encouragement played an important role to improve simultaneous movements of the cursor.

Table 5.4. The β values averaged across all subjects for single and combined DOF targets are shown using mean ± standard error. The significant comparisons are marked with *.

	Single DOF targets	*Combined DOF targets*	*p-value*
Visual Training	0.34 ± 0.04	2.37 ± 0.23	<0.001*

The subjects' offline and real-time results of the proposed method are listed in Table 5.5 and are plotted in Figure 5.5.

Table 5.5. The offline R^2 value and real-time performance metrics for each subject in the *visual training* experiment (the *constrained mirrored training* experiment results are shown in brackets for comparison).

	R^2 (%)	*Completion rate (%)*	*Completion Time (s)*	*Path efficiency (%)*	*Overshoot*
S1	89 (90)	91 (96)	3.94 (3.66)	64 (65)	0.71 (0.59)
S2	88 (89)	98 (93)	3.19 (3.47)	75 (64)	0.37 (0.65)
S3	85 (90)	75 (74)	5.28 (5.69)	42 (39)	0.69 (0.87)
S4	87 (93)	80 (96)	3.85 (3.41)	63 (76)	0.83 (0.65)
S5	88 (88)	77 (84)	4.81 (4.53)	53 (60)	0.93 (0.43)
S6	86 (91)	88 (87)	3.21 (3.54)	71 (71)	0.46 (0.43)
S7	86 (91)	84 (88)	3.71 (3.34)	67 (72)	0.51 (0.61)
S8	83 (91)	75 (79)	5.47 (4.76)	38 (55)	0.62 (1.06)
S9	87 (88)	79 (70)	4.89 (5.04)	47 (42)	1.06 (0.91)
S10	85 (88)	80 (78)	5.23 (4.90)	44 (49)	0.47 (1.01)

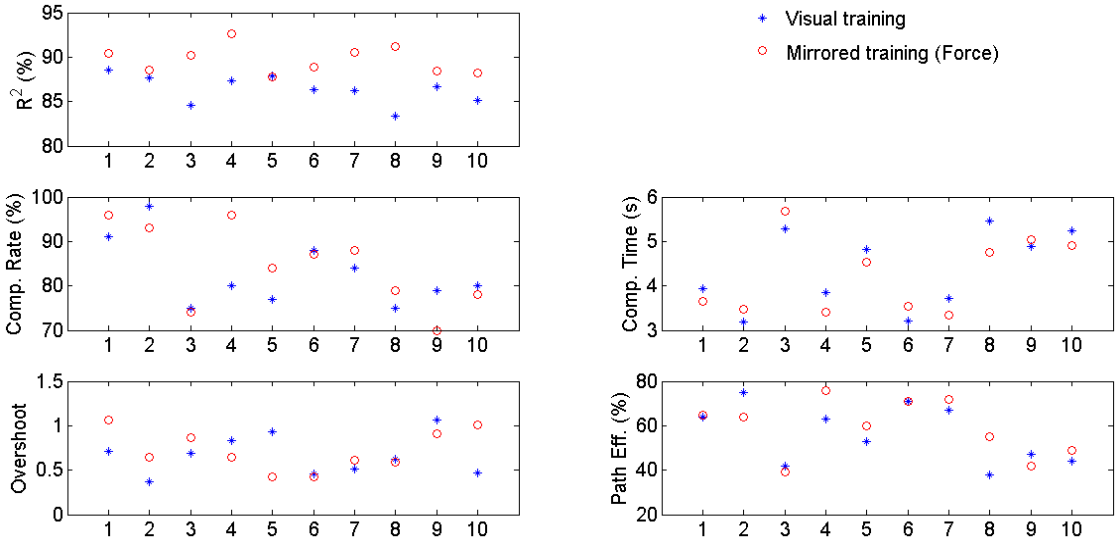

Figure 5.5. The R^2 values and real-time performance metrics for each subject for the *visual training* experiment and the *constrained mirrored training* experiment results are plotted for comparison.

5.3 Discussion

The offline estimation accuracies of the proposed method were found to be lower than those of the *constrained mirrored training*. This might be because the EMG levels were lower than those of the *constrained mirrored training* experiments, as the wrist was unconstrained.

The real-time results showed no significant difference between the *visual training* and *constrained mirrored training* methods. This suggests that the proposed *visual training* strategy may be preferable as it trains the estimators without the need for force/position data. The proposed training paradigm relied simply on the user's ability to synchronize dynamic contractions with the cursor movements on the computer screen.

In a clinical scenario, donning/doffing a prosthesis requires retraining the system. In this case, *mirrored bilateral training* is cumbersome since the training protocol requires complex force/position sensing apparatus which may be prohibitively expensive for the majority of clinics, and for home use. However, for the *visual training* approach, only a computer display is needed.

Nine out of ten subjects reported no difference between the control qualities using the *visual training* and *constrained mirrored training*, despite the fact that the wrist was unconstrained in the former and constrained in the latter. One subject noted a preference for the control quality of the *constrained mirrored training*, but it could possibly be due to a preference for the opposition of the wrist constraints.

To investigate the relationship between the offline estimation accuracies (R^2) and real-time performance metrics, scatter plots of performance metrics with respect to the offline

R^2 values are depicted in Figure 5.6. The correlation coefficients between the offline R^2 and each real-time performance metric are shown in Table 5.6.

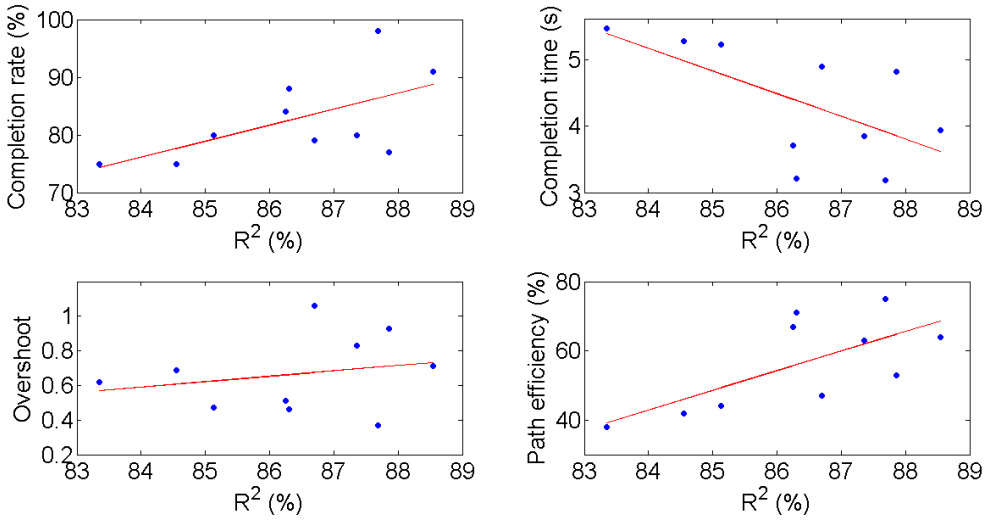

Figure 5.6. Scatter plots of the real-time performance metrics versus the offline R^2. The regression lines are shown in red.

Table 5.6. The correlation coefficients between the offline R^2 and each real-time performance metric

	Completion rate	*Completion time*	*Overshoot*	*Path Efficiency*
ρ	0.60	-0.63	0.23	0.70

Table 5.6 shows that in general, higher offline R^2 corresponded to improved real-time performance, as the ρ signs were as expected (except for *overshoot* in which the correlation was very low). However, correlation magnitudes between offline and real-time results were not strong. The correlation coefficients values are comparable to those of the *unconstrained experiment* from Chapter 4, which shared approximately the same

R^2 range with this experiment. A more thorough analysis of the relationship between the offline and real-time results would require a higher number of sample points (more subjects), and a wider range of estimation accuracies. The real-time test results provide a more relevant performance assessment because user interaction with the control scheme is reflected.

5.4 Summary

The mirrored training protocol discussed in Chapters 3 and 4 is not applicable to bilateral amputees. To overcome this issue, a training strategy using visual targets was proposed that removes the need for mirrored contractions. Because force or position sensing equipment is not required, the implementation complexity is also significantly reduced. Real-time test results showed that this method provided similar control performance as the previously used *mirrored training* strategy. These factors combined suggest that the proposed *visual training* method may be preferable to the previously described force and position based control paradigms.

Chapter 6- Comparison of SVM and ANN Based Control Schemes

In this chapter a comparison between the control performance of ANN and SVM based schemes using a three-dimensional Fitts' law test is conducted. For simultaneous estimation of DOFs, various linear and nonlinear estimators have been used in the literature, with multilayer perceptron ANNs as a common nonlinear approach (e.g. [8],[91]-[131]). Support vector regression has been previously used for single DOF, in offline force estimation for grasp [90],[151],[152], and flexion-extension [153]. In this work, for the first time, *real-time simultaneous* myoelectric control is performed using support vector regression. This experiment was motivated by the observation that SVM outperformed ANN in offline joint force and position estimation as shown in Chapter 3.

6.1 Experimental Design

Ten able bodied subjects (all right handed) participated in this experiment. A power analysis test (power=0.8) using pilot data was conducted and the minimum number of required subjects was found to be 3. Eight bipolar wireless surface electrodes (Delsys Inc.) were attached equally spaced around the circumference of subjects' right forearm. The electrodes were placed at approximately one-third of the forearm length, proximal to the elbow. The EMG data were sampled at 1 KHz using a 16 bit A/D converter (NI PCIe-6363).

6.1.1 Training Protocol

The novel visual training protocol (described in Chapter 5) was employed in this experiment. As described, the visual training approach is more practical than the mirrored training approaches, and yields comparable real-time performance. The protocol was the same as described in Section 5.1.1, in which, the subjects were prompted to elicit contractions consistent with a moving cursor on a computer screen. The same fourteen targets corresponding to the fourteen practical contractions of Table 4.1 were employed.

6.1.2 Data Processing

Data processing was conducted offline. An ANN and an SVM based system were trained using the same procedure explained in Section 5.1.2. The ANN based model used multilayer perceptron ANNs with the same structure described in Section 5.1.2. The SVM based model used SVMs with the previously described ν-support vector regression (ν-SVR) algorithm. A separate SVM was used for each DOF and their configuration was determined empirically. A radial basis function kernel was used, as well as a ν of 0.5, a cost of 0.2, and kernel function degree of 3. The Libsvm Matlab package [144] was used for simulation.

6.1.3 Fitts' Law Test

A Fitts' law [44] style target acquisition test was conducted to assess the usability of the ANN and SVM based control schemes. Unlike the target acquisition test described in

Chapters 4 and 5, here the estimated outputs of each DOF were mapped to the velocity (and not the displacement) of the control cursor in the corresponding DOF. Whereas displacement of the cursor was chosen in previous chapters to directly focus upon the controllability of the force/angle estimation methods, velocity control was chosen here to better reflect the control information imparted to commercial prosthetic devices as it was employed in [118]-[120].

A target was considered to be successfully acquired if the three dimensional Euclidean distance between the cursor and target was less than half the target width (W) for a full second (*dwell time*). If unsuccessful, the target was timed out after 15 seconds. Targets with combinations of three different widths and two different distances were used that generated six indices of difficulty as shown in Table 6.1.

Table 6.1. Different target distances and widths and the resulting indices of difficulty.

	Distance	*Width*	*ID*
1	1	0.10	3.46
2	1	0.15	2.94
3	1	0.25	2.32
4	0.5	0.10	2.59
5	0.5	0.15	2.12
6	0.5	0.25	1.59

The average processing time for estimation of a single sample using an ANN and an SVM was 20 ms and 2 ms, respectively. This allowed a faster screen update rate during SVM based control test. For the SVM control, the three SVMs required on average 6 ms. By taking into account the time taken for rendering and other data processing and adding a margin time (to ensure that the processing time does not exceed the update time, as the

processing times are variable), the screen was updated every 40 ms. For the ANN control, the three ANNs required on average 60 ms. Including the rendering and other data processing and a margin time (a larger margin was used as the ANN processing time variance was higher than the that of the SVM), the screen was updated every 100 ms.

To determine the effect of the estimation accuracy and processing speed separately, an additional SVM based scheme was included. With this system, delay was added after each intent estimation so that the screen was updated with the same rate as the ANN based system i.e. every 100 ms. This system is referred to as the *SVM-delayed*.

The targets used in the Fitts' law test corresponded to the fourteen practical contractions of Table 4.1. Six combinations of distances and widths were used for each target resulting in 14×6=84 targets. For every subject and control scheme (ANN, SVM, and SVM-delayed), the target order was randomized and the targets were divided into 6 trials of fourteen targets. For each subject, a complete test involved 84×3=252 targets. Each trial was completed using all control schemes performed in random order, before proceeding to the next trial.

In addition to the Fitts' law output of *throughput*, other performance metrics employed in the target acquisition test of Chapter 4 and 5, including the *completion rate*, *path efficiency*, and *overshoot*, were included to assess different aspects of the control quality. During the Fitts' law test, the estimated outputs of each DOF (limited to the range [-1,1]), were mapped to the cursor speed in the corresponding direction using a speed gain of 0.6 units per second. The speed gain was determined empirically in a pilot study with three

subjects. This gain was set to 0.6 units per second because it yielded the highest throughputs and path efficiency, and lowest overshoot.

To improve the control quality and to ensure that the cursor stopped when the user performed *no motion*, the cursor speed was set to zero for outputs smaller than a predefined threshold. This is another benefit of using velocity control that is not possible with position control (if thresholding is used for position control, close targets cannot be acquired).

The velocity thresholds were determined based on offline estimated outputs of *no motion* periods. The thresholds for the ANN and SVM based methods were determined independently. For every subject and every DOF, the threshold (*TH*) was computed using the formula below (determined empirically).

$$TH = \min\ \{0.2\ ,\ (\mu_y + 3\sigma_y)\} \tag{6.1}$$

where μ_y and σ_y are the mean and standard deviation of the offline estimated output of the corresponding DOF during *no motion*. The value of $(\mu_y + 3\sigma_y)$ was greater than 99% of the estimates during *no motion*. A maximum allowed threshold of 0.2 i.e. 20% of full range (determined empirically) was used. To avoid cursor speed discontinuity due to use of the threshold, the speed range was mapped to the output range above the threshold of each DOF. This is formulated in Equation (6.2).

$$\begin{aligned} &if\ \ |x| > TH \quad |v| = \frac{|x| - TH}{1 - TH} \\ &if\ \ |x| < TH \quad |v| = 0 \end{aligned} \tag{6.2}$$

where x is the estimated real-time output in a DOF, and $|v|$is the cursor speed magnitude in the corresponding DOF. This method allowed the user to generate near zero speeds, despite their contraction intensity being above the threshold.

6.1.4 Statistics

The offline estimation accuracies of the ANN and SVM based methods were compared using a one way repeated measures ANOVA test. The real-time control performance metrics of the ANN, SVM and SVM-delayed schemes were compared using a one way repeated measures ANOVA test followed by a *Bonferroni* post hoc test. The significance level was set to 0.05.

6.2 Results

6.2.1 Offline Results

The offline cursor displacement estimation accuracy results averaged across all subjects are listed in Table 6.2 using mean ± standard error. The statistical analyses results are also presented in Table 6.2, showing no significant difference between the offline R^2 of the ANN and SVM based methods in any DOF.

Table 6.2. The offline estimation accuracies R^2 (%) for all subjects are shown using mean ± standard error. The statistical analyses results are also listed.

	ANN	*SVM*	*p-value*
Fle/Ext	89.9 ± 1.1	89.7 ± 1.1	0.42
Abd/Add	82.4 ± 1.4	82.4 ± 1.2	0.96
Pro/Sup	83.9 ± 0.9	84.3 ± 0.9	0.47

Upon closer observation of the differences between the ANN and SVM estimates, the relative performance during *inactive periods* was identified. *Inactive periods* for a DOF are when the target displacements in that DOF are zero, but in other DOFs could be either zero or nonzero. This is different from *no motion* that denotes when all DOFs are zero (*no motion* is a subset of *inactive periods*).

Inactive periods are of special importance, as they impact the ability to be still in a DOF when desired, and may significantly affect the real-time control quality. For each DOF, the offline mean square error between the estimated and actual cursor displacements during inactive periods, are listed in Table 6.3.

Table 6.3. The offline mean square error results during the inactive segments for all subjects are shown using mean ± standard error. The statistical analyses results are also presented and the significant comparisons are marked with *.

	ANN	*SVM*	*p-value*
Fle/Ext	0.0039 ± 0.0006	0.0018 ± 0.0002	0.001*
Abd/Add	0.0089 ± 0.0010	0.0046 ± 0.0005	<0.001*
Pro/Sup	0.0101 ± 0.0006	0.0054 ± 0.0003	<0.001*

As shown in Table 6.3, the SVMs outperformed the ANNs during inactive periods in every DOF. The estimated outputs during inactive periods in each DOF are plotted for a representative subject in Figure 6.1 (a). The corresponding cumulative sums of the absolute values of the estimated outputs are plotted in Figure 6.1 (b) and show the higher accuracy of the SVMs during inactive periods.

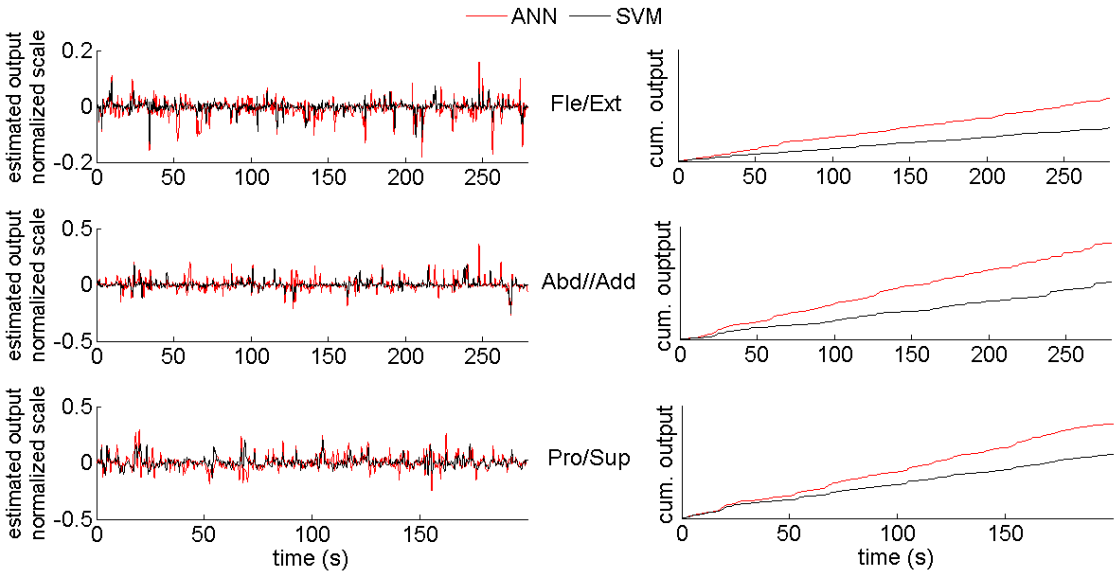

Figure 6.1. (a) The estimated outputs during inactive periods using ANNs and SVMs for a representative subject, (b) the cumulative sums of the absolute values of the corresponding estimated outputs during inactive periods.

To compare the efficacy of the SVMs and ANNs in estimation of different contraction intensities, for each DOF the data were divided into three segments where the target magnitude in the corresponding DOF was low (less than 20% of full range), medium (between 20% and 60% of full range) and high (greater than 60% of full range). The

offline mean square errors between the estimated and actual cursor displacements averaged across all subjects are presented in Tables 6.4, respectively.

Table 6.4. The offline mean square error results averaged across all subjects, are shown for the low, medium and high amplitude periods, respectively, using mean ± standard error. Significant comparisons are marked with *.

		ANN	*SVM*	*p-value*
Low amplitude periods	*Fle/Ext*	0.0047 ± 0.0007	0.0025 ± 0.0003	<0.001*
	Abd/Add	0.0097 ± 0.0010	0.0054 ± 0.0006	<0.001*
	Pro/Sup	0.0114 ± 0.0006	0.0068 ± 0.0004	<0.001*
Medium amplitude periods	*Fle/Ext*	0.0462 ± 0.0052	0.0487 ± 0.0055	0.48
	Abd/Add	0.0685 ± 0.0056	0.0715 ± 0.0054	0.29
	Pro/Sup	0.0653 ± 0.0030	0.0679 ± 0.0041	0.68
High amplitude periods	*Fle/Ext*	0.0302 ± 0.0034	0.0419 ± 0.0053	0.002*
	Abd/Add	0.0547 ± 0.0054	0.0712 ± 0.0072	0.002*
	Pro/Sup	0.0510 ± 0.0040	0.0607 ± 0.0040	0.006*

The results of Tables 6.4 show that the SVMs outperformed the ANNs in low amplitude periods (the MSEs of the ANNs were roughly two times those of the SVMs), while the ANNs estimation accuracies were higher during high amplitude periods.

The differences between the cost functions of SVM and ANN models appear to contribute to discrepancies between their estimation accuracies. For training an ANN, the cost function is the mean square error between the target and estimates. The support

vector regression (SVR), uses a kernel trick to map the input data to a high dimensional features space. For building the model, the data with estimates close to the target within a given threshold of ε are neglected. Only points outside the ε region (i.e. support vectors), contribute to the cost function. Also, the SVR seeks for the flattest function in the high dimensional features space, to reduce the complexity of the model.

Table 6.5 lists the threshold values computed using Equation (6.1) averaged across all subjects (the amputee results are shown in brackets), that were subsequently employed in the real-time test. Higher thresholds of the ANN based method imply that the SVMs outperformed the ANNs during *no motion* periods.

Table 6.5. Threshold values for each control scheme are listed using mean ± standard error.

	ANN	*SVM*
Fle/Ext	0.14 ± 0.01	0.09 ± 0.01
Abd/Add	0.18 ± 0.009	0.12 ± 0.02
Pro/Sup	0.16 ± 0.007	0.12 ± 0.01

The speed thresholds were determined using *no motion* periods, so that to ensure the control cursor stops when the user performs *no motion*. If thresholds were computed using *inactive periods* (where other DOFs can be zero or nonzero), the thresholds would increase, and without limiting the values, it would result in high thresholds for the ANNs (the average thresholds for abduction-adduction and pronation-supination would be 28%, and 30% of full range, respectively for able-bodied subjects). In this work, thresholds

based on *inactive periods*, were not used, because they are so high that they remove much of the usable range of motion, and can adversely affect the control quality.

Therefore, thresholds computed based on *no motion* periods were used. However, with these thresholds, it is possible that in some cases due to poor estimation accuracy (particularly with the ANNs) during inactive and low amplitude periods, outliers exceed the threshold, and negatively impact the control quality.

6.2.2 Fitts' Law Test Results

The real-time results obeyed Fitts' law as strong linear relationships were found between the movement times and indices of difficulty in every control scheme (Figure 6.2).

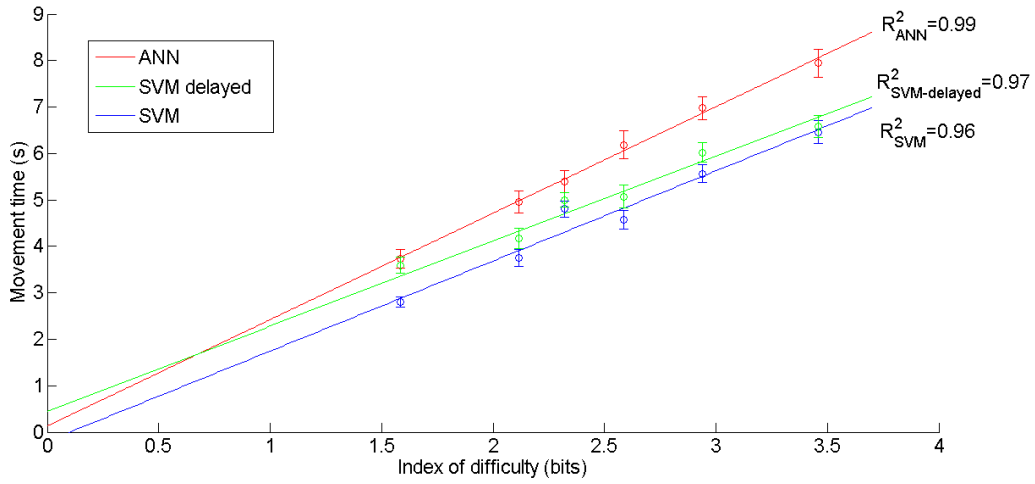

Figure 6.2. The relationships found between movement time and index of difficulty were strongly linear (R^2>0.95).

Figure 6.3 depicts a three dimensional representation (where cursor orientation is shown in the Z-direction for visualization purposes) of cursor path traces in the Fitts' law test for

a representative subject in (a) ANN and (b) SVM-delayed systems (only ten targets were shown for clarity). Figure 6.3 suggest that for cursor movements close to the target, during which the cursor had presumably low speed, the SVM control was smoother than the ANN control.

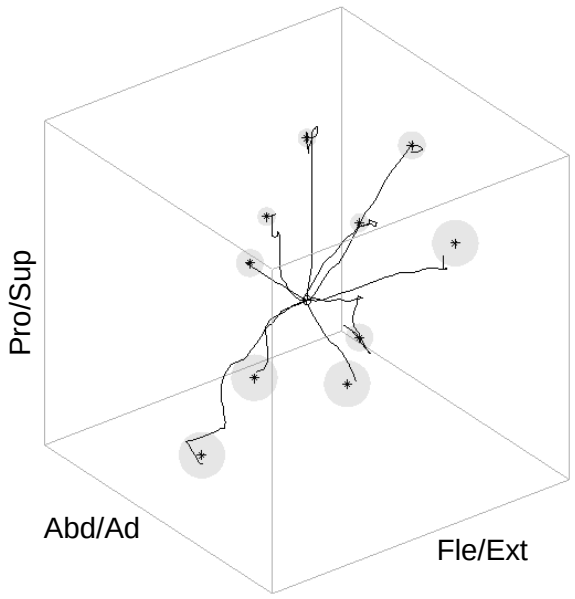

(a)

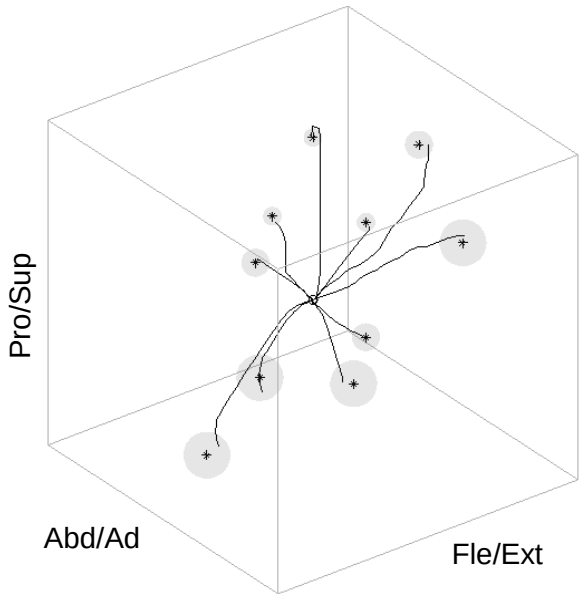

(b)

Figure 6.3. A 3D representation of path traces for a representative subject in the Fitts' law test; Ten targets are shown for clarity for (a) ANN, (b) SVM-delayed control schemes.

The Fitts' law test results averaged across all subjects are listed using mean ± standard error in Table 6.6. The corresponding statistical analyses results are shown in Table 6.7, which shows that the SVM and SVM-delayed control schemes outperformed the ANN based system in all four real-time performance metrics. The throughput of the SVM method was higher than that of the SVM-delayed system, but no difference was found between the SVM and SVM-delayed methods in other performance metrics.

Table 6.6. The Fitts' law test results for all subjects are shown using mean ± standard error.

	ANN	*SVM-delayed*	*SVM*
Throughput	0.54 ± 0.03	0.61 ± 0.04	0.66 ± 0.04
Completion rate (%)	92.5 ± 2.0	96.7 ± 1.1	98.9 ± 0.3
Overshoot	0.52 ± 0.06	0.27 ± 0.04	0.26 ± 0.02
Path Efficiency (%)	63.1 ± 2.1	75.1 ± 2.2	76.0 ± 1.9

Table 6.7. The statistical analyses results of the Fitts' law test (the significant comparisons are marked with *).

	ANN vs SVM	*ANN vs SVM-delayed*	*SVM vs SVM-delayed*
Throughput	$p<0.001$*	$p<0.001$*	$p=0.002$*
Completion rate	$p=0.001$*	$p=0.03$*	$p>0.1$
Overshoot	$p<0.001$*	$p<0.001$*	$p>0.1$
Path Efficiency	$p<0.001$*	$p<0.001$*	$p>0.1$

All subjects commented that they were able to use combined motions during the Fitts' law test. To investigate the use of simultaneous control of DOFs during Fitts' law test, a metric called β was defined as the ratio between the number of times that multiple DOFs were greater than 40% of full range and number of times that only one DOF was larger than 40% of full range. Table 6.8 shows the β values averaged across all subjects computed separately for single DOF and combined DOFs targets, and a comparison between single and combined DOF targets. It should be noted that if a combined DOFs target was not achieved in the first try (e.g. due to overshoot), single DOF motions might be needed to reach the target.

Table 6.8. The β values using mean ± standard error, and a comparison between single and combined DOF targets are shown. The significant comparisons are marked with *.

	Single DOF targets	*Combined DOFs targets*	*p-value*
ANN	0.24 ± 0.03	0.62 ± 0.04	<0.001*
SVM-delayed	0.08 ± 0.02	0.69 ± 0.11	<0.001*
SVM	0.11 ± 0.03	0.73 ± 0.10	<0.001*

As shown in Table 6.8, the use of combined motions during combined DOFs targets was significantly higher than that during single DOF targets. This was expected as combined motions were not needed to reach single DOFs targets, and shows that subjects performed combined motions to reach combined DOFs targets. Furthermore, the high β values of the ANN based system during single DOF targets might indicate an increase in inadvertent cursor movements. This is because when the user is trying to elicit one DOF, the second was also activated (due to estimation errors in inactive DOFs), or the case that user performing combined motions to correct this error. The offline mean R^2 values and real-time metrics for each subject are listed in Tables 6.90, 6.10, and 6.11.

Table 6.9. The offline R^2 and real-time performance metrics for each subject using the ANN scheme.

	R^2 (%)	*Completion rate (%)*	*Throughput (bit/s)*	*Path efficiency (%)*	*Overshoot*
S1	89	100	0.73	65	0.76
S2	86	87	0.42	54	0.27
S3	82	81	0.40	46	0.87
S4	88	94	0.59	47	0.53
S5	86	92	0.55	47	0.57
S6	82	92	0.46	52	0.36
S7	86	98	0.59	62	0.35
S8	85	86	0.43	54	0.36
S9	85	99	0.64	66	0.54
S10	86	98	0.61	61	0.62

Table 6.10. The offline R^2 and real-time performance metrics for each subject using the SVM-delayed scheme.

	R^2 (%)	*Completion rate (%)*	*Throughput (bit/s)*	*Path efficiency (%)*	*Overshoot*
S1	88	100	0.89	86	0.17
S2	87	92	0.42	60	0.12
S3	82	95	0.46	58	0.41
S4	88	98	0.63	68	0.29
S5	87	93	0.62	53	0.21
S6	81	92	0.51	61	0.31
S7	86	100	0.73	74	0.10
S8	86	99	0.45	59	0.28
S9	85	100	0.70	74	0.38
S10	85	99	0.67	75	0.41

Table 6.11. The offline R^2 and real-time performance metrics for each subject using the SVM scheme.

	R^2 (%)	*Completion rate (%)*	*Throughput (bit/s)*	*Path efficiency (%)*	*Overshoot*
S1	88	100	0.93	81	0.23
S2	87	98	0.48	64	0.30
S3	82	98	0.55	65	0.26
S4	88	99	0.69	68	0.28
S5	87	99	0.64	55	0.40
S6	81	99	0.53	63	0.23
S7	86	100	0.77	72	0.27
S8	86	99	0.55	72	0.17
S9	85	100	0.75	73	0.46
S10	85	99	0.73	77	0.30

The real-time performance metrics are plotted versus subject and control scheme in Figures 6.4, and 6.5, respectively.

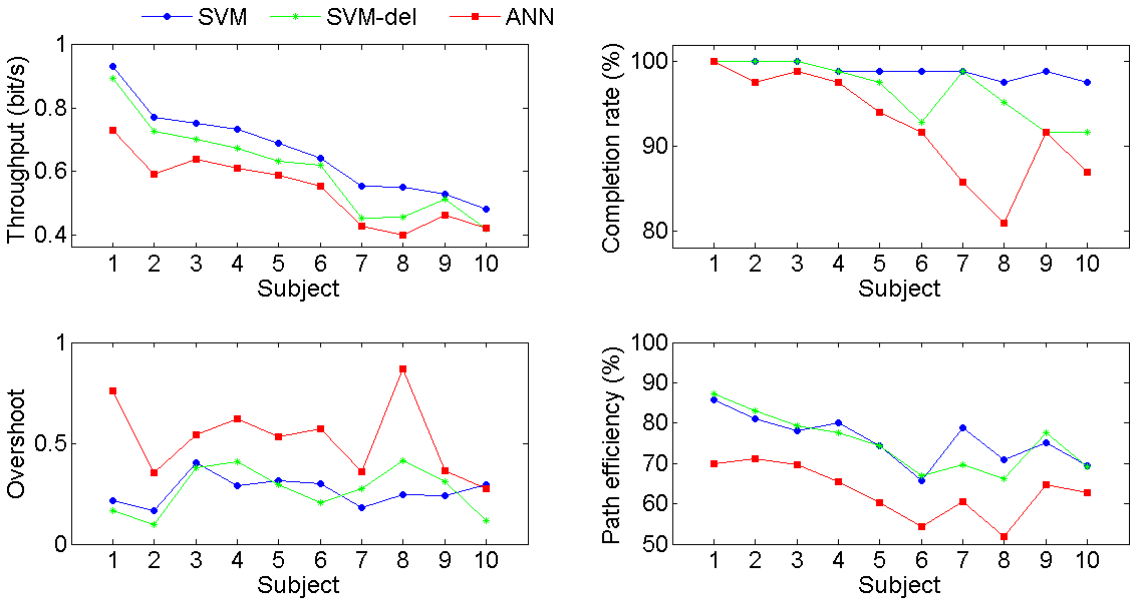

Figure 6.4. The real-time performance metrics for each control scheme are plotted versus subject.

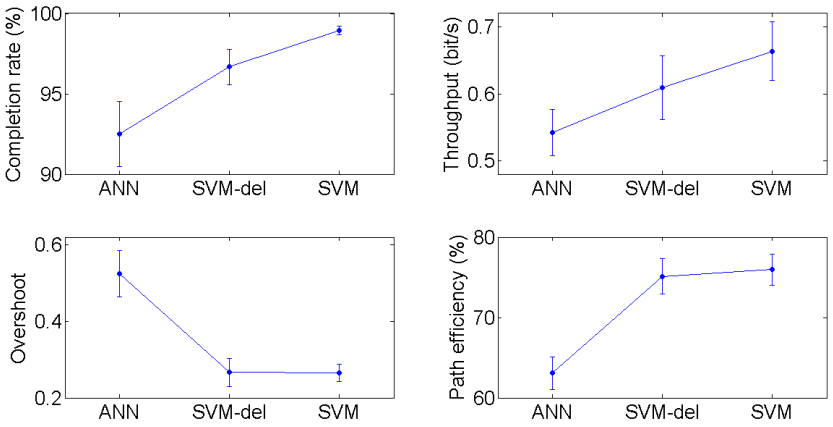

Figure 6.5. The real-time performance metrics averaged across all subjects are plotted versus control scheme.

6.3 Discussion

The subjects were asked to comment about the control quality during the breaks and after the experiment. All ten subjects found that inadvertent cursor movements were significantly less with the SVM and SVM-delayed methods than with the ANN based method. All subjects perceived the faster screen update of the SVM method, and preferred it. The subjects found that the control quality was more similar between the SVM and SVM-delayed tests, while the difference with the ANN based method was more noticeable.

The higher inadvertent cursor movements of the ANN based test may be explained by the low performance of the ANNs during low amplitude periods (the offline MSEs of the ANNs were roughly two times those of the SVMs during inactive and low amplitude periods as shown in Tables 6.3 and 6.4). This can significantly affect the control quality. For instance, when the users intended to perform pure wrist flexion during the real-time

test, the other DOFs should have remained inactive. However, low estimation accuracy during inactive periods (for those DOFs) may have resulted in unwanted cursor movements in these DOFs. Consequently, instead of pure movement of the cursor in the flexion direction, unwanted cursor rotation may have occurred. This deteriorates all real-time performance metrics. Similarly, when the cursor is near the target, low amplitude contractions are needed to control the small final movements. In this case, higher estimation accuracies of low amplitude contractions improve the target acquisition task, and therefore improve overall performance metrics.

The results of Table 6.4 suggest the possibility of using a hybrid system comprised of an ANN at higher intensities and a SVM at lower intensities. However, given that the processing speed of the SVM is much faster than that of the ANN for control (with computer), the hybrid method would slow the responsiveness of a purely SVM based system and possibly degrade the performance beyond the added benefit of the ANN. Such a hybrid system is outside the scope of this work.

All subjects perceived and used simultaneous control of multiple DOFs. All subjects also reported that combined motions were more efficient using the SVM and SVM-delayed systems than with the ANN based system. This could be due to inadvertent movements of the third DOF when combinations of two DOFs were used. Scatter plots of the real-time performance metrics versus offline R^2 are displayed in Figure 6.6. The correlation coefficients between the offline R^2 and each real-time performance metric are shown in Table 6.12.

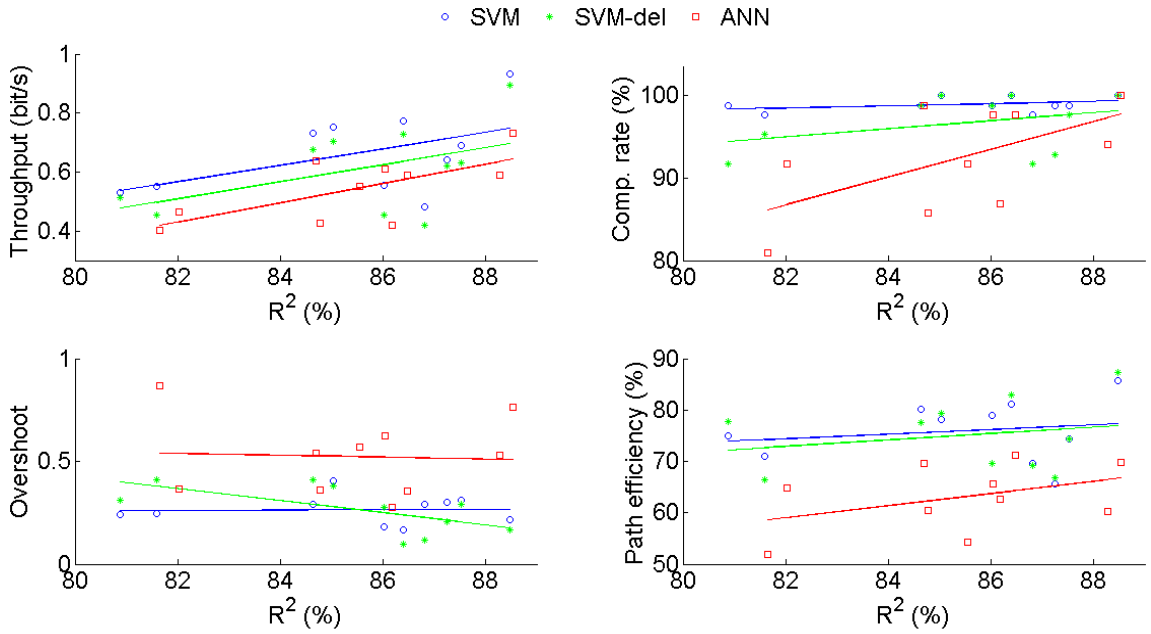

Figure 6.6. Scatter plots (with the regression lines) of the real-time performance metrics versus the offline R^2 values in the ANN, SVM-delayed, and SVM control schemes.

Table 6.12. The correlation coefficients between the offline R^2 and each real-time performance metric.

	ANN	*SVM-delayed*	*SVM*
Completion rate	0.60	0.36	0.36
Throughput	0.68	0.48	0.50
Overshoot	-0.05	-0.63	0.01
Path Efficiency	0.41	0.22	0.19

Table 6.12 shows that in general, higher offline R^2 corresponded to improved real-time performance in each metric (as the ρ signs were as expected), but the correlations were

not strong. For overshoot, in case of ANN and SVM, however, approximately no correlation was found, although there was mediocre correlation with SVM-delayed. Also, the correlation coefficient for the *overshoot* was close to zero in the *ANN* method. A complete description of the relationship between the offline and real-time results would require a higher number of subjects and a wider range of R^2. The lack of correlation between R^2 and overshoot might be because overshoot is more related to the estimation accuracy of low amplitudes, whereas R^2 represents the estimation accuracy across all amplitudes.

The histograms of the cursor speeds in each DOF during the Fitts' law test are plotted in Figures 6.7, 6.8, and 6.9, and show that the speed in every DOF is less than 10% of the full speed during the majority of the target acquisition time. This is because when a user performs a single DOF or combination of two DOFs contraction, other DOF(s) are inactive. Since the speed in a DOF is usually low, the performance of inactive and low amplitude periods significantly affects the real-time control performance.

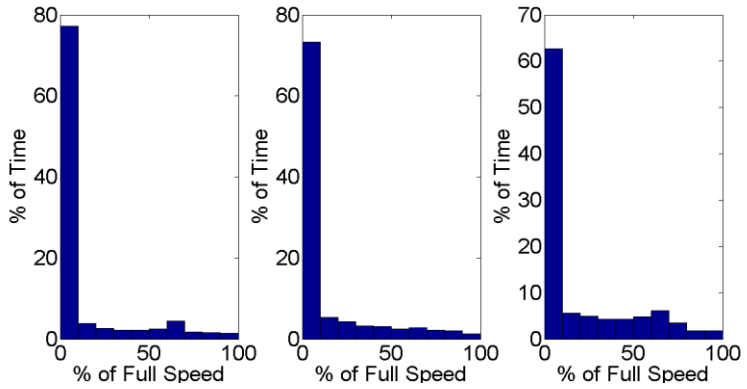

Figure 6.7. ANN control scheme speed histogram in (a) flexion-extension, (b) abduction-adduction, (c) pronation-supination.

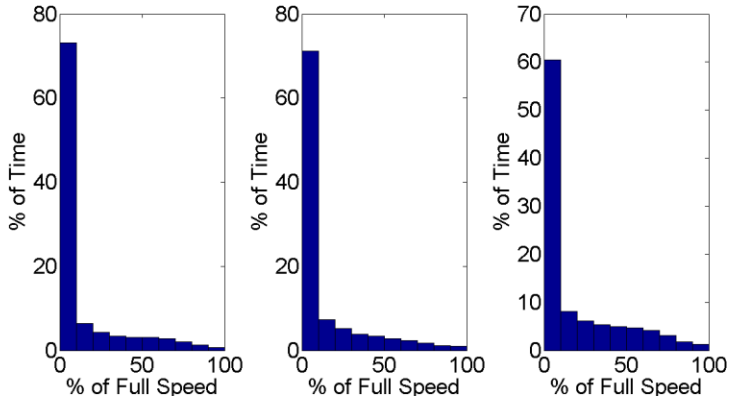

(a) (b) (c)

Figure 6.8. SVM-delayed control scheme speed histogram in (a) flexion-extension, (b) abduction-adduction, (c) pronation-supination.

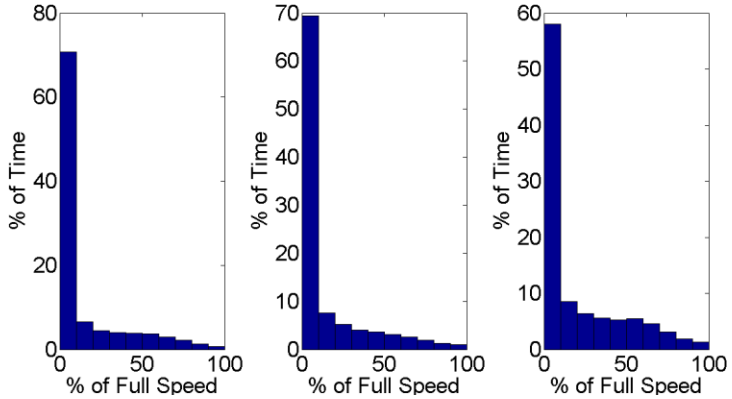

(a) (b) (c)

Figure 6.9. SVM control scheme speed histogram in (a) flexion-extension, (b) abduction-adduction, (c) pronation-supination.

Low amplitude periods were not only because of non-target DOFs, but also due to use of low speeds around the target (especially smaller targets). To demonstrate this, the speed histograms for the target DOFs, during single DOF targets, are plotted in Figure 6.10 and Figure 6.11 (for the SVM control), for the largest and lowest target widths (0.25, 0.10), respectively. The results show high use of low speeds which was due to periods during which the cursor was close to the target. Based on the plots, low speeds were more

frequent for smaller targets than larger targets. This is expected as smaller targets are more difficult to achieve, so that the cursor spends a longer time with low speed around the target before successfully acquiring the target.

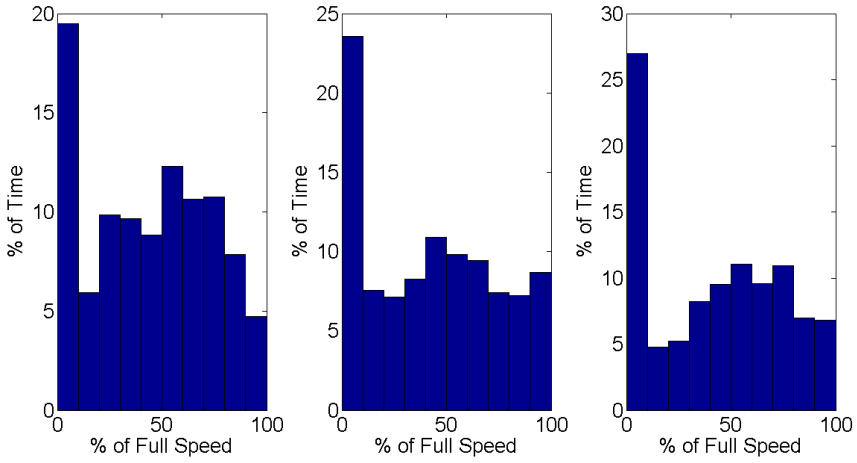

(a) **(b)** **(c)**

Figure 6.10. SVM control scheme speed histogram for target DOFs during single DOF targets with width of 0.25 in (a) flexion-extension, (b) abduction-adduction, (c) pronation-supination.

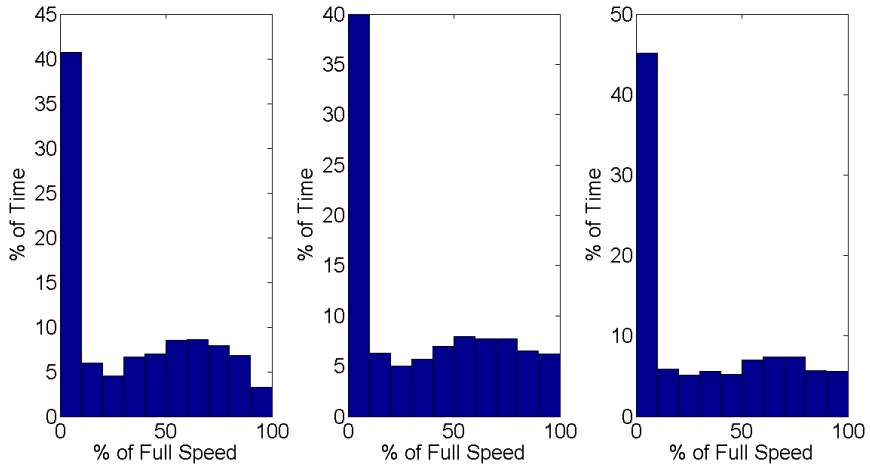

(a) **(b)** **(c)**

Figure 6.11. SVM control scheme speed histogram for target DOFs during single DOF targets with width of 0.1 in (a) flexion-extension, (b) abduction-adduction, (c) pronation-supination.

6.4 Amputee Results

Four trans-radial amputees participated in this study. Based on our clinical observation, it is extremely difficult for amputees to visualize simultaneous contractions of all three DOFs of the wrist. This visualization ability is necessary even with single DOF motions, as the user is required to maintain the non-target DOFs in an inactive state. Consequently, the abduction-adduction DOF was removed from the protocol to simplify the conceptual task and reduce the training complexity. The resultant number of training trials was eight (corresponding to the eight contractions from Table 4.1). During the Fitts' law test, the screen was updated every 80 ms for the ANN and SVM-delayed control, as the control involved two DOFs, so one ANN less than able-bodied experiment was needed, which reduced the processing time by 20 ms. For the SVM system, the screen update rate was 40 ms. The number of presented targets was 8×6=48 for each control scheme, and the total number of targets was 48×3=144.

Due to the fact that each amputee had substantially different residual limb morphologies, motor and sensory capabilities, and suitable options for electrode placement, the results cannot be directly compared between amputee participants. Instead, they are treated here as case studies.

6.4.1 Amputee I

The first amputee subject (male, 42 years old) had a congenital absence, with a long residual forearm (Figure 6.12). The offline R^2 values are listed in Table 6.13, and show that the SVM outperformed the ANN in pronation-supination, but there was no major difference in flexion-extension.

Figure 6.12. Amputee I's residual forearm.

Table 6.13. The offline R^2 (%) values for amputee I.

	ANN	*SVM*
Fle/Ext	80.7	81.7
Pro/Sup	76.3	80.8

The mean square estimation errors for low (<20% full range), medium (between 20% and 60% full range) and high (>60% full range) amplitude segments for every DOF are listed

in Table 6.14, which shows that the SVM outperformed the ANN in low amplitudes. For high amplitude estimates, the ANN outperformed the SVM in flexion-extension, but the SVM outperformed the ANN in pronation-supination. For medium amplitude segments, there was no major difference between the two methods. The offline estimates are plotted for combined DOF trials in Figure 6.13.

Table 6.14. The offline mean square error results are shown for the low, medium and high amplitude periods, respectively for amputee I.

		ANN	*SVM*
Low amplitude periods	*Fle/Ext*	0.0249	0.0156
	Pro/Sup	0.0253	0.0166
Medium amplitude periods	*Fle/Ext*	0.0686	0.0709
	Pro/Sup	0.0827	0.0816
High amplitude periods	*Fle/Ext*	0.0521	0.0610
	Pro/Sup	0.0718	0.0602

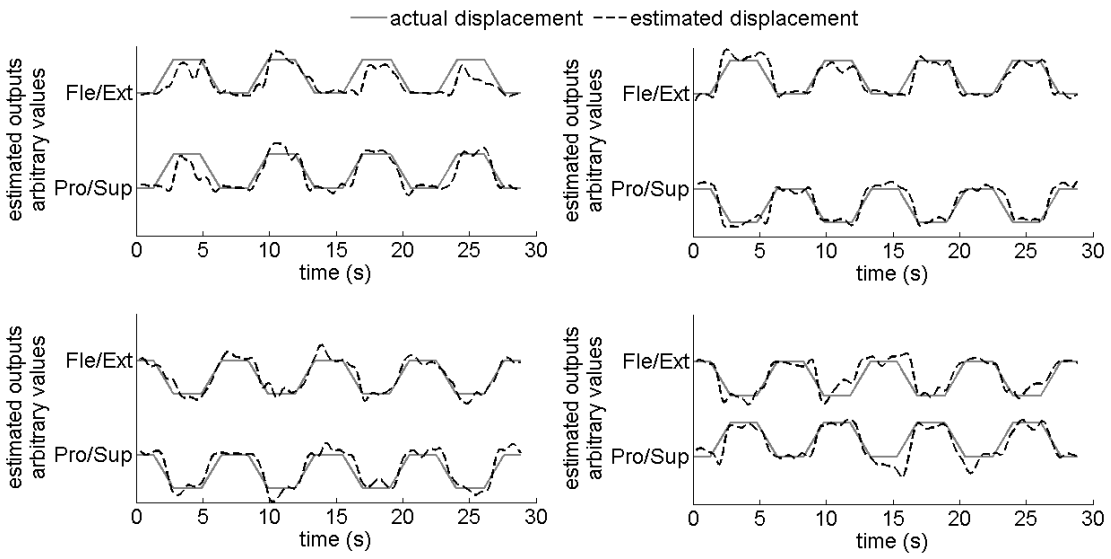

(a)

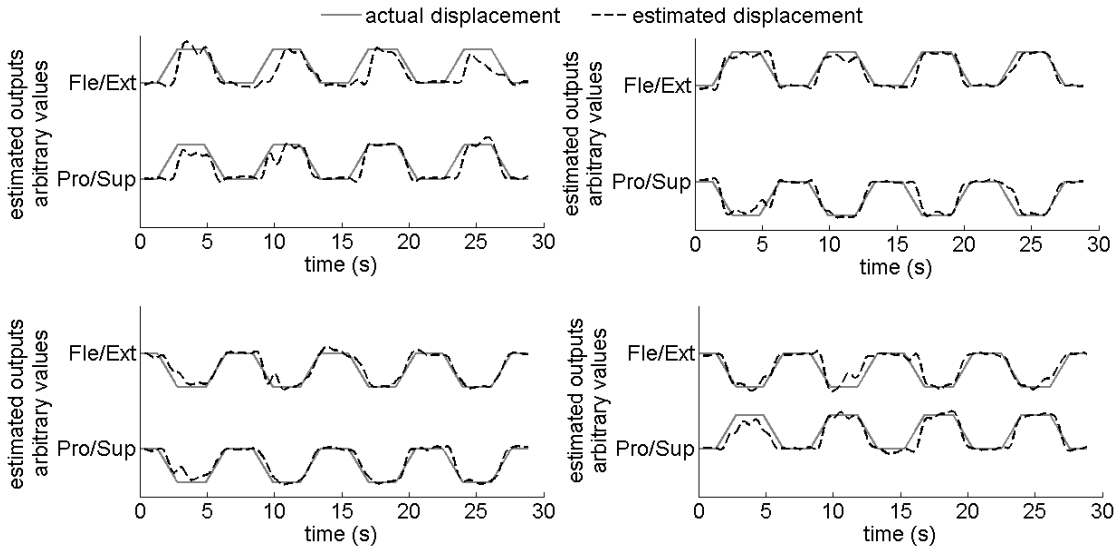

(b)

Figure 6.13. Amputee I: Offline estimated outputs are plotted for combined DOF trials for (a) ANN, and (b) SVM based methods. The four plots correspond to top left: simultaneous extension & supination, top right: simultaneous extension & pronation, bottom left: simultaneous flexion & pronation, bottom right: flexion & supination.

The Fitts' law test results are listed in Table 6.15, showing that the SVM and SVM-delayed control schemes outperformed the ANN based system in *throughput* and *path efficiency*, but that no large difference was found in *completion rate* and *overshoot*. Also, the *throughput* of the SVM system outperformed that of the SVM-delayed, but no significant difference was found between them in other performance metrics.

Table 6.15. The Fitts' law test results for amputee I.

	ANN	*SVM-delayed*	*SVM*
Throughput (bps)	0.57	0.59	0.62
Completion rate (%)	95.8	95.8	100
Overshoot	0.13	0.02	0.10
Path Efficiency (%)	76.7	85.1	84.5

The *path efficiency* of the SVM and SVM-delayed systems was much higher than that of the ANN scheme. For other metrics, however, the difference between the ANN and SVM based control was not as large as that with able-bodied subjects. This appears to be because the experiment was limited to two DOFs, in which the number of inactive DOFs was less than that of a three DOF experiment. The advantage of the SVMs over the ANNs appears to be a consequence, at least partially, of more reliable characterization of inactive DOFs. With fewer DOFs under control (and therefore inactive DOFs during single DOF or combination of two DOFs motions), this advantage is reduced.

The subject indicated that he perceived simultaneous and proportional control of DOFs. He remarked that he was able to control the cursor using combined motions. The β values (described in Section 6.2.2) are shown for single and combined DOF targets in Table 6.16, which shows that the β values of combined DOF targets were considerably higher than those of single DOF targets. This demonstrates that the use of combined motions was substantially higher with combined DOF targets, which was expected, as there was no need for combined motions with single DOF targets. More importantly, it shows that the subject performed combined motions to acquire combined DOF targets (although he did not have to use combined motions for velocity control).

Table 6.16. The β values are shown separately for single and combined DOF targets for amputee I.

	Single DOF targets	*Combined DOFs targets*
ANN	0.07	0.45
SVM-delayed	0.03	0.49
SVM	0.01	0.50

The user subjectively preferred the SVM and SVM-delayed control over the ANN control, because inadvertent movements with the ANN were noticeably higher than those of the SVM based control. He commented that with the ANN control, during single DOF contractions, the cursor sometimes had unwanted movements in the other DOF. He did not perceive a significant difference between the SVM and SVM-delayed control. The higher real-time performance of the SVM over the ANN can be related to their estimation

accuracy during inactive and low amplitude periods. Moreover, the overall estimation accuracy of pronation-supination with the SVM was higher than that with the ANN.

6.4.2 Amputee II

The second amputee subject (male, 62 years old) had a traumatic amputation, with a medium length residual forearm and substantial scarring of the distal end (Figure 6.14). The offline R^2 values are listed in Table 6.17, which shows that there was no major difference between the ANN and SVM systems.

Figure 6.14. Amputee II's residual forearm.

Table 6.17. The offline R^2 (%) values for amputee II.

	ANN	*SVM*
Fle/Ext	83.2	83.8
Pro/Sup	83.6	82.7

The mean square estimation errors for low (<20% full range), medium (between 20% and 60% full range) and high (>60% full range) amplitude levels for every DOF are listed in Table 6.18 which shows that the SVM outperformed the ANN in low amplitudes. For high amplitudes, the ANN outperformed the SVM. For medium amplitudes, there was no major difference between the two methods. The offline estimates are plotted for combined DOF trials in Figure 6.15.

Table 6.18. The offline mean square error results are shown for the low, medium and high amplitude periods, respectively for amputee II.

		ANN	*SVM*
Low amplitude periods	*Fle/Ext*	0.0171	0.0099
	Pro/Sup	0.0092	0.0053
Medium amplitude periods	*Fle/Ext*	0.0549	0.0562
	Pro/Sup	0.0506	0.0543
High amplitude periods	*Fle/Ext*	0.0591	0.0684
	Pro/Sup	0.0564	0.0798

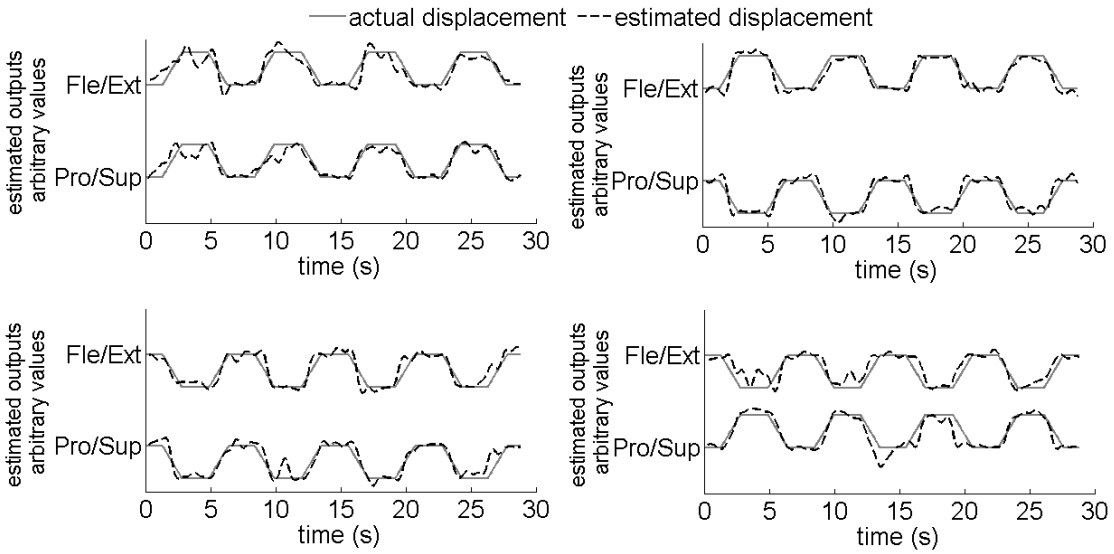

(a)

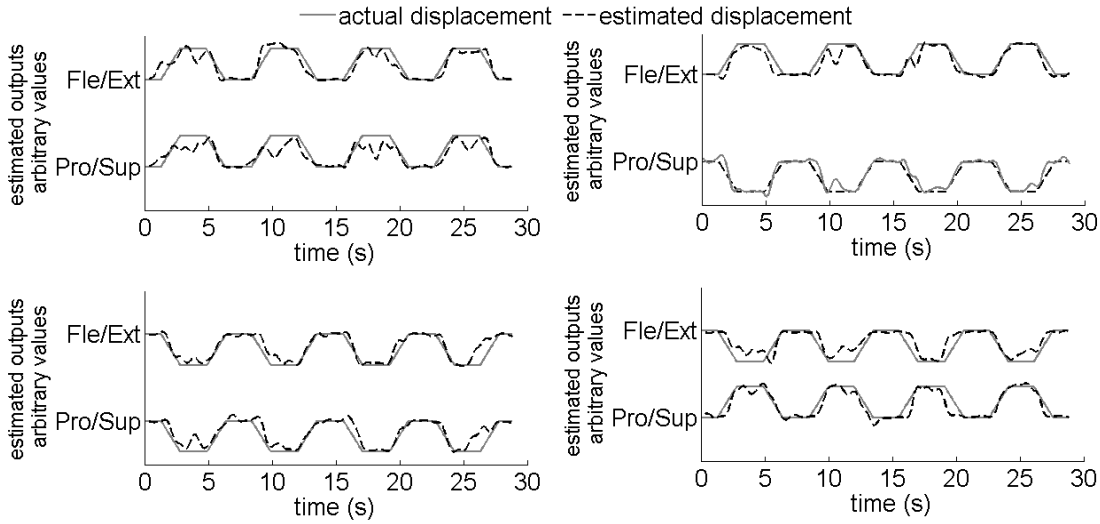

(b)

Figure 6.15. Amputee II: Offline estimated outputs are plotted for combined DOF trials for (a) ANN, and (b) SVM based methods. The four plots correspond to top left: simultaneous extension & supination, top right: simultaneous extension & pronation, bottom left: simultaneous flexion & pronation, bottom right: flexion & supination.

The Fitts' law test results are listed in Table 6.19, which shows that the SVM and SVM-delayed systems outperformed the ANN system in *throughput* and *completion rate*. For *overshoot* and *path efficiency*, the control schemes had similar performance. Again, the differences between the results of ANN and SVM based schemes were not as large as that with able-bodied users. Similar to the first amputee subject, this may be because the experiment was limited to two DOFs.

Table 6.19. The Fitts' law test results for amputee II.

	ANN	*SVM-delayed*	*SVM*
Throughput (bps)	0.37	0.41	0.40
Completion rate (%)	83.3	89.6	93.8
Overshoot	0.42	0.35	0.40
Path Efficiency (%)	63.6	70.7	66.1

The subject commented that he was able to use combined movements. However, he seemed to prefer performing sequential movements to achieve combined DOF targets (always first completing the desired rotation). It is expected that the use of combined motions would improve with practice and encouragement. The β values are shown for single and combined DOF targets in Table 6.20. The β values for combined DOF targets were somewhat low due to use of sequential movements in some cases.

Table 6.20. The β values are shown separately for single and combined DOF targets for amputee II.

	Single DOF targets	*Combined DOFs targets*
ANN	0.11	0.31
SVM-delayed	0.08	0.16
SVM	0.07	0.16

The subject remarked that he did not feel a major difference between the three control schemes, but noted that the ANN felt slightly faster.

6.4.3 Amputee III

The third amputee subject (male, 24 years old) had a congenital absence with a short forearm (Figure 6.16). The offline R^2 results are listed in Table 6.21, and show that the SVM again outperformed the ANN in pronation-supination, but there was no considerable difference in flexion-extension.

Figure 6.16. Amputee III's residual forearm.

Table 6.21. The offline R^2 (%) values for amputee III

	ANN	*SVM*
Fle/Ext	78.6	77.4
Pro/Sup	81.3	84.5

The mean square estimation errors for low, medium and high amplitude levels for every DOF are shown in Table 6.22, which demonstrates that the SVM outperformed the ANN in low and medium amplitude estimates. For high amplitude segments, the ANN outperformed the SVM in flexion-extension, but the SVM outperformed the ANN in pronation-supination.

Table 6.22. The offline mean square error results, are shown for the low, medium and high amplitude periods, respectively for amputee III.

		ANN	*SVM*
Low amplitude periods	*Fle/Ext*	0.0137	0.0122
	Pro/Sup	0.0085	0.0059
Medium amplitude periods	*Fle/Ext*	0.0714	0.0629
	Pro/Sup	0.0816	0.0758
High amplitude periods	*Fle/Ext*	0.0913	0.1080
	Pro/Sup	0.0767	0.0613

The offline estimates are plotted for combined DOF trials in Figure 6.17. The plots demonstrate that in general the estimation performance for combined motions was relatively low. This is most evident in the top-right plot (simultaneous extension and supination). Similarly poor performance was observed with single DOF trials, as with extension and supination single DOF motions, considerable estimation error was found in inactive DOF. It was observed that if the system was only trained with only single DOF trials, the estimation plots for single DOF trials considerably improved, and the inactive DOF was close to zero (the interference between the DOFs was removed). The low performance of combined motions could be because the subject may not have elicited the motions using the same relative intensities making it more similar to a single DOF contraction. Also, it can be seen in Figure 6.17, that the timing between the visual prompt and the contractions was poor in comparison with that of the previous subjects.

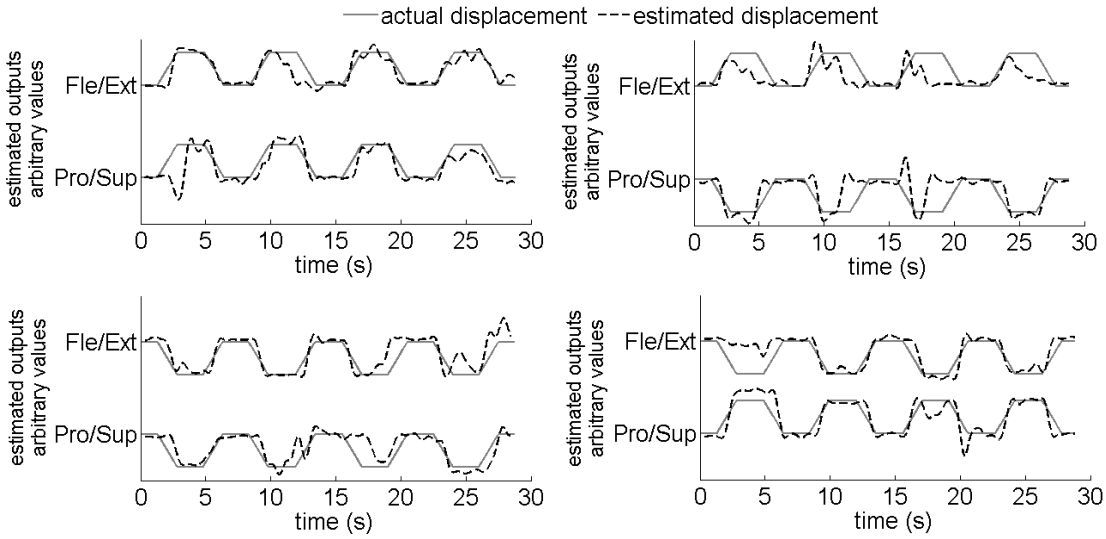

(a)

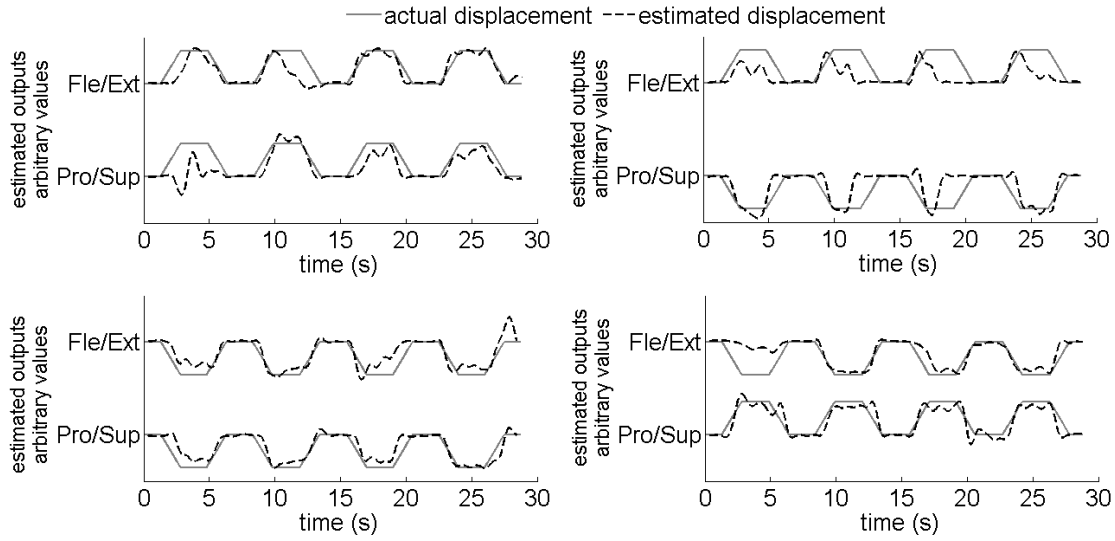

(b)

Figure 6.17. Amputee III: Offline estimated outputs are plotted for combined DOF trials for (a) ANN, and (b) SVM based methods. The four plots correspond to top left: simultaneous extension & supination, top right: simultaneous extension & pronation, bottom left: simultaneous flexion & pronation, bottom right: flexion & supination.

For the Fitts' law test, it was found that when the system was trained using only data from single DOF trials, the control quality was higher than the case that the system was

trained with the full data set. This appears to be because perhaps some combined contractions (such as simultaneous extension and pronation) did not result in repeatable patterns, as the subject did not perform those contractions correctly. This can be because of the complexity or unnaturalness of these motions (for the subject) or lack of experience of the user. Since the experiment duration was kept less than an hour to avoid fatigue, the user did not have a chance for more practice with the motions. Considerable care was taken to avoid imposition of the amputee subjects, which limited the ability for extensive training, or iteration of the trials. Also, access to the amputees was limited, preventing the option of sessions over multiple days.

Although the system was trained with only single DOF contractions, the real-time test could have included combined DOF targets as in [99],[100]. In this experiment, however, the combined DOF targets were excluded from the Fitts' law test due to time constraints. The SVM-delayed test was also omitted. The control cursor was, however, allowed to move in both DOFs simultaneously. In other words, the outputs of the non-target DOF were allowed to move.

The Fitts' law test results (with single DOF targets only) are listed in Table 6.23. The results show that the SVM control substantially outperformed the ANN control. This is particularly reflected in the *completion rate*. The user strongly preferred the SVM over the ANN control. The considerable difference between the ANN and SVM appears to be because the SVM outperformed the ANN in all low, medium and high amplitude levels (except for flexion-extension in high amplitudes). Also, it shows the user's inability to accommodate the unwanted movements associated with the ANN control, and demonstrates the higher robustness of the SVM based method. The poorer results for this

subject reflect a possible challenge with this approach. In order for proper training, it is assumed that the user contractions are well synchronized with the visual prompts. This subject did not consistently coordinate with the cursor motion (particularly during combined motions with equal intensity).

Table 6.23. The Fitts' law test results for amputee III

	ANN	*SVM*
Completion rate (%)	45.8	83.3
Throughput (bit/s)	0.42	0.50
Overshoot	0.54	0.15
Path Efficiency (%)	81.2	91.3

6.4.4 Amputee IV

The fourth amputee subject (male, 47 years old) had a traumatic amputation with a short residual forearm. The offline R^2 results are listed in Table 6.24, and show no difference between the ANN and SVM based systems.

Table 6.24. The offline R^2 (%) values for amputee IV

	ANN	*SVM*
Fle/Ext	75.3	75.5
Pro/Sup	82.2	82.6

The mean square estimation errors for low, medium and high amplitude levels for every DOF are shown in Table 6.25. The SVM outperformed the ANN in low amplitude segments, but the ANN outperformed the SVM in high amplitudes. For medium amplitudes, the ANN outperformed the SVM in pronation-supination, but no difference was found in flexion-extension.

Table 6.25. The offline mean square error results are shown for the low, medium and high amplitude periods, respectively, for amputee IV.

		ANN	*SVM*
Low amplitude periods	*Fle/Ext*	0.0203	0.0135
	Pro/Sup	0.0118	0.0052
Medium amplitude periods	*Fle/Ext*	0.0767	0.0794
	Pro/Sup	0.0694	0.0806
High amplitude periods	*Fle/Ext*	0.0928	0.1165
	Pro/Sup	0.0623	0.0709

The offline estimates are plotted for the combined DOF trials in Figure 6.18, showing that the estimation performance for combined motions were generally low. This is particularly evident in the simultaneous flexion-pronation (the top-left plot).

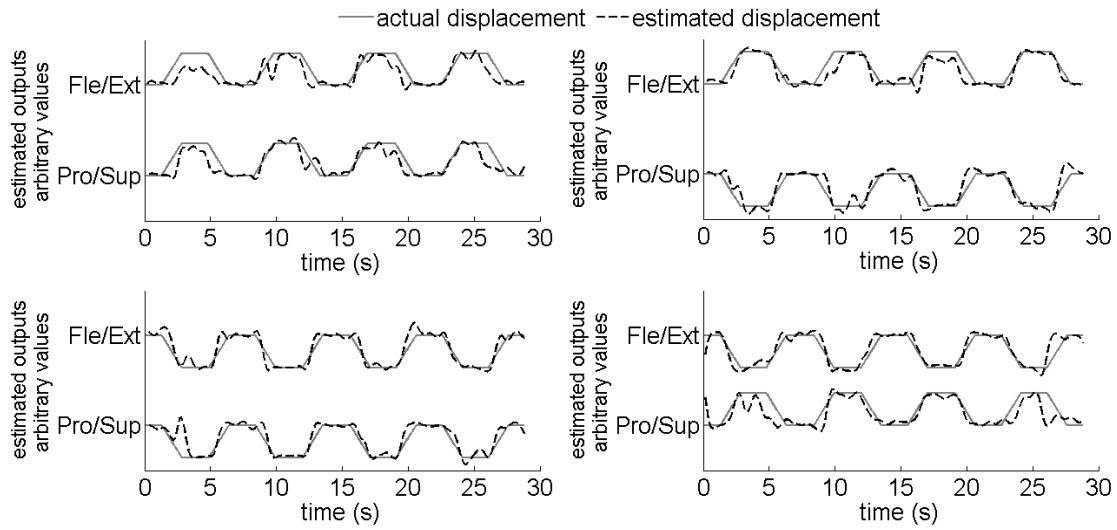

(a)

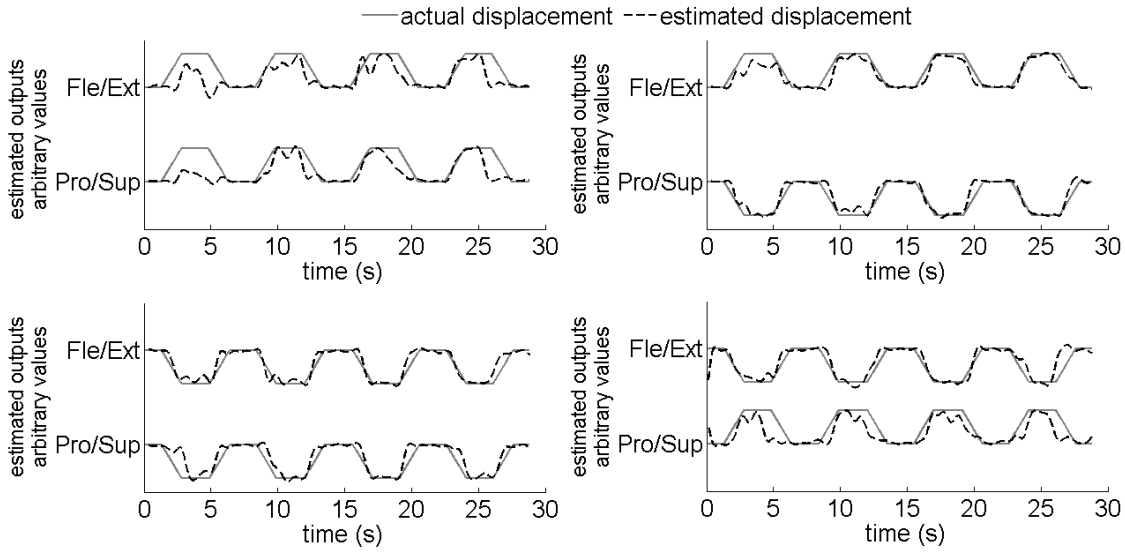

(b)

Figure 6.18. Amputee IV Offline estimated outputs are plotted for combined DOF trials for (a) ANN, and (b) SVM based methods. The four plots correspond to top left: simultaneous flexion & pronation, top right: simultaneous flexion & supination, bottom left: simultaneous extension & supination, bottom right: extension & pronation.

As with amputee III, it was found that the control quality was higher when the system was trained only with single DOF trials, rather than training with the full data set. Again, this may be because of poor contraction-cursor coordination during some combined DOF contractions. This was likely because the subject did not perform these contractions correctly because of the complexity or unnaturalness of these contractions.

Due to time constraints and concerns about fatigue, the targets in the Fitts' law test were again limited to single DOF targets. However, the control cursor was allowed to move in both DOFs simultaneously.

The Fitts' law test results of the SVM control are listed in Table 6.26. The subject was not able to control the cursor with the ANN based system. Despite several attempts, no targets were completed, and ultimately the trials were ended to avoid further frustrating the subject. The fact that the SVM based system obtained 75% completion again demonstrates the superiority of the SVM based system, particularly in avoiding unwanted cursor motions.

Table 6.26. The Fitts' law test Results for amputee IV

	SVM
Completion rate (%)	75.0
Throughput (bit/s)	0.53
Overshoot	0.39
Path Efficiency (%)	84.8

6.5 Amputee Discussion

The offline and Fitts' law tests results of the amputee subjects are summarized in Tables 6.27, and 6.28.

Table 6.27. The offline R^2 (%) values for amputee subjects. The residuum length is annotated by L, M, S, for long, medium and short, respectively.

	Subject	*ANN*	*SVM*
Fle/Ext	*AI(L)*	80.7	81.7
	AII(M)	83.2	83.8
	AIII(S)	78.6	77.4
	AIV(S)	75.3	75.5
Pro/Sup	*AI(L)*	76.3	80.8
	AII(M)	83.6	82.7
	AIII(S)	81.3	84.5
	AIV(S)	82.2	82.6

Table 6.28. The Fitts' law test results for amputee subjects. For amputee III, IV the Fitts' law test was limited to single DOF targets. With amputee III, only ANN and SVM tests and with amputee IV, only SVM test was completed. The residuum length is annotated by L, M, S, for long, medium and short, respectively.

	Subject	*ANN*	*SVM-delayed*	*SVM*
Throughput (bps)	*AI(L)*	0.57	0.59	0.62
	AII(M)	0.37	0.41	0.40
	AIII(S)	0.42	-	0.50
	AIV(S)	-	-	0.53
Completion rate (%)	*AI(L)*	95.8	95.8	100
	AII(M)	83.3	89.6	93.8
	AIII(S)	45.8	-	83.3
	AIV(S)	-	-	75.0
Overshoot	*AI(L)*	0.13	0.02	0.10
	AII(M)	0.42	0.35	0.40
	AIII(S)	0.54	-	0.15
	AIV(S)	-	-	0.39
Path Efficiency (%)	*AI(L)*	76.7	85.1	84.5
	AII(M)	63.6	70.7	66.1
	AIII(S)	81.2	-	91.3
	AIV(S)	-	-	84.8

The Fitts' law test results showed that the control performance and length of the residual limb had a direct relationship. This was expected, because longer residual muscles enable more synergistic muscle activation, and generally higher contraction intensities (and EMG levels) which in turn improve the estimation accuracy. Furthermore, eliciting combined motions is difficult with a short residuum, as muscle length change is limited. Additionally, the elicitation of these contractions is unintuitive for congenital amputees.

The flexion-extension offline R^2 values for amputees III and IV were lower than those of amputees I and II (Table 6.27). The pronation-supination R^2 values, however, were

similar between amputees (Table 6.27). Although there was not a large difference in overall R^2 results between amputees, the real-time control performances were quite different (Table 6.28). Also, it suggests that offline test result may not be indicative of real-time performance assessment. In the case of amputees III and IV, performing incorrect combined contractions during training resulted in estimation errors of both single and combined motions. Specifically for single DOF motions, this led to accidental co-activation of the non-target DOF with activation of the target DOF. This caused poor control quality with amputees III and IV when combined motions were included in the training set. Consequently, combined motions were removed from the training set for these users.

Subjectively, amputee I (with a long residuum) exhibited excellent control similar to that of able-bodied users. He comfortably and easily performed combined motions during combined DOF targets. This is reflected in the high β values (Table 6.16) and high path efficiencies (Table 6.28). Amputee II's control performance was notably lower than that of amputee I as supported by the Fitts' law test results (Table 6.28). He perceived simultaneous control and used combined motions for some combined DOF targets. However, in many cases, amputee II did not try to perform combined motions. Instead, he preferred to perform contractions sequentially. This is reflected in the low β values (Table 6.20), and low path efficiencies (Table 6.28). This might result from an inability to quickly conceptualize combined motions (or the required DOFs to elicit the desired cursor movement), and therefore he tended to perform sequential motions. Also, this could be because his control of single DOF may have been more comfortable than combined motions, and therefore he chose to use single DOF motions. It is expected that

simultaneous control would improve with practice as he showed the ability to correctly produce combined DOF contractions when verbally prompted.

For amputees III and IV, the real-time control performance was lower than that of amputee I and II. Amputee IV was unable to control the ANN system, and amputee III's ANN completion rate was also poor (46%) in comparison with that of the SVM (83%). This suggests that the superiority of the SVM control method is amplified when the control ability is limited. This could be due to the lack of users' ability to accommodate inadvertent cursor motions associated with the ANN control. As previously noted, this is largely due to the ANN's inferior performance at low contraction levels.

In the case of amputees I and II, the difference between ANN and SVM control was less than that with able-bodied users. This was likely because the experiment was limited to two DOFs, and therefore the number of inactive DOF was reduced (considering that the SVM advantage over the ANN appeared to be at least in part due to inactive periods). Also, the difference between SVM and SVM-delayed performance was less than that of able-bodied users. This was because the SVM-delayed screen update rate (80 ms) was faster than that with able-bodied users (100 ms). The SVM screen update rate (40 ms) was the same between the amputees and able-bodied users (because reduction of one SVM corresponded to only 2 ms faster processing time, so it was neglected and the same 40 ms update rate was used with amputees). Amputees I and II did not report any perceived difference between the SVM and SVM-delayed control quality.

Amputees III and IV (with short forearms) had difficulty eliciting combined motions. It is postulated that performing wrist combined contractions requires a sufficient amount of

limb rotation and therefore muscle length change. To perform combined contractions, with maximum preferred intensity, users must maintain their forearm fully rotated and perform either flexion or extension. If the rotation range is limited due to a short residuum, it becomes difficult to perform both motions simultaneously. Therefore, when subjects tried to elicit combined motions, instead they might have actually performed the single DOF motions sequentially, or performed one DOF more strongly than the other. This lack of coordination between the contraction and the visual prompt is detrimental to the estimation performance. In the case of the long residual forearm, the amputee more comfortably performed flexion/extension while the forearm is rotated without confusing single and combined DOF contractions. Based on these results, the residual forearm length is a very important factor affecting the control performance.

The visual target based training protocol had fast setup, so it was practical for amputee users, however, amputees with shorter residuum found eliciting combined motions in synchronization with the visual prompt to be difficult. Because visualization of combined motions is difficult for amputees, inclusion of user feedback may help the subject during such complex motions. However, feedback is confusing during dynamic contractions, and may require training with static targets. However, training using static targets would require a longer training session, because targets with different amplitudes have to be included. The long training session can cause fatigue with amputees.

An advantage of the proposed visual training protocol was that it did not involve awkward constraining of the intact limb (as with force based mirrored training protocol), or attaching markers on the intact limb (as with position based mirrored training). The intact limb was not used with this approach, and the only setup required was attaching

electrodes to the impaired limb. An amputee was able to choose his maximum preferred contraction intensity in each DOF independent of other DOFs. The dynamic contractions had an appropriate speed that amputees were subjectively comfortable with. It should be noted that no amputee that participated in this work had previously performed simultaneous myoelectric control. Therefore, it is expected that their control performance would improve with more training sessions.

6.6 Summary

Multilayer perceptron ANNs have been widely used in previous work for simultaneous estimation of multiple DOFs from EMG. In this chapter an SVM based control scheme was proposed. The usability of the ANN and SVM based methods were assessed using a Fitts' law test. The processing times of the SVMs and ANNs were 6 and 60 ms, respectively (for three DOFs). Therefore, two SVM based systems were used. The first system used the original speed of the SVM estimation and the screen was updated every 40 ms. The second system was delayed to have the same delay and screen update rate as those of the ANN based system. In the SVM-delayed and ANN based methods, the screen was updated every 100 ms. The SVM-delayed and SVM systems outperformed the ANN based control in all real-time performance metrics. Since the ANNs and SVMs had similar offline estimation accuracies (R^2), the difference in the real-time results appear to be due (at least in part) to significantly higher estimation accuracy of the SVMs during inactive and low amplitude periods (the MSEs of the ANNs were approximately two times those of the SVMs during inactive periods). The throughput of the SVM

scheme was higher than that of the SVM-delayed system. This is likely due to the higher screen update rate of the SVM method that enhanced the efficacy of the user interaction with the system, by increasing the responsiveness of the system. In summary, the SVM based scheme provided significantly better control in comparison with the ANN based system. Furthermore, the use of the SVMs substantially lowered the training and estimation processing times.

Four amputees also participated in this experiment. The abduction-adduction DOF was removed from the experiment, and consequently, for the SVM-delayed and ANN based methods, the screen was updated every 80 ms (the SVM control screen was updated every 40 ms). With the first amputee (with long residuum), in offline results, the SVM outperformed the ANN in the pronation-supination, but the flexion-extension results were close. For the real-time test results, the SVM and SVM-delayed outperformed the ANN in *throughput* and *path efficiency*. With the second amputee (with medium length residuum), the ANN and SVM based offline results were similar. In real-time control, the SVM outperformed the ANN in *throughput* and *completion rate*. With the third amputee (with short residuum), in offline results, the SVM outperformed the ANN in pronation-supination, but the flexion-extension results were similar between the ANN and SVM. All real-time performance metrics of the SVM were considerably higher than those of the ANN. With the fourth amputee (with short residuum), the offline results were similar between the SVM and ANN. The subject completed the SVM based test, but was unable to control the cursor with the ANN based system. For the third and fourth amputees, the considerable difference between the ANN and SVM based methods in the real-time control appears to be caused by the inability of the users to accommodate inadvertent

cursor motions associated typically with the ANN control. The amputee results suggest that the SVM is more robust than the ANN, when the user's control ability is limited.

An important point that should be noted in studies of simultaneous control, is that sequential activations of a task does not necessarily demonstrates the inability of a user to perform simultaneous motions. For instance, with *amputee II*, it was observed that despite having the ability of simultaneous control (which was shown in many trials), he chose to use sequential motions in other trials. In other words, the preference of the user to perform a specific task, sequentially or simultaneously, must be taken into account, as this is a very important factor. Therefore, in many cases, encouragement might be required to perform simultaneous motions, as sequential movements might be the first choice that comes to the mind of the user.

Chapter 7- Conclusions

7.1 Summary

It has been suggested that simultaneous and proportional control of multiple DOFs may improve the naturalness and intuitiveness of the use of prostheses. Mirrored bilateral training has been proposed in previous work to address the case of unilateral amputees. In this thesis, a direct comparison was made between constrained contractions (force targeted) and unconstrained contractions (position targeted) for mirrored bilateral training strategies. It was shown that when the EMG (and effort) levels were similar between constrained and unconstrained contractions, these methods yielded similar performance in both offline estimation accuracies and in real-time control testing. During a usability test, *position control* was used in which the estimated outputs were mapped to cursor displacements. Different aspects of control were assessed using four metrics including *completion rate*, *completion time*, *overshoot*, and *path efficiency*.

Mirrored bilateral training is only applicable to unilateral amputees and requires complex equipment to record limb force or position. To address this issue, a novel training paradigm (*visual training*) was proposed, during which subjects were prompted to elicit contractions synchronized with a moving cursor on a computer screen. Based on the results, no difference was observed between the real-time control performance of the *visual training* and *mirrored training* based systems. The proposed visual training method is preferable for potential clinical applications as it significantly reduces the training cost and complexity (for clinician and user), while it can be used for both unilateral and bilateral amputees.

Furthermore, a novel application of a support vector machine (SVM) was proposed for simultaneous control of multiple DOFs. SVMs implemented using ν-support vector regression (ν-SVR) was used for estimation. The proposed SVM based scheme was compared with the previously used multilayer perceptron ANNs using a three dimensional Fitts' law test. A velocity control modality was employed where the estimated outputs were mapped to the cursor velocities. The results showed that in comparison to the ANN based system the SVM based scheme significantly improved all real-time performance metrics including *throughput*, *completion rate*, *overshoot*, and *path efficiency*. In each DOF, the offline estimation accuracies of the SVMs and ANNs were similar, but the SVMs outperformed during periods where the target amplitude (in the corresponding DOF) was inactive or less than 20% of full range. In these periods, the MSE of the SVM was approximately half that of the ANN. The low amplitude periods were found to greatly affect the control quality. During both single DOF and combinations of two DOFs contractions, low estimation accuracy of inactive DOFs can cause unwanted cursor movements in the other DOFs. Moreover, when the cursor is close to the target, low level contractions are needed to acquire the target (especially in the case of targets with small widths). Speed histograms calculated using the data from the Fitts' law tests showed that in each DOF, the inactive and low amplitude periods comprised the majority of the target acquisition time. Therefore, the higher real-time control performance of the SVM based scheme can be explained, at least in part, by its higher estimation accuracy during inactive and low amplitude periods. Furthermore, the SVM significantly reduced the training and estimation processing times. The average estimation time of one sample was 6 ms and 60 ms for SVMs and ANNs, respectively

(three estimators for three DOFs were used). This allowed for a faster screen update rate. In this case, the screen was updated every 40 ms for SVM method (limited by rendering delays). When this system was compared to an SVM based system with the same delay and update rate (every 100 ms) as those of the ANN based model, the faster system improved the throughput metric, although other performance metrics did not change.

Also, four amputees participated in this study. The abduction-adduction DOF was removed from the experiment, and therefore the screen was updated every 80 ms for the ANN and SVM-delayed tests. For the first amputee (congenital, with long forearm), the SVM offline results were higher than those of the ANN in pronation-supination. In real-time control, the SVM outperformed the ANN in *path efficiency* and *throughput*. With the second amputee subject (traumatic, with medium length forearm), no appreciable difference between the ANN and SVM based methods were found for the offline results. In real-time control, the SVM outperformed the ANN in *throughput* and *completion rate*. For the third amputee (congenital, with short forearm), the SVM offline results were higher than those of the ANN in pronation-supination. In all real-time performance metrics, the SVM control substantially outperformed the ANN control. For the fourth amputee (traumatic, with short forearm), no difference was found between the offline results of the ANN and SVM. The subject was not able to control the ANN system in real time, but he completed the SVM based test. For all amputees, during inactive and low amplitude periods, the SVM outperformed the ANN in offline estimation accuracy. As with able-bodied users, this might be at least in part the reason for the higher performance of the SVM over ANN in real-time control with amputees.

For the third and fourth amputees, the training was limited to single DOF contractions, as it led to improvement of the control quality. For these subjects, the offline estimates plots demonstrated poor performance for some combined motions. This suggests that they did not perform these contractions correctly, because of either lack of experience or unnaturalness of the motions. It is expected that their performance will improve with more practice unless certain motions are impossible. One of the difficulties of the combined motions for amputees is that unlike able-bodied individuals they do not receive visual feedback to ensure the correctness of their contractions. For the third and fourth amputees, the SVM substantially outperformed the ANN in the real-time test. This appears to be due to inability of these users to accommodate inadvertent cursor motions (often associated with the ANN control). It may be concluded that the SVM is more robust than the ANN when the controllably is low.

During the experiments, the control performance did not systematically decline, implying that fatigue, electrodes shift or impedance changes did not occur.

In this thesis, real-time simultaneous myoelectric control was investigated. In chapters 4 and 5, a position control modality was used, where successful acquisition of combined DOF targets required performing combined DOF contractions. In chapter 6, a velocity control modality was used for the real-time test. In this case, acquisition of targets with combined DOF targets did not necessarily require combined motions. During the experiments (in chapter 4, 5 and 6), the users were encouraged to move simultaneously towards the target in the corresponding DOFs. Based on the results of the β values (in chapters 4, 5 and 6), the subjects chose to move in multiple DOFs simultaneously towards the target. It should be noted that, the subject plays an important role in the

simultaneous movements performance, and encouragement and the subject's experience are important factors. Some users might find it more straight-forward to move towards the target using one DOF at a time. This can be due to lack of experience so that the required combined motion cannot be recalled immediately, whereas the required single DOF motions are more apparent. Also (with a velocity control), this might be because of having physical difficulty to perform a specific combined motion, so that the subject chose to employ sequential movements to reach the target.

7.2 Contributions

1. For the first time, a direct comparison of constrained and unconstrained contractions based strategies using mirrored training was conducted in this work. Based on the results, when using similar EMG levels, no difference was observed between the constrained and unconstrained contractions based systems in both offline and real-time control performance.
2. Several analytical approaches were investigated to improve the offline control performance, as measured by the coefficient of determination (R^2). Alternative feature sets, estimators, feature projection and coordinate systems were considered. An interesting estimator termed an ensemble of bagged decision trees was introduced that improved the estimation accuracies in abduction-adduction, and reduced the processing time. This estimator had not been previously applied to EMG processing. Although no significant advantage over the baseline

configuration comprising TD features and an ANN estimator was found, these results will inform future research.

3. This work provided the first assessment of continuous force / angle estimation in real time. Meaningful metrics were used to capture the usability of the control schemes.
4. As an alternative for *mirrored bilateral training*, a novel training strategy called *visual training* was introduced. No difference was found between the real-time control performance of the *visual training* and *mirrored training* based systems. The *visual training* is preferred because it does not require force or position sensing equipment. Moreover, it can be used for both unilateral and bilateral amputees.
5. A support vector machine (SVM) with the ν-support vector regression algorithm was applied to this problem for the first time. A three dimensional Fitts' law test was used to assess the usability of ANN and SVM estimators. It was shown that the results obeyed Fitts' law as the relationships between the indices of difficulty and completion times were strongly linear. The results showed that the SVMs significantly improved the real-time control performance. This was likely due to higher performance of the SVMs during inactive and low amplitude periods.

7.3 Future Work

This work proposed a practical training protocol (*visual training*) and a more effective estimator (SVM) than the baseline (ANN). The system usability was assessed with able-

bodied and amputee subjects. A thorough investigation of these methods with a larger number of amputees tested over a longer time period can better indicate their suitability for potential clinical applications, as the residual limb musculature of amputees can be very different from those of intact-limbed individuals. Moreover, amputees do not receive proprioceptive and visual feedback from the limb, so their ability to coordinate their contractions with computer based prompting (during the training session) may be impaired. Also, they may have difficulty in generating smooth dynamic contractions. Furthermore, certain combined motions might be unnatural and cumbersome for these users.

A comprehensive comparison of constrained and dynamic contractions using mirrored training also needs inclusion of amputee results. However, generalization of the results requires a large number of amputees with different amputation types and forearm lengths.

An alternative strategy for visual training could include displaying feedback about the user's control (as a control cursor) by employing a system trained with previous data at iterative stages during training. This might be useful for amputees as it provides visual feedback to them to ensure they are performing relevant contractions. However, since dynamic contractions were used in the training protocol of this work, pilot work including feedback was found to be confusing and impractical. Inclusion of control feedback may be more applicable for training protocols that use static targets, to prompt users to position the cursor on the target. Our pilot experiments with able-bodied subjects, however, showed that the dynamic protocol outperformed the static protocol. It is possible that the benefit of the feedback may outweigh the dynamics for amputee subjects.

It would be of great interest to compare the proposed method with pattern recognition based approaches to simultaneous control. A recent study by Young et al. [150] employed a set of conditional parallel classifiers to classify simultaneous movements of wrist and hand. The main drawback of this method was high misclassification rates of combined motions as "no motion". The SVM based method proposed here which showed promise in providing robust control with high performance over inactive periods, can be directly compared with the pattern recognition based approach to determine the relative efficiency of each method.

Three wrist DOFs were investigated in this work, however, future work should also incorporate hand and finger motions. For this purpose, a hierarchical control scheme may suitable, employing the methods described here for the wrist component.

Most commercially available prostheses use a velocity control paradigm. This has been implemented because it "integrates" the instantaneous intent of the user, and results in greater controllability with a noisy input from the EMG. With continuous estimates of force and / or position described in this work, a velocity control scheme may not be best approach to impart dexterous control. Alternative methods to velocity control to take advantage of the force and position information estimated from neural activity must be developed. This is because it is likely that human arm movements do not operate with velocity control, but with position (or force) control.

References

[1] http://www.stanford.edu/class/engr110/2011/LeBlanc-03a.pdf

[2] P. A. Parker, K. B. Englehart, and B.Hudgins, “Myoelectric signal processing for control of powered limb prostheses,” *J. Electromyogr. Kinesiol.*, vol. 16, no. 6, pp. 541–548, 2006.

[3] http://www.coaptengineering.com/

[4] M. Winkler, A. Boschmann, P. Kaufmann and M. Platzner, "Towards multi-movement hand prostheses: combining adaptive classification with high precision socket," *Proceedings of the 2nd European Conference on Technically Assisted Rehabilitation*, 2009.

[5] J. Sensinger, B. Lock and T. Kuiken, "Adaptive pattern recognition of myoelectric signals: exploration of conceptual framework and practical algorithms.," *IEEE Trans Neural Syst Rehabil Eng.*, vol. 17, no. 3, pp. 270-278, Jun. 2009.

[6] A. J. Young, L. H. Smith, E. J. Rouse, L. J. Hargrove, “A new hierarchical approach for simultaneous control of multi-joint powered prostheses,” *Biomedical Robotics and Biomechatronics (BioRob) IEEE RAS & EMBS International Conference*, 2012, pp.514-520.

[7] E. Kamavuako, J. Rosenvang, R. Horup, W. Jensen, D. Farina, and K. Englehart, “Surface Versus Untargeted Intramuscular EMG Based Classification of Simultaneous and Unconstrainedally Changing Movements,” *Neural Systems and Rehabilitation Engineering, IEEE Transactions on* , 2013.

[8] J. L. Nielsen, S. Holmgaard, N. Jiang, K. B. Englehart, D. Farina, and P. A. Parker, “Simultaneous and Proportional Force Estimation for Multifunction Myoelectric Prostheses Using Mirrored Bilateral Training,” *IEEE Trans Biomed Eng*, vol. 58, no. 3, Mar. 2011.

[9] P. V. Komi, M. Ishikawa, “Muscle; Producing force and movement,” *book chapter of The Olympic Textbook of Science in Sport*, 1st edition, Edited by R.J. Maughan, 2009, Blackwell Publishing.

[10] J. T. Francis, “The neural representation of kinematics and dynamics in multiple brain regions: The use of force field reaching paradigms in the primate and rat.”

Mechanosensitivity of the Nervous System. Springer Netherlands, pp 215-247, 2009.

[11] H. S. Milner-Brown, R. B. Stein, "The relation between the surface electromyogram and muscular force", *J Physiol*, vol. 246, no. 3, pp 549–69, 1975.

[12] D. Staudenmann, K. Roeleveld, D. F. Stegeman, J. H. van Dieën, "Methodological aspects of SEMG recordings for force estimation – A tutorial and review". *Journal of Electromyography and Kinesiology*, vol. 20, no. 3, pp 375-387, 2010.

[13] R. M. Enoka, A. J. Fuglevan, "Motor unit physiology: some unresolved issues. Muscle Nerve", vol. 24, no. 1, pp 4-17, 2001.

[14] B. M. Nigg, and W. Herzog, "Biomechanics of the musculo-skeletal system" Vol. 2. New York, Wiley, 1999.

[15] Z. Moussavi, "An Introduction to Muscles & EMG Signal", *online tutorial*, http://www.ee.umanitoba.ca/~moussavi/BME4610/Lectures/Intro_muscles.pdf.

[16] C. J. De Luca, "Electromyography. Encyclopedia of Medical Devices and Instrumentation", Wiley, 2006.

[17] J. Basmajian, and C. DeLuca, "Muscles Alive: Their Functions Revealed By Electromyography," Baltimore, MD: Williams & Wilkins, 1985.

[18] C. Antfolk, C. Cipriani, M. Controzzi, M. C. Carrozza, G. Lundborg, B. Rosén, F. Sebelius, "Using EMG for Real-time Prediction of Joint Angles to Control a Prosthetic Hand Equipped with a Sensory Feedback System," *Journal of Medical and Biological Engineering*, vol. 30, no. 6, pp. 399-406, 2010.

[19] B. Bigland, O. C. Lippold, "The relation between force, velocity and integrated electrical activity in human muscles", *J Physiol*, vol. 123, no. 1, pp 214–24, 1954.

[20] R. H. De Jong, F. G. Freund, "Relation between electromyogram and isometric twitch tension in human muscle," *Archives of physical medicine and rehabilitation*, vol. 48, no.10, pp 539-542, 1967.

[21] H. A. DeVries, "Efficiency of electrical activity as a physiological measure of the functional state of muscle tissue," *American Journal of Physical Medicine & Rehabilitation*, vol. 47, no. 1, pp 10-22, 1968.

[22] L. Korner, P. Parker, C. Almstrom, G. B. Andersson, P. Herberts, R. Kadefors et al., "Relation of intramuscular pressure to the force output and myoelectric signal of skeletal muscle," *Journal of orthopaedic research*, vol. 2, no.3, pp 289-296, 1984.

[23] B. A. Alkner, P. A. Tesch, H. E. Berg, "Quadriceps EMG/force relationship in knee extension and leg press," *Medicine and science in sports and exercise*, vol. 32, no. 2, pp 459-463, 2000.

[24] C. J. De Luca, "The use of surface electromyography in biomechanics," *J Appl Biomech*, vol. 13, no.2, pp 135–63, 1997.

[25] P. V. Komi, E. R. Buskirk, "Reproducibility of electromyographic measurements with inserted wire electrodes and surface electrodes," *Electromyography*, vol. 10, no. 4, pp 357–67, 1970.

[26] J. R. Potvin, R. W. Norman, S. M. McGill, "Mechanically corrected EMG for the continuous estimation of erector spinae muscle loading during repetitive lifting. *European journal of applied physiology and occupational physiology*, vol. 74, no. 1-2, pp 119-132, 1996.

[27] M. Solomonow, R. Baratta, H. Shoji, R. D. D'Ambrosia, "The myoelectric signal of electrically stimulated muscle during recruitment: an inherent feedback parameter for a closed-loop control scheme," *IEEE Trans Biomed Eng*, vol. 33, no. 8, pp 735–45, 1986.

[28] P. Vink, E. A. van der Velde, A. J. Verbout, "A functional subdivision of the lumbar extensor musculature. Recruitment patterns and force-RA-EMG relationships under isometric conditions," *Electromyogr Clin Neurophysiol*; vol. 27, no. 8, pp 517–25, 1987.

[29] E. N. Zuniga, E. G. Simons, "Nonlinear relationship between averaged electromyogram potential and muscle tension in normal subjects," *Arch Phys Med Rehabil*, vol. 50, no. 11, pp 613–20, 1969.

[30] T. Finni, P. V. Komi, J. Lukkariniemi, "Achilles tendon loading during walking: application of a novel optic fiber technique," *Eur J Appl Physiol Occup Physiol*, vol. 77, no. 3, pp 289–91, 1998.

[31] P. Zhou, W. Z. Rymer, "Factors governing the form of the relation between muscle force and the EMG: a simulation study," *J Neurophysiol*, vol. 92, no. 5, pp 2878–86, 2004.

[32] A. J. Fuglevand, D. A. Winter, A. E. Patla, "Models of recruitment and rate coding organization in motor-unit pools," *J Neurophysiol*, vol. 70, no. 6, pp 2470–88, 1993.

[33] K. Roeleveld, D. F. Stegeman, H. M. Vingerhoets, A. Van Oosterom, "Motor unit potential contribution to surface electromyography," *Acta Physiol Scand*, vol. 160, no. 2, pp 175–83, 1997b.

[34] J. J. Woods, and B. Bigland-Ritchie, "Linear and non-linear surface EMG/force relationships in human muscles: an anatomical/functional argument for the existence of both," *American Journal of Physical Medicine & Rehabilitation*, vol. 62, no. 6, pp 287-299, 1983.

[35] A. V. Hill, "First and last experiments in muscle mechanics," *Cambridge University Press*, 1970.

[36] M. F. Bobbert, K. G. M. Gerritsen, M. C. A. Litjens, A. J. Van Soest, "Why is countermovement jump height greater than squat jump height?" *Med Sci Sports Exer*, vol. 28, no. 11, pp 1402–12, 1996.

[37] K. P. Granata, W. S. Marras, "An EMG assisted model of loads on the lumbar spine during asymmetric trunk extensions," *J Biomech*, vol. 26, no. 12, pp 1429–38, 1993.

[38] J. Cholewicki, S. M. McGill, "Mechanical stability of the in vivo lumbar spine: implications for injury and chronic low back pain," *Clin Biomech*, vol. 11, no. 1, pp 1–15, 1996.

[39] B. Laursen, B. R. Jensen, G. Nemeth, G. Sjogaard, "A model predicting individual shoulder muscle forces based on relationship between electromyographic and 3D external forces in static position," *J Biomech*, vol. 31, no. 8, pp 731–9, 1998.

[40] T. S. Buchanan, S. L. Delp, J. A. Solbeck, "Muscular resistance to varus and valgus loads at the elbow," *J Biomech Eng*, vol. 120, no. 5, pp 634–9, 1998.

[41] A. Ridderikhoff, C. L. Peper, R. G. Carson, P. J. Beek, "Effector dynamics of rhythmic wrist activity and its implications for (modeling) bimanual coordination," *Hum Mov Sci*, vol. 23, no (3–4), pp 285–313, 2004.

[42] S. J. Piazza, S. L. Delp, "The influence of muscles on knee flexion during the swing phase of gait," *J Biomech*, vol. 29, no. 6, pp 723–33, 1996.

[43] F. M. M. O. Campos, J. M. F. Calado, "Approaches to human arm movement control—A review," *Annual Reviews in Control*, vol. 33, pp 69–77, 2009.

[44] P. Fitts, “The information capacity of the human motor system in controlling the amplitude of movement," *Journal of Exp. Psychol.*, vol. 47, pp. 381-391, 1954.

[45] W. Abend, E. Bizzi, and P. Morasso, “Human arm trajectory formation,” *Brain: a journal of neurology*, vol. 105, pp 331-348, 1982.

[46] F. Lacquaniti, C. Terzuolo, and P. Viviani, “The law relating the kinematic and figural aspects of drawing movements,” *Acta psychologica*, vol. 54, no.1, pp 115-130, 1983.

[47] T. Flash, N. Hogan, “The coordination of arm movements: An experimental confirmed mathematical model,” *Journal of Neurosciences*, vol. 7, pp 1688–1703, 1985.

[48] D. Wolpert, “Computational approaches to motor control,” *Trends in Cognitive Sciences*, vol. 1, no. 7, 1997.

[49] Y. Uno, M. Kawato, and R. Suzuki, “Formation and control of optimal trajectory in human multijoint arm movement—Minimum torque change model,” *Biologic Cybernetics*, vol. 61, pp 89-101, 1989.

[50] C. M. Harris, and D. M. Wolpert, “Signal-dependent noise determines motor planning.” Nature, vol. 394, pp. 780–784, 1998.

[51] P. H. Clammam, “Statistical analysis of motor unit firing patterns in human skeletal muscle.” *J. Biophysics*, vol. 9, pp. 1233–51, 1969.

[52] P. B. C. Matthews, ”Relationship of firing intervals of human motor units to the trajectory of post-spike after-hyper polarization and synaptic noise.” *J. Physiol*., vol. 492, pp. 597–628, 1996.

[53] E. Todorov, M. Jordan, “Optimal feedback control as a theory of motor coordination,” Nature, vol. 5, No. 11, 2002.

[54] E.E. Fetz, Are movement parameters recognizably coded in the activity of single neurons? Behav Brain Sci. 15 (1992) 679–690.

[55] D. R. Humphrey, J. Tanji, “What features of voluntary motor control are encoded in the neuronal discharge of different cortical motor areas?” *Motor Control: Concepts and Issues*, pp. 307-330, 1991.

[56] J. F. Kalaska, “What parameters of reaching are encoded by discharges of cortical cells?” *Motor Control: Concepts and Issues*, pp. 307-330, 1991.

[57] L.E. Sergio, C. Hamel-Paquet, J. F. Kalaska, "Motor cortex neural correlates of output kinematics and kinetics during isometric-force and arm-reaching tasks," *J. Neurophysiol*, vol. 94, pp 2353–2378, 2005.

[58] A. P. Georgopoulos, R. Caminiti, J. F. Kalaska, J. T. Massey, "Spatial coding of movement: a hypothesis concerning the coding of movement direction by motor cortical populations," *Exp. Brain Res. Suppl.*, vol. 7, 327–336, 1983.

[59] M. T. V. Johnson, T. J. Ebner, "Processing of multiple kinematic signals in the cerebellum and motor cortices," *Brain Res. Rev.*, vol. 33, pp. 155–168, 2000.

[60] M. T. V. Johnson, C. R. Mason, T. J. Ebner, "Central processes for the multiparametric control of arm movements in primates," *Curr. Opin. Neurobiol.*, vol. 11, pp. 684–688, 2001.

[61] U. Windhorst, "Muscle proprioceptive feedback and spinal networks," *Brain Research Bulletin*, vol. 73, pp. 155–202, 2007.

[62] A. Prochazka, "Proprioceptive feedback and movement regulation," *Comprehensive Physiology*,1996.

[63] C. J. De Luca, L. D. Gilmore, M. Kuznetsov, S. H. Roy, "Filtering the surface EMG signal: Movement artifact and baseline noise contamination," *Journal of biomechanics*, vol. 43, no. 8, pp. 1573-1579, 2010.

[64] E. Huigen, A. Peper, C. A. Grimbergen, "Investigation into the origin of the noise of surface electrodes," *Medical and Biological Engineering and Computing*, vol. 40, pp. 332–338, 2002.

[65] D. A. Winter, G. Rau, R. Kadefors, H. Broman, and C. J. De Luca, "Units, terms and standards in the reporting of EMG research," *A Report of the ad hoc Committee of the International Society of Electrophysiological Kinesiology*, 1980.

[66] R. Merletti, "Standards for reporting EMG data. Journal of Electromyography and Kinesiology", vol. 9, no. 1, 1999.

[67] D. F. Stegeman and H. J. Hermens, "Standards for surface electromyography: the European project (SENIAM)," In: Hermens H.J., Rau G., Disselhorst-Klug C., Freriks B. (Eds.), Surface Electromyography Application Areas and Parameters. Proceedings of the Third General SENIAM Workshop on surface electromyo- graphy, Aachen, Germany, pp. 108–112, 1998.

[68] R. N. Scott, "Bio-Engineering Institute. *An introduction to myoelectric prostheses*," *Bio-Engineering Institute, University of New Brunswick*, 1984.

[69] T. R. Farrell, and R. F. Weir. "The optimal controller delay for myoelectric prostheses," *Neural Systems and Rehabilitation Engineering, IEEE Transactions on,* vol. 15, no. 1, pp. 111-118, 2007.

[70] K. Englehart, and B. Hudgins. "A robust, real-time control scheme for multifunction myoelectric control," *Biomedical Engineering, IEEE Transactions on,* vol. 50, no.7, pp. 848-854, 2003.

[71] N. Jiang, K. B. Englehart, and P. A. Parker, "Extracting simultaneous and proportional neural control information for multiple-DOF prostheses from the surface electromyographic signal," *IEEE Trans Biomed Eng,* vol. 56, no. 4, pp. 1070-80, Apr. 2009.

[72] L. Hargrove, E. Scheme, K. Englehart, and B. Hudgins, "Multiple binary classifications via linear discriminant analysis for improved controllability of a powered prosthesis," *IEEE Trans. Neural Syst. Rehabil. Eng.,* vol. 18, no. 1, pp. 49–57, Feb. 2010.

[73] B. Hudgins, P. A. Parker, and R. N. Scott, "A new strategy for multifunction myoelectric control," *IEEE Trans Biomed Eng,* vol. 40, no. 1, pp. 82-94, 1993.

[74] K. B. Englehart, B. Hudgins, P. A. Parker, and M. Stevenson, "Classification of the myoelectric signal using time-frequency based representations," *Med. Eng. Phys.,* vol. 21, no. 6-7, pp. 431–438, Jul-Sep. 1999.

[75] Y. Huang, K. B. Englehart, B. Hudgins, and A. D. C. Chan, "Gaussian mixture model based classification scheme for myoelectric control of powered upper limb prostheses," *IEEE Trans. Biomed. Eng.,* vol. 52, no. 11, pp. 1801–1811, Nov. 2005.

[76] M. F. Lucas, A. Gaufriau, S. Pascual, C. Doncarli, and D. Farina, "Multichannel surface EMG classification using support vector machines and signal-based wavelet optimization," *Biomed. Signal Process Control,* vol. 3, no. 2, pp. 169–174, Apr. 2008.

[77] M. Asghari Oskoei, and H. Hu, "Myoelectric control systems—A survey," *Biomedical Signal Processing and Control,* vol. 2, no.4, pp. 275-94, 2007.

[78] A. Phinyomark, F. Quaine, S. Charbonnier, C. Serviere, F. Tarpin-Bernard, and Y. Laurillau, "EMG feature evaluation for improving myoelectric pattern recognition robustness," *Expert Systems with Applications,* vol. 40, no. 12, pp. 4832-40, 2013.

[79] A. Phinyomark, P. Phukpattaranont, C. Limsakul, “Feature reduction and selection for EMG signal classification,” *Expert Systems with Applications,* vol. 39, no. 8, pp. 7420-31, 2012.

[80] D. S. Dorcas and R. N. Scott, “A three-state myoelectric controller,” *Med. Biol. Eng*., vol. 4, pp. 367–372, 1966.

[81] D. Childress, “A myoelectric three state controller using rate sensitivity,” presented at the Int. Conf. Mathematical Biology and Ecology, Chicago, IL, 1969.

[82] T. W. Williams, “Practical methods for controlling powered upper-extremity prostheses,” *Assist Technol*., vol. 2, no. 3, pp. 3–18, 1990.

[83] D. Graupe, J. Salahi, and K. H. Kohn, “Multifunctional prosthesis and orthosis control via microcomputer identification of temporal pattern differences in single-site myoelectric signals,” *J. Biomed. Eng.*, vol. 4, pp. 17–22, Jan. 1982.

[84] A. Fougner, O. Stavdahl, P. J. Kyberd, Y. G. Losier, P. A. Parker, “Control of Upper Limb Prostheses: Terminology and Proportional Myoelectric Control - A Review,” *IEEE Trans. Neural Syst. Rehabil. Eng.*, vol. 20, no.5, pp. 663-677, Sep. 2012.

[85] E. Scheme, K. Englehart, “Training Strategies for Mitigating the Effect of Proportional Control on Classification in Pattern Recognition–Based Myoelectric Control” , *Journal of Prosthetics and Orthotics*, vol. 25, no. 2, pp. 76-83, Apr. 2013.

[86] P. K. Artemiadis and K. J. Kyriakopoulos, “An EMG-based robot control scheme robust to time-varying EMG signal features,” *IEEE Transactions on Information Technology in Biomedicine*, vol. 14, no. 3, pp.582-588, May. 2010.

[87] S. Oda, “Motor control for bilateral muscular contractions in humans,” *Jpn. J. Physiol,* vol. 47, no. 6, pp. 487-498, Dec. 1997.

[88] De Luca, Carlo J., and Zeynep Erim. "Common drive of motor units in regulation of muscle force." *Trends in neurosciences* 17.7 (1994): 299-305.

[89] N. Jiang, J. L. Vest-Nielsen, S. Muceli, and D. Farina, “EMG-based simultaneous and proportional estimation of wrist/hand unconstraineds in uni-lateral trans-radial amputees,” *J. Neuro Eng. Rehabil*., vol. 9, p. Epub, Jun. 2012.

[90] C. Castellini, E. Gruppioni, A. Davalli, and G. Sandini, "Fine detection of grasp force and posture by amputees via surface electromyography," *Journal of Physiology-Paris*, vol. 103, pp. 255-262, Sep-Dec 2009.

[91] E. N. Kamavuako, D. Farina, K. Yoshida, and W. Jensen, "Estimation of grasping force from features of intramuscular EMG signals with mirrored bilateral training," *Ann. Biomed. Eng.*, vol. 40, no. 3, pp. 648–656, Mar. 2012.

[92] F. Sebelius, L. Eriksson, C. Balkenius and T. Laurell, "Myoelectric control of a computer animated hand: A new concept based on the combined use of a tree-structured artificial neural network and a data glove," *Journal of Medical Engineering and Technology*, vol. 30, no. 1, pp. 2-10, Jan-Feb. 2006.

[93] S. Muceli, N. Jiang, D. Farina, "Multichannel surface EMG based estimation of bilateral hand kinematics," during movements at multiple degrees of freedom," *Conf. Proc. IEEE Eng. Med. Biol. Soc.*, vol. 2010, pp. 6066-6069.

[94] S. Muceli, D Farina, "Simultaneous and proportional estimation of hand kinematics from EMG during mirrored movements at multiple degrees of freedom," *IEEE Trans Neural Sys & Rehab Eng*, vol. 20, no. 3, pp. 371-378, May. 2012.

[95] R. J. Smith, F. Tenore, D. Huberdeau, R. Etienne-Cummings, and Nitish V. Thakor, "Continuous Decoding of Finger Position from Surface EMG Signals for the Control of Powered Prostheses", *30th Annual International IEEE EMBS Conference Vancouver*, 2008, pp. 197-200.

[96] C. Choi; J. Kim, "Development of a myoelectric joystick: A preliminary study," *Biomedical Robotics and Biomechatronics (BioRob), 3rd IEEE RAS and EMBS International Conference on*, pp.173,178, Sept. 2010.

[97] C. Choi; J. Kim, "Synergy matrices to extract fluid wrist motion intents via surface electromyography," *Engineering in Medicine and Biology Society (EMBC), Annual International Conference of the IEEE*, pp. 3511-3514, 2010.

[98] C. Choi, and J. Kim, "Synergy matrices to estimate fluid wrist movements by surface electromyography," *Medical engineering & physics*, vol. 33, no. 8, pp. 916-923, 2011.

[99] N. Jiang, H. Rehbaum, I. Vujaklija, B. Graimann, D. Farina, "Intuitive, Online, Simultaneous and Proportional Myoelectric Control Over Two Degrees of Freedom in Upper Limb Amputees," *IEEE Trans. Neural Syst. Rehabil. Eng.* 2013, in press.

[100] S. Muceli, N. Jiang, D. Farina, "Extracting Signals Robust to Electrode Number and Shift for Online Simultaneous and Proportional Myoelectric Control by Factorization Algorithms," *IEEE Trans. Neural Syst. Rehabil. Eng.* 2013, in press.

[101] H. Rehbaum, N. Jiang, L. Paredes, S. Amsuess, B. Graimann, D. Farina, "Real Time Simultaneous and Proportional Control of Multiple Degrees of Freedom from surface EMG: preliminary results on subjects with limb deficiency," *Conf. Proc. IEEE Eng. Med. Biol. Soc.*, (2012) pp. 1346-1349.

[102] F. C. Sebelius, B. N. Rosen, and G. N. Lundborg, "Refined myoelectric control in below-elbow amputees using artificial neural networks and a data glove," *J. Hand Surg. Am.*, vol. 30, pp. 780–789, Jul. 2005.

[103] C. Cipriani, C. Antfolk, M. Controzzi, G. Lundborg, B. Rosen, M.C. Carrozza, F. Sebelius, "Online Myoelectric Control of a Dexterous Hand Prosthesis by Transradial Amputees," *Neural Systems and Rehabilitation Engineering, IEEE Transactions on* , vol. 19, no. 3, pp. 260-270, Jun. 2011.

[104] P. Shenoy, K. J. Miller, B. Crawford, R. P. N. Rao, "Online Electromyographic Control of a Robotic Prosthesis," *Biomedical Engineering, IEEE Transactions on* , vol. 55, no. 3, pp. 1128-1135, Mar. 2008.

[105] R. Davoodi, G. E. Loeb, "Real-Time Animation Software for Customized Training to Use Motor Prosthetic Systems," *Neural Systems and Rehabilitation Engineering, IEEE Transactions on* , vol.20, no.2, pp.134,142, Mar. 2012.

[106] J. M. Lambrecht, C. L. Pulliam, and R. F. Kirsch, "Virtual reality environment for simulating tasks with a myoelectric prosthesis: an assessment and training tool," *J Prosthet Orthot.*, vol. 23(2), pp. 89–94, Apr. 2011.

[107] B. Lock, K. Englehart, and B. Hudgins, "Real-time myoelectric control in a virtual environment to relate usability vs. accuracy," Myoelectric Symposium, 2005.

[108] A. Simon, L. Hargrove, B. Lock and T. Kuiken, "Target Achievement Control Test: Evaluating real-time myoelectric pattern-recognition control of multifunctional upper-limb prostheses," *Journal of Rehabil. Research and Development*, vol. 48, no. 6, pp. 619-628, 2011.

[109] L. Hargrove, Y. Losier, B. Lock, K. Englehart, B. Hudgins, "A real-time pattern recognition based myoelectric control usability study implemented in a virtual environment," *Conf Proc IEEE Eng Med Biol Soc*, pp. 4842–45, 2007.

[110] M. R. Dawson, F. Fahimi, and J. P. Carey, "The Development of a Myoelectric Training Tool for Above-Elbow Amputees," *Open Biomed Eng J.*, vol. 6, pp. 5–15, Feb. 2012.

[111] M. R. Dawson, F. Fahimi, J. P. Carey, "Myoelectric training systems," *Expert Review of Medical Devices,* vol. 8, no. 5, pp. 581–589, Sep. 2011.

[112] J. Sensinger, R. Weir, "User-Modulated Impedance Control of a Prosthetic Elbow in Unconstrained, Perturbed Motion," *Biomedical Engineering, IEEE Transactions on* , vol.55, no.3, pp.1043,1055, March 2008.

[113] S. Zhai, and P. Milgram, "Human performance evaluation of manipulation schemes in virtual environments," *Virtual Reality Annual International Symposium, 1993, IEEE*.

[114] T. A. Kuiken, G. Li, B. Lock, R. Lipschutz, L. Miller, K. Stubblefield, and K. Englehart, "Targeted muscle reinnervation for real-time myoelectric control of multifunction artificial arms," *JAMA: the journal of the American Medical Association,* vol. 301, no. 6, pp. 619-628, 2009.

[115] R. J. Smith, D. Huberdeau, F. Tenore, N. V. Thakor, "Real-time myoelectric decoding of individual finger movements for a virtual target task," *Engineering in Medicine and Biology Society, Annual International Conference of the IEEE,* pp. 2376-2379, Sept. 2009.

[116] C. Choi; S. Micera, J. Carpaneto, J. Kim, "Development and Quantitative Performance Evaluation of a Noninvasive EMG Computer Interface," *Biomedical Engineering, IEEE Transactions on* , vol. 56, no. 1, pp. 188,191, Jan. 2009.

[117] M. Williams and R. Kirsch, "Evaluation of Head Orientation and neck muscle EMG signals as command inputs to a human-computer interface for individuals with high tetraplegia," *IEEE Trans. Neural Syst. Rehabil. Eng.,* vol. 16, no. 5, pp. 485-496, Oct. 2008.

[118] E. Scheme and K. Englehart, "Validation of a Selective Ensemble-Based Classification Scheme for Myoelectric Control Using a Three Dimensional Fitts' Law Test," *IEEE Trans. Neural Syst. Rehabil. Eng.,* vol. 21, no.4, pp.616-623, Jul. 2013.

[119] E. Scheme, B. Hudgins, K. Englehart, "Confidence-Based Rejection for Improved Pattern Recognition Myoelectric Control," *Biomedical Engineering, IEEE Transactions on*, vol.60, no.6, pp.1563,1570, June 2013.

[120] E. Scheme, B. Lock, L. Hargrove, W. Hill, U. Kuruganti, K. Englehart, "Motion Normalized Proportional Control for Improved Pattern Recognition-Based Myoelectric Control," *Neural Systems and Rehabilitation Engineering, IEEE Transactions on* , vol.22, no.1, pp.149,157, Jan. 2014.

[121] P. Shenoy, K. J. Miller, B. Crawford, R. P. N. Rao, "Online Electromyographic Control of a Robotic Prosthesis," *Biomedical Engineering, IEEE Transactions on* , vol. 55, no. 3, pp. 1128-1135, March 2008.

[122] Z. O. Khokhar, G. X. Zhen, and C. Menon, "Surface EMG pattern recognition for real-time control of a wrist exoskeleton," *Biomedical engineering online*, vol. 9, no.41, 2010.

[123] K. Momen, S. Krishnan, T. Chau, "Real-Time Classification of Forearm Electromyographic Signals Corresponding to User-Selected Intentional Movements for Multifunction Prosthesis Control," *Neural Systems and Rehabilitation Engineering, IEEE Transactions on* , vol. 15, no. 4, pp. 535-542, Dec. 2007.

[124] A. B. Ajiboye, R. F. Weir, "A heuristic fuzzy logic approach to EMG pattern recognition for multifunctional prosthesis control," *Neural Systems and Rehabilitation Engineering, IEEE Transactions on* , vol. 13, no. 3, pp. 280-291, Sept. 2005.

[125] J. L. Nielsen, S. Holmgaard, N. Jiang, K. Englehart, D. Farina, and P. Parker, "Enhanced EMG signal processing for simultaneous and proportional myoelectric control," *Conf Proc IEEE Eng Med Biol Soc*, Sep 2009, pp. 4335-8.

[126] Zajac, Felix E. "Muscle and tendon: properties, models, scaling, and application to biomechanics and motor control." *Critical reviews in biomedical engineering* 17.4 (1988): 359-411.

[127] F. V. Wright, "Measurement of functional outcome with individuals who use upper extremity prosthetic devices: Current and future directions," *J Prosthet Orthot*, vol. 18, no. 2, pp. 46–56, 2006.

[128] L. A. Miller, S. Swanson, "Summary and recommendations of the Academy's State of the Science Conference on Upper Limb Prosthetic Outcome Measures," *J Prosthet Orthot*, vol. 21, no.9, pp. 83–89, 2009.

[129] W. Hill, Ø. Stavdahl, L. N. Hermansson, P. Kyberd, S. Swanson, S. Hubbard, "Functional outcomes in the WHO-ICF model: Establishment of the Upper Limb Prosthetic Outcome Measures Group," *J Prosthet Orthot*, vol. 21, no.2, pp. 115–19, 2009.

[130] C. Shannon, "Mathematical theory of communication," *Bell Syste. Tech. J.*, vol. 27, pp. 623-656, 1948.

[131] E. N. Kamavuako, J. C. Rosenvang, M. F. Bøg, A. Smidstrup, E. Erkocevic, MJ Niemeier , W Jensen, and D. Farina, "Influence of the feature space on the estimation of hand grasping force from intramuscular EMG," *Biomedical Signal Processing and Control*, vol 8, no. 1, pp. 1-5, Jan. 2013.

[132] A. Phinyomark, C. Limsakul, and P. Phukpattaranont, "A novel feature extraction for robust EMG pattern recognition," *arXiv preprint arXiv:0912.3973*, 2009.

[133] H. Lu, M. Gargesha, Z. Wang, D. Chamie, D., G. Attizzani, T. Kanaya, M. Costa, A. Rollins, H. Bezerra, D. Wilson, "Automatic stent detection in intravascular OCT images using bagged decision trees," *Biomedical optics express*, vol. *3*, No. 11, pp. 2809-24, 2012.

[134] M. C. Tu, D. Shin, D. Shin, "Effective Diagnosis of Heart Disease through Bagging Approach," *Biomedical Engineering and Informatics, BMEI '09. 2nd International Conference on*, pp.1-4, Oct. 2009.

[135] L. Breiman, J. H. Friedman, R. A. Olshen, and C. J. Stone, "Classification and regression trees," *Wadsworth & Brooks*, *Monterey*, *CA*, 1984.

[136] L. Breiman, "Bagging Predictors", *Technical Report 421*, September 1994, Department of Statistics, University of California Berkeley, CA, http://statistics.berkeley.edu/sites/default/files/tech-reports/421.pdf.

[137] C. Cortes, and V. Vapnik, "Support-vector networks," *Machine learning*, vol. 20, No. 3, pp. 273-297, 1995.

[138] B. E. Boser, I. M. Guyon, and V. N. Vapnik, "A training algorithm for optimal margin classifiers," *Proceedings of the fifth annual workshop on Computational learning theory*, *ACM*, 1992.

[139] B. Scholkopf, P. L. Bartlett, A. J. Smola, and R. Williamson, "Shrinking the tube: a new support vector regression algorithm," *Advances in neural information processing systems* 330-336, 1999.

[140] W. Karush, "Minima of functions of several variables with inequalities as side constraints", *Masters' thesis, Dept. of Mathematics, Univ. of Chicago.*, 1939.

[141] H. Kuhn and A. Tucker, "Nonlinear programming," *In Proc. 2nd Berkeley Symposium on Mathematical Statistics and Probabilistics, Berkeley, University of California Press*, pp. 481–92, 1951.

[142] C. Chang, C. Lin, "Training ν-support vector regression: theory and algorithms," *Neural Computation*, vol.14, no.8, pp. 1959-77, 2002.

[143] P. Chen, C. Lin, and B. Schölkopf, "A tutorial on ν-support vector machines," *Applied Stochastic Models in Business and* Industry, vol. 21, no. 2, pp. 111-36, 2005.

[144] http://www.csie.ntu.edu.tw/~cjlin/libsvm/

[145] A. B. Graf, and S. Borer, "Normalization in support vector machines," *Pattern Recognition. Springer Berlin Heidelberg*, pp. 277-282, 2001.

[146] S. Li, X. Hou, H. Zhang, and Q. Cheng, "Learning spatially localized, parts-based representation," *In Proc. IEEE Computer Vision and Pattern Recognitio*n, pp. 207-212, 2001.

[147] D. Lee and H. S. Seung, "Algorithms for non-negatvie matrix factorization," *In Advances in Neural Information Processing Systems*, vol. 13, pp. 1-8, 2001.

[148] C. Wang, Z. Song, S. Yan, L. Zhang, and H. Zhang, "Multiplicative NonNegative Graph Embedding," *In Proc. IEEE Conference on Computer Vision and Pattern Recognition*, 2009.

[149] M. Borga, H. Knutsson, "A canonical correlation approach to blind source separation," *Technical Report LiU-IMT-EX-0062, Department of Biomedical Engineering, Linköping University*, 2001.

[150] A. Young, L. Smith, E. Rouse, L. Hargrove, "Classification of simultaneous movements using surface EMG pattern recognition," *Biomedical Engineering, IEEE Transactions on*, Vol. 60, No. 5, pp. 1250-1258, Jan 2013.

[151] C. Castellini, P. Van der Smagt, "Surface EMG in advanced hand prosthetics," Biol Cybern, vol. 100, pp. 35-47, 2009.

[152] D. Yang D, J. Zhao, Y. Gu, L. Jiang, H. Liu, "EMG Pattern Recognition and Grasping Force Estimation: Improvement to the Myocontrol of Multi-DOF Prosthetic Hands," *IEEE/RSJ International Conference on Intelligent Robots and Systems* 2009.

[153] A. Ziai, and M. Carlo, "Comparison of regression models for estimation of isometric wrist joint torques using surface electromyography," *Journal of neuroengineering and rehabilitation*, vol. 8, no.1, 2011.

Curriculum Vitae

Ali Ameri Mahabadi

PhD. Candidate
Department of Electrical and Computer Engineering,
University of New Brunswick
15 Dineen Dr., Fredericton, NB, Canada, E3B 5A3
Phone(c): 1-506-999-0333
Email: ali.ameri@unb.ca

Education

University of New Brunswick, (Expected 2014) **2010 – 2014**
Doctor of Philosophy in Electrical Engineering (Ph.D.)
Department of Electrical Engineering, Institute of Biomedical engineering
Thesis topic: Real-time simultaneous myoelectric control of multiple degrees of freedom
Supervisors: K. Englehart, P. Parker, E. Scheme.

Shahid Beheshti University, Tehran **2004 – 2007**
Master of Science in Electrical Engineering (M.Sc.),
Department of Electrical Engineering
Thesis topic: Speech enhancement using wavelet transform
Supervisors: M. Eshghi

Sharif University of Technology, Tehran, **2000 – 2004**
Bachelor of Science in Electrical Engineering (B.Sc.); Electronics
Department of Electrical Engineering

Current research interests

- Statistical signal processing
- Myoelectric control of powered prostheses
- Machine learning
- Speech processing

Publications

Journal publications

A. Ameri, E. Kamavuako, E. Scheme, K. Englehart, P. Parker, "Support Vector Regression for Improved Real-Time, Simultaneous Myoelectric Control," *IEEE Trans. Neural Syst. Rehabil. Eng.*, in press, 2014.

A. Ameri, E. Scheme, E. Kamavuako, K. Englehart, P. Parker, "Real Time, Simultaneous Myoelectric Control Using Force and Position Based Training Paradigms," *IEEE Trans. Biomed. Eng,* vol. 61, no. 2, pp. 279-287, 2014.

A. Ameri, E. Kamavuako, E. Scheme, K. Englehart, P. Parker, "Real-time, simultaneous myoelectric control using visual target-based training paradigm," *Biomed. Signal Proc. & control,* vol. 13, pp. 8-14, 2014.

Conference publications

A. Ameri, K. B. Englehart, and P. A. Parker, "A comparison between force and position control strategies in myoelectric prostheses," in *Conf. Proc. IEEE Eng. Med. Biol. Soc.*, vol. 2012, pp. 1342–1345.

A. Ameri, K. B. Englehart, and P. A. Parker, "Simultaneous and proportional estimation of multiple DOFs for myoelectric prostheses: a comparison between force and position control paradigms," in *Conf. Proc. ACCES17 & CMBEC, Jun 2012, Halifax, Canada.*

A. Ameri, A. Hejazi, et al., "A Combinational Adaptive Noise Canceller Using Filter Bank", *in Proc. the 6th IEEE Int. Symposium on Image and Signal Processing and Analysis (ISPA),* 2009.

A. Ameri, M. Eshghi, "Half-Zone Quantization Based Algorithm for Information Hiding", *in Proc. the 5thIEEE Int. Conf. on Intelligent Information Hiding and Multimedia Signal Processing (IIH-MSP),* 2009.

A. Ameri, M. A. Akhaee, F. Marvasti, "Semi-Reversible Quantization Based Data Hiding Using Missing Samples Recovery Technique", *in Proc. IEEE Int. Conf. on Telecommunications (ICT),* 2009.

A. Ameri, M. Eshghi, "Speech Enhancement Using Affine Projection Algorithm in Subband", *in Proc. IEEE Int. Conf. on Multimedia Computing and Systems (ICMCS),* 2009.

M. A. Akhaee, A. Ameri, F. A. Marvasti, "Speech Enhancement by Adaptive Noise Cancellation in the Wavelet Domain", *in Proc. 5th IEEE Int. Conf. on Information, Communications, and Signal Processing (ICICS)*, 2005.

Memberships

IEEE, student member	2010-2014
Canadian Medical and Biological Society	2010-2014